공학박사학위논문

A study on the preparation of supramolecular and polymeric materials containing lanthanide ions and their luminescent or catalytic properties

란탄족 이온을 함유한 초분자와 고분자 재료의 제조 및 발광 또는 촉매 특성에 관한 연구

2014년 2월

서울대학교 대학원

재료공학부

김 형 우

A study on the preparation of supramolecular and polymeric materials containing lanthanide ions and their luminescent or catalytic properties

란탄족 이온을 함유한 초분자와 고분자 재료의 제조 및 발광 또는 촉매 특성에 관한 연구

지도교수 장 지 영

이 논문을 공학박사 학위논문으로 제출함

2013년 10월

서울대학교 대학원

재료공학부

김 형 우

김형우의 공학박사 학위논문을 인준함

2013년 12월

위 원 장 조 원 호 (인)

부위원장 장 지 영 (인)

위 원 박 종 래 (인)

위 원 안 철 희 (인)

위 원 임 순 호 (인)

Abstract

A study on the preparation of supramolecular and polymeric materials containing lanthanide ions and their luminescent or catalytic properties

Hyungwoo Kim

Department of Materials Science and Engineering

Seoul National University

Lanthanide(III) ions are of great interest due to their characteristic optical properties such as narrow emission and long lifetime originated from intraconfigurational f-f transition. In this study, lanthanide(III) ions were utilized as a luminescence center in organogelators after coordination with aromatic molecules, showing enhanced luminescence and color change during gelation in organic solvents. A lanthanide(III) ion was also incorporated in the binding sites of a molecularly imprinted polymer as a signal transducer in luminescence sensing. When a lanthanide(III) ion was doped in microporous organic polymer, gas adsorption and catalytic activity of the polymer were enhanced.

Firstly, Eu(III) and Tb(III) complexes (**Eu2** and **Tb2**) were prepared with phenanthroline derivatives, which formed organogels in *n*-decane. The organogels of **Eu2** and **Tb2** showed red and green emissions, respectively, when excited at 330 nm. TEM images of dry gels of **Eu2** and **Tb2** showed entangled fiber network structures with fiber diameters ranging from 20 to 80 nm. Because of the structural similarity of **Eu2** and **Tb2**, they formed stable mixed gels of different compositions in *n*-decane. The emission spectrum of a mixed gel showed emission peaks from Eu(III) at 595 and 618 nm and from Tb(III) at 496 and 551 nm when excited at 330 nm. A broad emission was observed around 470 nm that was attributed primarily to the ligands of **Tb2**. At a ratio of **Eu2** / **Tb2** of 1 : 19 by weight, the mixed gel exhibited white luminescence. The 1931 CIE color coordinates of the mixed gel were x = 0.36 and y = 0.30 in the white region. The TEM image of the dry gel revealed entangled fibers with diameters ranging from 20 to 80 nm without evidence of self-sorting. Trimetallic organogelators, **Eu4** and **Tb4**, were prepared by coordination of **Eu2** and **Tb2** with two 1,3-diketone groups. **Eu4** showed three transitions of Eu(III) ion in red region and a ligand-centered emission but **Tb4** showed only a broad emission in greenish blue region from the ligands. **Eu4** and **Tb4** also formed a homogeneous mixed gel in *n*-decane, showing a whitish luminescence at the ratio of 3 : 1 by weight. Furthermore, **Eu4** showed film-

forming property. The complex was fabricated as a not only thin film by spin casting but also free-standing film by melt casting without losing the red luminescence. A Er(III) complex, **Er4** was also synthesized and fabricated as fiber network embedded in cross-linked EGDMA film. The film showed an emission in NIR region ranging from 1450 to 1650 nm, potentially utilized in telecommunication.

Secondly, it was demonstrated that the molecularly imprinted system bearing the Eu(III) ions could be used for the direct detection of chromophoric organic molecules. A molecularly imprinted polymer containing Eu(III) ions in binding cavities (**MIP-Eu**) was prepared by polymerization of a complex of non-chromophoric monomer (3-allylpentane-2,4-dione) and the Eu(III) ion. Picloram was used as a template molecule, which is a widely used chlorinated herbicide persistent in water or soil. The ability of **MIP-Eu** to recognize the template was investigated by photoluminescence spectroscopy. It was able to detect the template molecules captured in the cavities directly by observing the sensitized luminescence of the Eu(III) ions. The emission peak intensities of the Eu(III) ions at 594 and 616 nm intensified with the increase in the picrolam concentration. The specific recognition ability of **MIP-Eu** was also investigated for the template against its structural analogs such as dicamba and 2-amino-4,6-dichloropyrimidine-5-carboxaldehyde by photoluminescence spectroscopy.

Lastly, a Yb(III)-incorporated microporous polymer (**Yb-ADA**) was synthesized and its gas adsorption property and catalytic activity were studied. The adamantane-based porous polymer (**ADA**) was obtained from an ethynyl-functionalized adamantane derivative and 2,5-dibromoterephthalic acid through Sonogashira-Hagihara cross-coupling. **ADA** had carboxyl groups which were used for Yb(III) coordination under basic condition. The Brunauer-Emmett-Teller (BET) surface area of **ADA** was 970 $m^2 g^{-1}$. As Yb(III) ions were incorporated into **ADA**, the surface area of the polymer (**Yb-ADA**) was reduced to 885 $m^2 g^{-1}$. However, **Yb-ADA** exhibited a significantly enhanced CO_2 and H_2 adsorption capacities despite the reduction of the surface area. The CO_2 uptakes of **ADA** and **Yb-ADA** were 1.56 and 2.36 mmol g^{-1} at 298 K, respectively. The H_2 uptake of **ADA** also increased after coordination with Yb(III) from 1.15 to 1.40 wt% at 77 K. **Yb-ADA** showed a high catalytic activity in the acetalization of 4-bromobenzaldehyde and furfural with trimethylorthoformate and could be reused after recovery without severe loss of activity.

Keywords: Lanthanide, luminescence, organogel, molecular imprinting, microporous polymer, catalysis.

Student Number: 2008-20639

Contents

List of Schemes

List of Tables

List of Figures

Figure II-4. TEM images of dry gels obtained from (a) 1 wt% of **Eu2** in *n*-decane, (b) 2 wt% of **Tb2** in *n*-decane, (c) 1 wt% of **Eu4** in *n*-decane, (d) 1 wt% of **Tb4** in *n*-decane and (e) 1 wt% of **Er4** in *n*-decane.

Figure II-5. (a) Emission spectra from **Eu2** and **Tb2** in chloroform excited at 330 nm. The absorption spectra of the two complexes are included as an inset. (b and c) Photographs of organogels of **Eu2** (b) and **Tb2** (c) (2 wt% in *n*-decane) taken under 365 nm irradiation.

Figure II-6. (a) TEM image of the dry gel obtained from **Eu2-Tb2** in *n*-decane (2 wt%). (b) Emission spectra of the sol and gel of **Eu2-Tb2** in *n*-decane (2 wt%) when excited at 330 nm. The absorption spectra of two states are shown in the inset.

Figure II-7. Emission spectra obtained from (a) a solution of **Eu2** (0.1 wt%) in *n*-decane and (b) a solution of **Eu2-Tb2** (2 wt%) in toluene when excited at 330 nm.

Figure II-8. (a) Emission spectra of the sol (100 ^{o}C) and gel (25 ^{o}C) of **Eu2** in *n*-decane (2 wt%) excited at 330 nm. The absorption spectra of two states are shown in the inset. (b and c) Photographs of the sol (b) and the gel (c) of **Eu2** in *n*-decane (2 wt%) under 365 nm irradiation.

Figure II-9. (a) Emission spectra of the sol (100 ^{o}C) and gel (25 ^{o}C) of **Tb2** in *n*-decane (2 wt%) excited at 330 nm. The absorption spectra of two states are

shown in the inset. (b and c) Photographs of the sol (b) and the gel (c) of **Tb2** in *n*-decane (2 wt%) under 365 nm irradiation.

Figure II-10. Photographs of the sol at 100 ^{o}C (a) and gel at 25 ^{o}C (b) of **Eu2-Tb2 (**2 wt%, *n*-decane) taken under 365 nm irradiation. (c) CIE color coordinates of **Eu2-Tb2** at the sol and gel states in *n*-decane (2 wt%).

Figure II-11. Emission spectra from **Eu4** and **Tb4** in chloroform excited at 330 nm. The absorption spectra of the two complexes are shown in the inset.

Figure II-12. Emission spectra of the sol (70 ^{o}C) and gel (25 ^{o}C) of **Eu4** (a) and **Tb4** (b) in *n*-decane (1 wt%) excited at 330 nm. The absorption spectra of two states are shown in the inset.

Figure II-13. (a) TEM image of the dry gel obtained from **Eu4-Tb4** (3 : 1 by weight) in *n*-decane (1 wt%). (b) Emission spectra of the sol (70 ^{o}C) and gel (25 ^{o}C) of **Eu4-Tb4** in *n*-decane (1 wt%) excited at 330 nm. Absorption spectra of two states are shown in the inset.

Figure II-14. (a) Emission spectra of **Eu4** in toluene with various concentrations obtained at 25 ^{o}C (λ_{ex} = 310 nm). (b) Emission spectra of **Eu4** in toluene obtained at 25 and 70 ^{o}C (λ_{ex} = 310 nm).

Figure II-15. UV-Vis spectra (left) and emission spectra excited at 275 nm (right) of **Eu4** in the solution and gel states. Photographs of the sol (left) and the gel (right) were taken after 365 nm irradiation.

Figure III-2. (a) Emission spectra of **MIP-Eu** in aqueous methanol in the presence of various concentrations of picloram. Emission spectra were obtained at 250 nm excitation. (b) The concentration effect of picloram on emissions of **MIP-Eu** and **NIP-Eu**. ΔI: emission intensity change upon addition of picloram ($I - I_0$), I_0: emission intensity in the absence of picloram.

Figure III-3. Photographs of the as-synthesized polymer, **MIP-Eu** and **MIP-Eu** incubated in a 0.4 mM picloram solution in methanol for 1 h taken in (a) daylight and (b) under 365 nm irradiation.

Figure III-4. The effect of pH on emission of **MIP-Eu** in 0.4 mM of picloram solution. ΔI : emission intensity change upon addition of picloram ($I-I_0$), I_0 : emission intensity without picloram.

Figure III-5. (a) Emission spectra of **MIP-Eu** in aqueous methanol in the presence of picloram and its analogs (0.4 mM). Emission spectra were obtained at 250 nm excitation. (b) Structures of analytes and their effect on emissions of **MIP-Eu** and **NIP-Eu**. ΔI: emission intensity change upon addition of picloram ($I - I_0$), I_0: emission intensity in the absence of picloram.

Figure IV-1. XPS spectra of **ADA** and **Yb-ADA**.

Figure IV-2. Solid-state ^{13}C NMR spectra of **ADA** and **Yb-ADA**.

Figure IV-3. TGA thermograms of **ADA** and **Yb-ADA**.

Chapter I.

Introduction

I-1. Lanthanide(III) Ions and Applications

I-1-1. Principle of Lighting on Lanthanide(III) Ions

The trivalent lanthanide ions have shown their abilities in various fields due to their unique luminescent properties. They have been used in lasing phosphor, electroluminescent materials for organic light-emitting diode (OLED), optical fibers for signal amplification and sensors for biological and clinical purposes. Intraconfiguraltional 4f-4f transitions of lanthanide(III) ions are responsible for long-lasting and narrow emissions. The emissions cover not only visible light region but also ultraviolet (UV) and near-infrared (NIR) regions. Typically, Eu(III) emits red light, Sm(III) orange light, Dy(III) yellow light, Tb(III) green light and Tm(III) blue light in visible region. Also, Yb(III), Nd(III) and Er(III) emit NIR light and Gd(III) UV light. The f-f transitions are less affected by external chemical environment because 4f orbitals are perturbed and shielded by $5s^2$ and $5p^6$ subshells in proximity. Sometimes, 4f-5d transitions occur in special

case such as Ce(III) with exhibition of intense and various colored emissions depending on the ligands, indicating the 5d orbitals interact directly with external ligands. Most of electronic transitions are spin-fobidden f-f transitions according to the selection rule, having low absorption coefficients less than 10 L mol^{-1} cm^{-1}. This weak absorption inhibits the direct excitation of lanthanide(III) ions, resulting the only feeble luminescence. This has been overcome by the coordination of organic ligand to lanthanide(III) ions after Weissman investigated an indirect excitation of lanthanide(III) complexes.[1] The ligands in the complexes absorb the light instead of metal ions and induce the photo-induced energy transfer to excited lanthanide(III) ions, named sensitization or antenna effect.[2] Following this method, the luminescence of lanthanide(III) ions can be obtained efficiently with a high quantum yield.

The sensitization mechanism is shown in Figure I-1. Once the organic ligand is irradiated by light energy, the ligand is excited to the first excited singlet energy state (S_1). Then, the excited energy is quickly relaxed to the lowest vibrational level in S_1 state by internal conversion and deactivated radiatively or non-radiatively. The radiative deactivation generates fluorescence, but the non-radiative deactivation populates the first excited triplet state (T_1) by intersystem crossing. The intersystem crossing is known to be processed by spin-orbit coupling and enhanced by a heavy paramagnetic ion effect. The excited energy in

T_1 is immediately relaxed to the lowest vibrational level and also decayed radiatively or non-radiatively. The radiative decay from T_1 to S_0 emits phosphorescence having a long lifetime and large stokes shift due to the parity-forbidden transition. On the other hand, in the case of non-radiative transition, the energy is transferred to excited states in lanthanide(III) ion by phonon-assisted pathways. In principle, two mechanisms are possibly included. One of the mechanisms is Dexter energy transfer, meaning that electrons are exchanged between the ligand and the metal ion through the good overlap of orbitals. The other one is Förster resonance energy transfer. This mechanism transfers energy by dipole-dipole coupling and less dependent on the distance than the Dexter mechanism. The S_1 state could be involved in the energy transfer towards the metal ion, but the lifetime was desperately short to transfer the energy compared to T_1 state. After the energy transfer and internal conversion, the emitting level of lanthanide(III) ion is indirectly populated and ready to emit the line-like luminescence efficiently.[3]

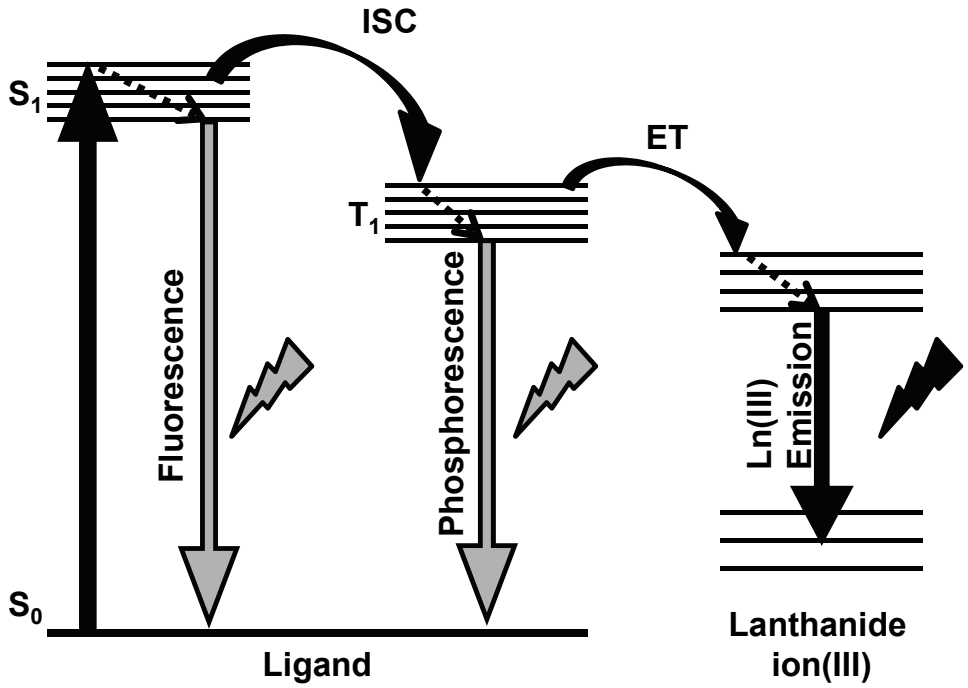

Figure I-1. Schematic description of energy transfer by sensitization mechanism in lanthanide(III) complex. The main energy transfer is shown in solid black arrows. The dotted black arrows indicate internal conversion. S = singlet, T = triplet, ISC = intersystem crossing, ET = energy transfer.

Otherly, charge transfer states such as ligand-to-metal charge transfer (LMCT) or intra-ligand charge transfer (ILCT) are also related to the energy transfer. Those states should be positioned much higher than resonance level of lanthanide(III) ion to transfer energy. Otherwise, they work as a quencher of lanthanide(III) ion.

To improve the luminescent properties of lanthanide(III) ions, the energy transfer is sufficiently facilitated and non-radiative processes should be suppressed. The chromophore group of the ligand should be located near the lanthanide(III) ion because the energy transfer is highly dependent on the distance between the sensitizer and the metal ion. Vibrational deactivation should be diminished. The bond vibrations such as O-H, N-H and C-H nearby dissipate excited energy and severely devastate the quantum effciency. Also, the collision with solvent molecules has an detrimental effect on the luminescence. The energy back transfer hinders the lanthanide(III) ion from achieving the high quantum yield. In each step of energy migration, there are possiblities for the back transfer. There are theoretically and empirically optimized energy gaps, for instance the energy gap between S_1 and T_1 state should be approximately 5000 cm^{-1} to efficiently prevent the back transfer and the gap between T_1 and resonance level of lanthanide(III) ion should range from 2500 to 4000 cm^{-1}.[4,5] The above issues can be unraveled by the coordination with proper organic ligands which preserve the metal ion from external atmosphere.

I-1-2. Application of Lanthanide(III) Ions in Organogels

Low molecular weight organogels are thermally reversible and vicoelastic materials. Generally they are composed of an organic solvent with a low

concentration (<2 wt%) of a small molecule gelator. Above the critical gelation concentration, they are self-assembled to form one-dimensional fiber-like supramolecules through non-covalent driving forces such as hydrogen bonding, π-π interaction, donor-acceptor interaction, solvophobic interaction, van der Waals interaction, metal coordination and so on. The fibrous strands are entangled physically to form a three-dimensional network and immobilize whole solvent molecules. The organic solvent is absorbed by surface tension and the resulitng substance becomes as a solid-like gel.[6] This type of gel is also called a physical gel or supramolecular gel (Figure I-2a). Cholresterol and fatty acid groups have been considerably incorporated in organogelators for self-assembly. Also the rigid aromatic rings are used to enhance intermolecular interactions by π-π interaction. Urea and amide bonds can induce multiple hydrogen bondings.

Polymer gels are also known, which are obtained chemically or physically. The chemical gels are constructed by cross-linking of the polymer chain through covalent bonding, which fixes the gel to be thermally irreversible. However, the physical gels are formed by non-covalent cross-linking, mainly hydrogen bonding, without losing thermo-reversibility (Figure I-2b). Various conformational changes of polymer promote the intra- and intermolecular interactions in the gels. Syndiotactic[7] or isotactic[8] polystyrene polymers show gelation properties. Syndiotatic poly(methyl methacrylate)[9] and poly(γ-benzyl-$_L$-

glutamate)[10] also gelate organic solvents. Furthermore, some copolymers are known to form organogels.[11,12]

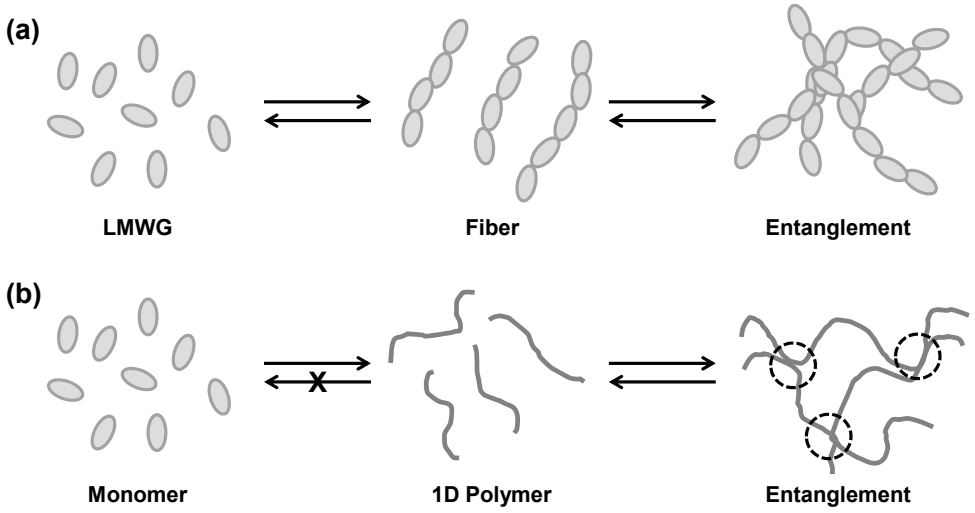

Figure I-2. Schematic descriptions of the gelation processes from (a) low molecular weight gelator and (b) conventional polymer. The dotted circles mean physical entanglements.

A number of luminescent organogels containing lanthanide(III) ions have been reported. Mostly, luminescent lanthanide(III) ions were incorporated in polymers having carboxylic acid functionality, for example, poly(acrylic acid) and photophysical properties were investigated.[13,14] Supramolecular polymer gels were fabricated based on the coordination bonds with lanthanide(III) ions. Lanthanide(III) ions have high coordination numbers ranging from 6 to 12,

facilitating cross-linking to fabricate the gel. Rowan groups explored the metallo-supramolecular polymer gels with tridentate ligand **1** (Figure I-3a).[15,16] The ligand could not only bind lanthanide(III) ions but also sensitize them. Besseling group also synthesized bifunctional ligands and induced chemical cross-linking by using lanthanide(III) ions (Figure I-3b).[17]

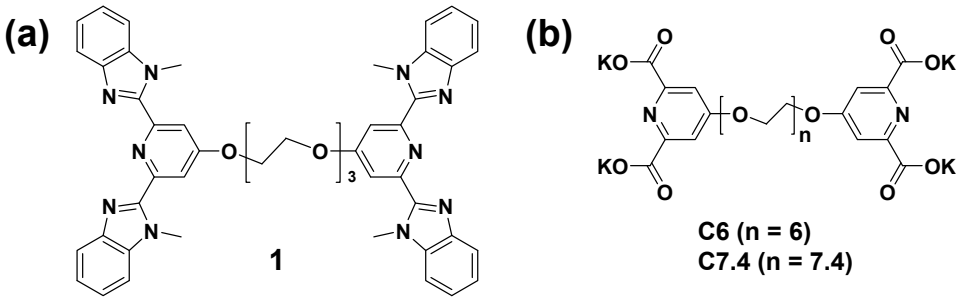

Figure I-3. Structures of bis(tridentate) ligands (a) **1** and (b) **C6** and **C7.4**.

Some physical gels were doped with lanthanide(III) ions or lanthanide(III) complexes. In Figure I-4, low molecular weight gelators of **1** and **2** could form the supramolecular gels doped with an europium complex, **3**.[18] In the gel state, luminescence was enhanced noticeably, suggesting the excited energy in the ligand migrated to an europium(III) ion efficiently.

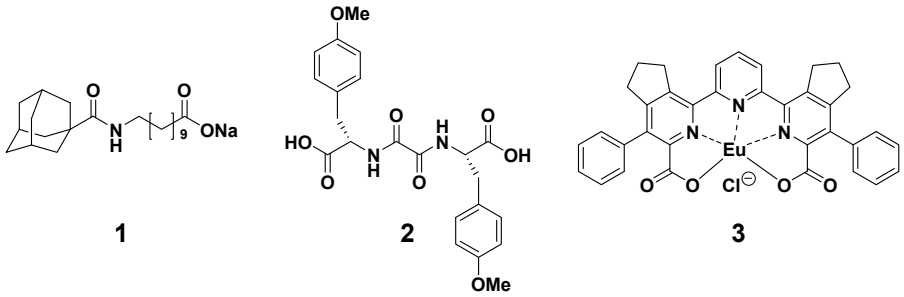

Figure I-4. Structures of low molecular weight gelators (**1** and **2**) and europium(III) complex (**3**).

Wang *et al.* incorporated dysprosium(III) ion in an ethanol gel formed by **1** (Figure I-5).[19] During the sol-gel transition by the temperature change, the metal-centered blue emission was switched on and off reversibly. Only in the gel state, the energy transfer occurred.

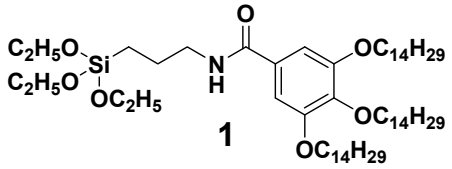

Figure I-5. Structure of **1**.

A low molecular weight organogelator with an europium(III) complex was also reported (Figure I-6). In this research, photophysical properties as NIR emission and two-photon absorption were studied.

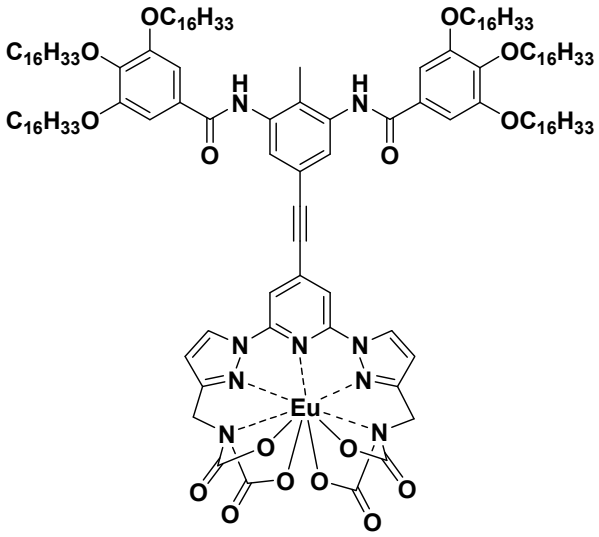

$(NH_4)[Eu\mathbf{L}_3]$

Figure I-6. Structure of lanthanide(III) ion-containing organogelator.

I-2. Molecular imprinting

I-2-1. Principle of Molecularly Imprinted Polymers

As enzyme-related catalysis was started to be elucidated,[20] the interest in the molecular recognition, binding process, control of chirality has been grown. Among the related studies, a molecular imprinting is a feasible strategy to synthesize an artificial receptor, mimicking the biological receptor. During the process of the molecular imprinting, tailored binding sites are formed in cross-linked polymeric matrices. Molecularly imprinted polymers abbreviated as MIPs have been investigated widely due to their application potentials in many fields including separation, sensing, enzyme-like catalysis, solid-phase extraction and so on.[21-24]

Compared to the biological receptors, MIPs have several advantages. The most advantageous feature is that MIPs can be prepared quite simply on a large scale. Because of the cross-linked structures, MIPs are stable physically and thermally and inert to external environments. Furthermore, they can be chemically modified with ease to control their binding properties. However, fundamentally, MIPs have drawbacks such as low sensitivity and selectivity.[25]

The MIPs are fabricated as follows. Firstly, template molecules are assembled with functional monomers via covalent or non-covalent bonds.

The resulting complexes are polymerized with suitable monomers and cross-linkers to form the polymer matrices. The template molecules in the polymer matrices are extracted to leave cavities. The cross-linking density influences the rigidity of the polymer matrices. When the polymers are rigid, it is beneficial to form shape-resistant cavities. However, it could be detrimental for the template removal and the binding site accessibility. Porogenic solvents can be used in the polymerization to improve the accessibility. All processes are shown in Figure I-7.

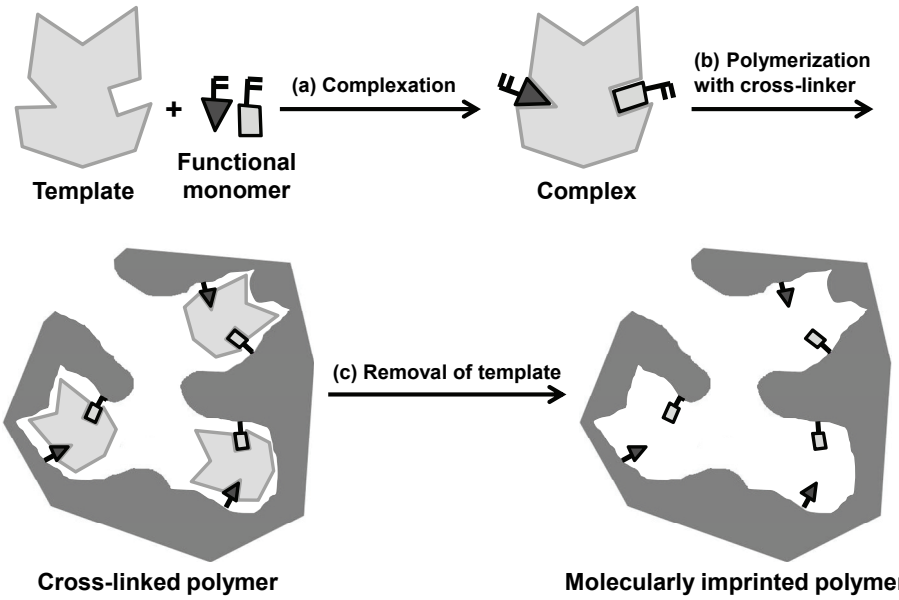

Figure I-7. Schematic description for preparation of molecularly imprinted polymer including three steps of (a) complexation, (b) cross-linking and (c) removal of template molecules.

For the complexation of a template with a functional monomer, covalent or non-covalent bondings can be used. The covalent approach was early suggested by Wulff and coworkers.[26] They used a boronate ester as a linkage (Figure I-8a). The complexes were also obtained by ketal and Schiff base formation (Figure I-8b and I-8c).[27,28] In the case of the covalent imprinting, template molecules are covalently attached to functional monomers. Because of this, the more homogeneous cavities are expected after removing the template molecules. However, it is difficult to find proper chemical bondings, which can be easily formed and cleaved.

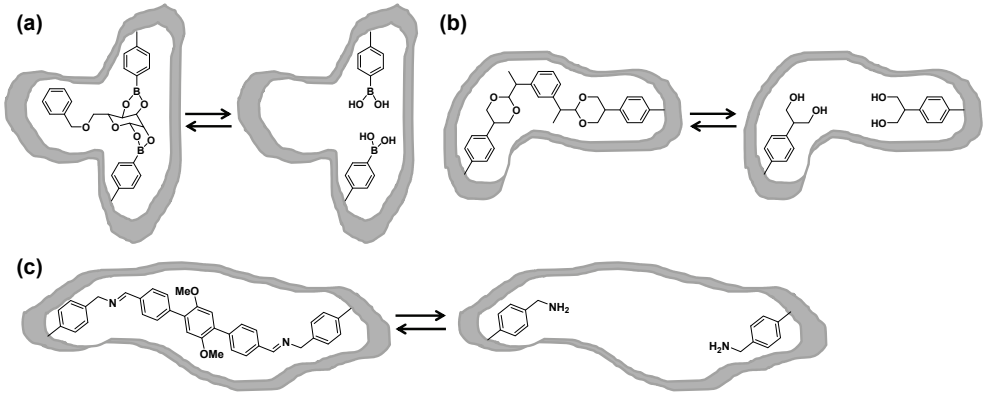

Figure I-8. Schematic descriptions for covalent imprinting based on (a) boronate ester, (b) ketal and (c) Schiff base.

On the other hand, the non-covalent approach uses various physical interactions e.g., hydrogen bonding, dipole-dipole interaction, ion paring, van der Waals interaction and hydrophobic interaction for the template-monomer complexation. Mosbach and coworkers intensively investigated this approach.[29,30] The complexes obtained from these interactions are not stable and can be easily broken under polymerization conditions. Excess of functional monomers are required to maintain the complex structure, bringing about the structural heterogeneity in binding sites. After cross-linking, the template molecules can be removed easily. Some functional groups can strongly interact with a specific template molecule. For example, amidine[31] and urea groups[32] could form stable complexes with a phosphonic monoester and a salt form of penicillin G respectively through multipoint hydrogen bonds (Figure I-9a and I-9b). Metal coordination between a Ni(II) ion and His-Ala is also utilized for imprinting the dipeptide (Figure I-9c).[33] In addition, post-treatment methods such as blocking free functional monomer[34] or tuning the size of imprinted sites[35] are known to improve the binding performance.

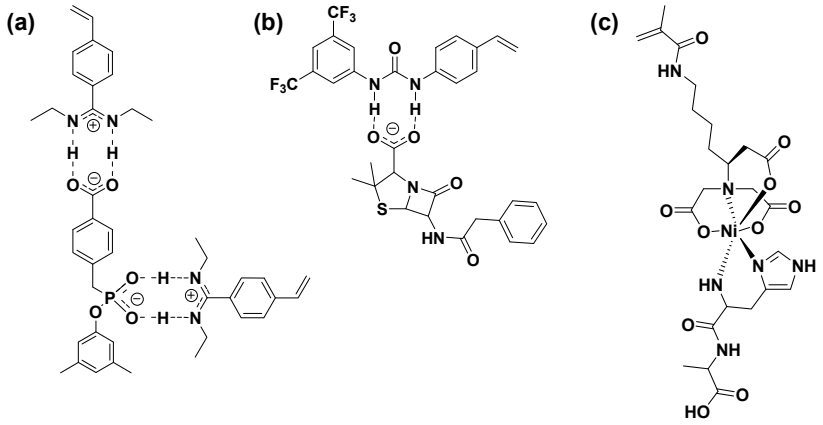

Figure I-9. Schematic descriptions for noncovalent complexes based on (a) amidine, (b) urea and (c) metal coordination.

A *sacrificial spacer* can be used in the formation of the template-monomer complex.[36] In this method, it is critical to use easily cleavable chemical bonds such as carbonate[37] or urea[38] bonds. The phenyl urethane bond is thermally reversible.[39] It is stable at room temperature, but cleaved to be isocyante and phenol groups on heating (Scheme 1-1). The resulting electrophilic isocyanate group can be easily converted to various functional groups by the reaction with nucleophiles. Several template molecules were complexed with functional monomers via thermally reversible urethane bonds. After polymerization, the templates were easily removed by simple heating. At the same time, the functionality in binding sites could be controlled by the reaction between the dissociated isocyanate groups and the added nucleophiles (Figure I-10).[40,41]

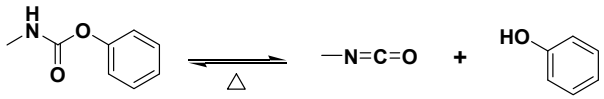

Scheme 1-1. Thermo-reversible urethane bond.

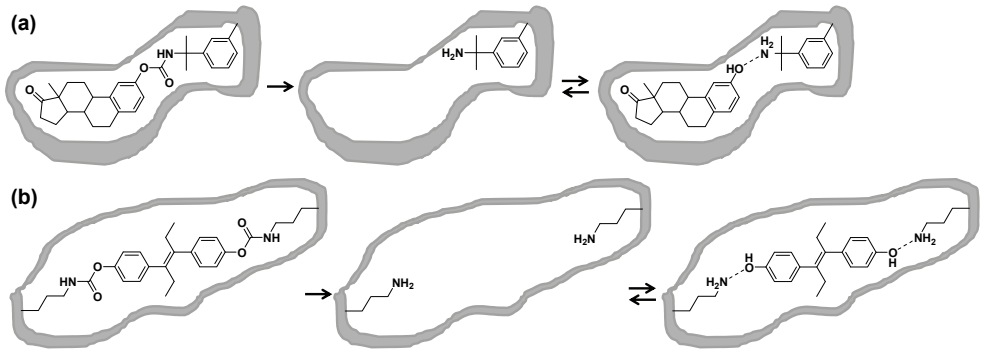

Figure 1-10. Schematic descriptions for urethane bond-assisted hybrid systems imprinted by (a) estrone and (b) diethylstilbestrol.

I-2-2. Application of Molecularly Imprinted Polymers for Luminescent Sensing

Conventionally, rebound template molecules are analyzed indirectly by liquid and gas chromatography and mass spectrometry, which involves tedious isolation and sample preparation steps. The direct detection of analytes with MIPs has been also developed using quartz crystal microbalance (QCM), surface plasmon resonance (SPR) and optical or electrical methods. Among them, the use of luminescence in sensing is practically useful because the

luminescence is quite sensitive to environment, lowering the limit of detection.

A variety of luminophore have been used for sensing the analytes bound to MIPs. Quantum dots (QDs) are very promising luminescent nanoparticles for detecting analytes, showing sharp emissions with high quantum yields.[42]

A molecularly imprinted matrix was fabricated with co-loading of magnetic nanoparticles and QDs (Figure I-11).[43] The Fe_3O_4 nanoparticles were used for easy separation of the MIP by applying an external magnetic field. The luminescence of Mn^{2+}-doped ZnS QDs incorporated in a pesticide pentachlorophenol (PCP) imprinted silica was quenched in the presence of PCP. The quenching was originated from the photo-induced charge transfer. The excited charges in the conduction bands of the QDs could be transferred to the LUMO level of the analytes. The quenching efficiency of PCP was the highest, indicating that PCP was bound to the imprinted matrix selectively compared to those of other structure analogs.

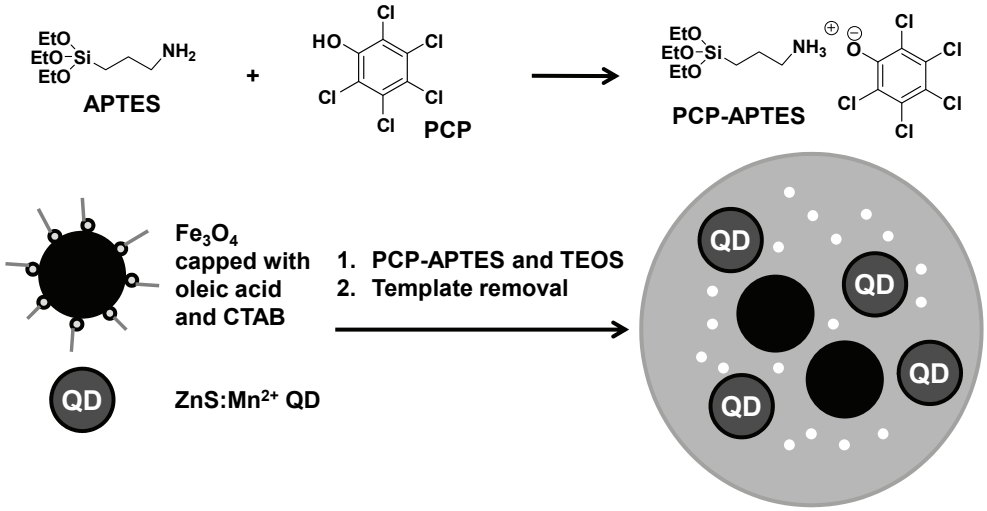

Figure I-11. Synthetic procedure of PCP-imprinted silica particles doped with magnetic particles and QDs.

The CDs@MIP for the detection of dopamine was prepared using highly luminescent carbon dots (CDs) functionalized with methyldimethoxy silane groups (Figure I-12). CDs as a signal transducer have some attractive attributes including tunable photoluminescence properties, biocompatibility and low cytotoxicity. CDs were synthesized by pyrolysis of anhydrous citric acid.[44] The luminescence of the CDs@MIP was quenched depending on the concentration of dopamine, demonstrating that the CDs@MIP could be served as a fluorescence sensor for dopamine.

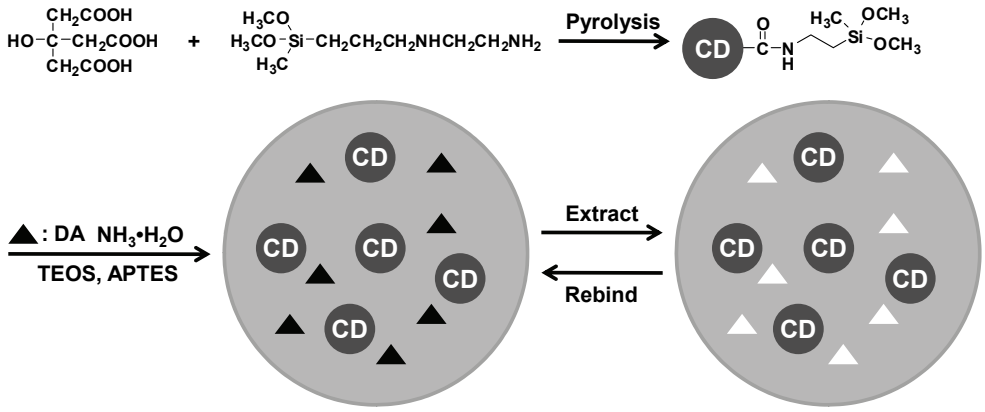

Figure I-12. Preparation of dopamine-imprinted silica particles doped with luminescent carbon dots.

Several organic fluorescent dyes were incorporated into binding sites of MIPs.[45-47] Rurack group introduced a fluorescent monomer from a nitrobenzoxadiazole fluorophore containing a urea group that turned on upon binding to the target analyte having the carboxylate unit into a MIP matrix (Figure I-13).[48] Core-shell silica microparticles with the MIP as a thin shell showed fast response to the template molecules.

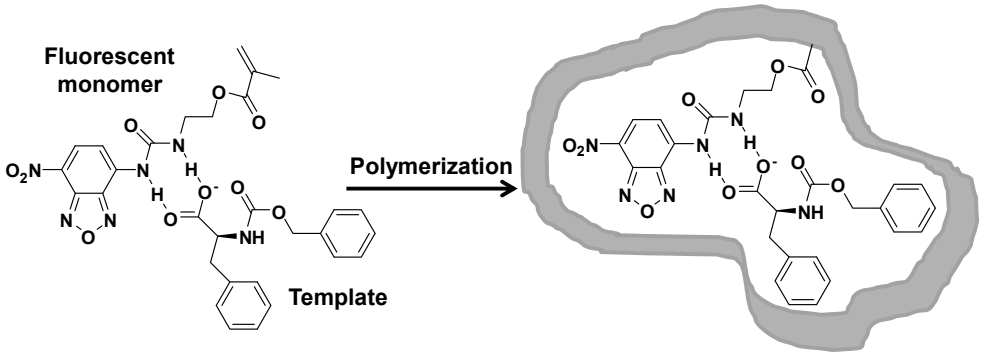

Figure I-13. Schematic route for a turn-on fluorescence sensor based on MIP.

The lanthanide ions with unique photophysical properties have also been used in luminescent sensing. Liu *et al.* reported the Eu(III) complex-based MIP sensor for optosensing of λ-cyhalothrin (LC).[49] Mesoporous silica particles were covalently tethered with a red luminescent Eu(III) complex, $Eu(TTA)_3Bpc$ (TTA, 2-thenoyltrifluoroacetone; Bpc, 2,2'-bipyridine-4,4'-dicarboxylic acid) (Figure I-14). These particles ($mSiO_2$-$Eu(TTA)_3Bpc$) were used as stabilizers for Pickering emulsion polymerization of the template-monomer complex. The characteristic emission of Eu(III) complex centered at around 615 nm was gradually quenched with the increasing concentrations of LC.

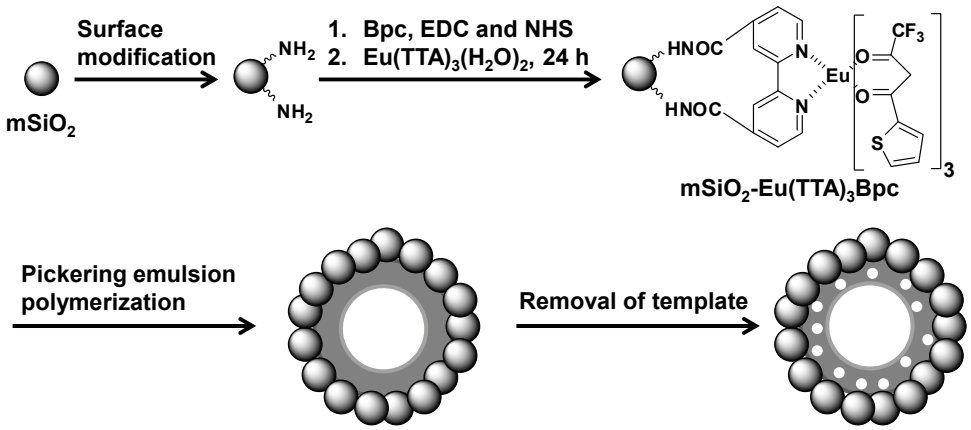

Figure I-14. Synthetic strategy of europium(III)-containing MIP by Pickering emulsion polymerization.

I-3. Microporous Organic Polymers

I-3-1. Principle of Microporous Organic Polymers

As zeolite, discovered in 1756, and activated carbon were broadly explored in adsorption applications, porous materials have attracted a great deal of attention. According to the pore diameter, pores are classified as micropore (<2 nm), mesopore (2-50 nm) and macropore (>50 nm) following the IUPAC definition. Among them, microporous materials have been widely used due to their high surface areas in various fields such as gas storage, fluid absorption, separation, catalysis, sensing and so on.[50]

There are many types of microporous materials. Metal-organic frameworks (MOFs) have been intensively researched so far.[51,52] Generally, MOFs have crystalline structures and high surface areas (Figure I-15a).[53] However, most of MOFs are structurally fragile and it is still challenging to fabricate durable MOFs with maintaining their unique porosities. Covalent organic frameworks (COFs) are also crystalline materials, composed of organic elements. Most of COFs were constructed via B-O bonds showing reversibility to induce crystalline structures similar in the metal coordination (Figure I-15b).[54] However, the fabrication of COFs is still complicated and the surface areas are insufficient compared to MOFs. Polymers of intrinsic microporosity (PIMs)

were firstly developed by Mckeown group.[55] PIMs are not cross-linked polymers, but show the intrinsic porosity generated by the contorted structures in the solid state. Some PIMs have a good processability, but relatively low surface areas than cross-linked porous polymers (Figure I-15c).

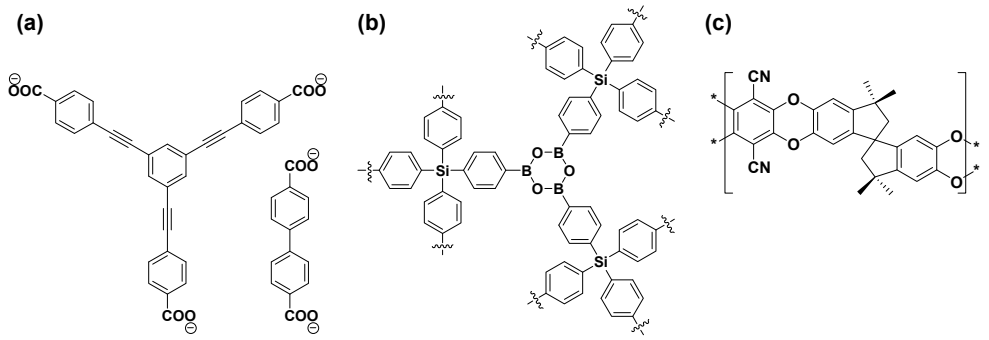

Figure I-15. Structures of (a) ligands in MOF-210, (b) COF-103 and (c) PIM-1.

Recently, cross-linked microporous organic polymers (MOPs) have been widely investigated as a promising class of porous materials showing high surface areas and physicochemical stability. A variety of organic building blocks and synthetic methodologies to link them are available, which has drawn more attention to MOPs in recent years, compared to traditional porous materials. A vast majority of MOPs have been prepared in forms of highly cross-linked networks by transition metal-mediated coupling reactions.

Suzuki coupling reaction was used for synthesizing PAF-11 and PP-CMP. PAF-11 showed high adsorption performance for small molecules such as methanol, benzene and toluene with a surface area of 952 m^2 g^{-1} calculated by the Langmuir model (Figure I-16a).[56] PP-CMP having a conjugated structure was found to harvest light with a BET surface area of 1,083 m^2 g^{-1} (Figure I-16b).[57]

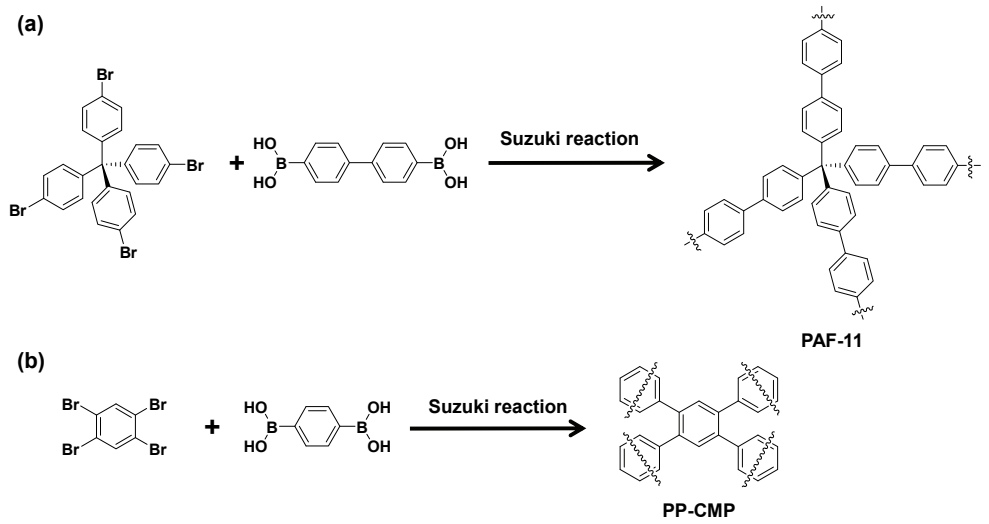

Figure I-16. Synthetic descriptions of microporous organic polymers by Suzuki reaction.

Another palladium-mediated coupling reaction, Sonogashira-Hagihara reaction is also used for preparing porous frameworks such as adamantane-based porous polymers (Figure I-17a).[58] Cooper group synthesized a series of conjugated microporous polymers having different functional groups by Sonogashira-Hagihara reaction. They researched the effect of functionalities on gas adsorption property of the polymers (Figure I-17b).[59]

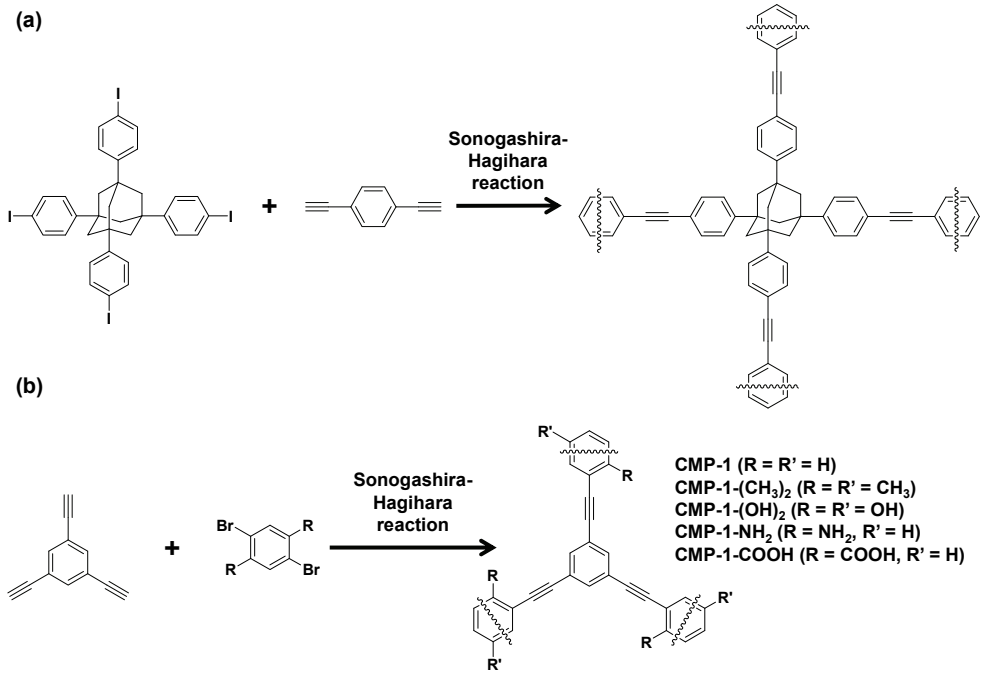

Figure I-17. Synthetic descriptions of microporous organic polymers by Sonogashira-Hagihara reaction.

Ullmann reaction has been used in the synthesis of a porous polymers from a macrocycle as a monomer[60] and a boroxine ring[61] (Figure I-18).

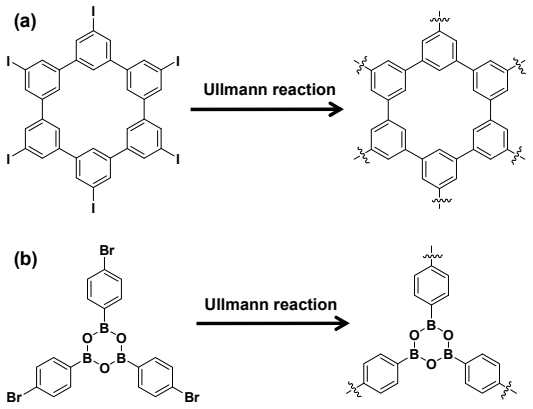

Figure I-18. Synthetic descriptions of microporous organic polymers by Ullmann reaction.

Yamamoto reaction has been particularly successful in coupling phenyl rings to produce porous aromatic frameworks with extremely high surface areas.[62,63] PAF-1 and PPN-4 showed the significantly high BET surface areas of 5,600 and 6,461 $m^2 g^{-1}$ respectively (Figure I-19).

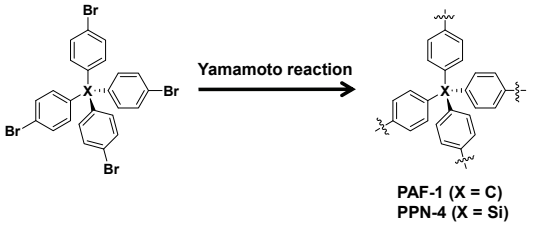

Figure I-19. Synthetic descriptions of microporous organic polymers by Yamamoto reaction.

There has been continuous interest in metal catalyst-free reactions for the mass production of MOPs that can alleviate environmental and economic concerns. Transition metal-mediated coupling reactions have often suffered from problems such as difficulty in the purification of the products, high cost of the catalysts and complicated reaction pathways.[64] One of the most familiar metal catalyst-free reactions for polymer synthesis is a condensation reaction where the elements of water are eliminated. A number of highly cross-linked MOPs have been prepared by the condensation of multiamino-functionalized monomers with aldehydes, carboxylic acids, and anhydrides. The reaction between amino and aldehyde functional groups preferably formed aminal linkages through pre-formed imine linkages (Figure I-20a).[65] From *o*-benzenedianmine and aldehyde monomer, a benzimidazole-linkage was obtained (Figure I-20b).[66] Porous aromatic poly(amide) and poly(imide) networks have been synthesized by the reaction of a multiamine with an aromatic diacid and an aromatic dianhydride, respectively (Figure I-21).[67,68]

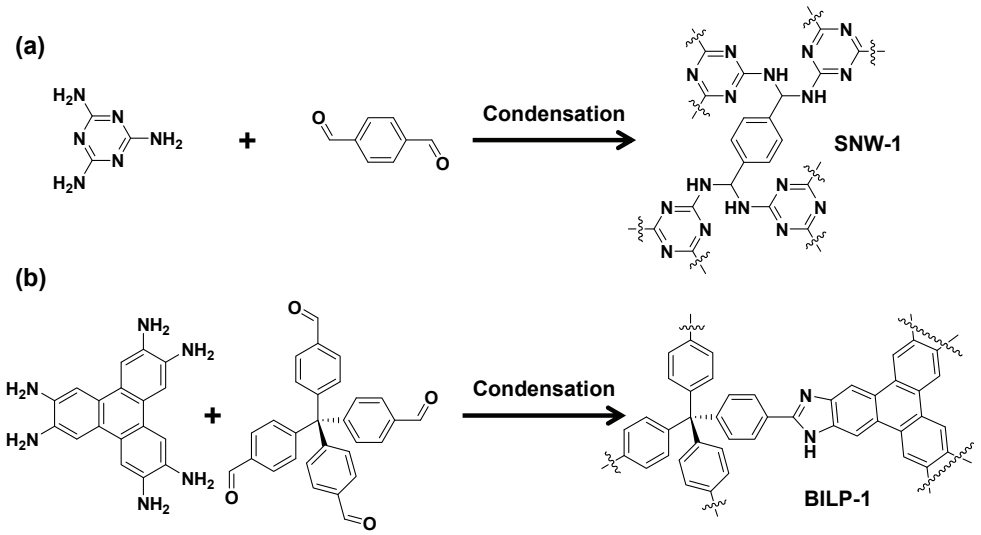

Figure I-20. Synthetic descriptions of microporous organic polymers having (a) aminal and (b) benzimidazole linkages.

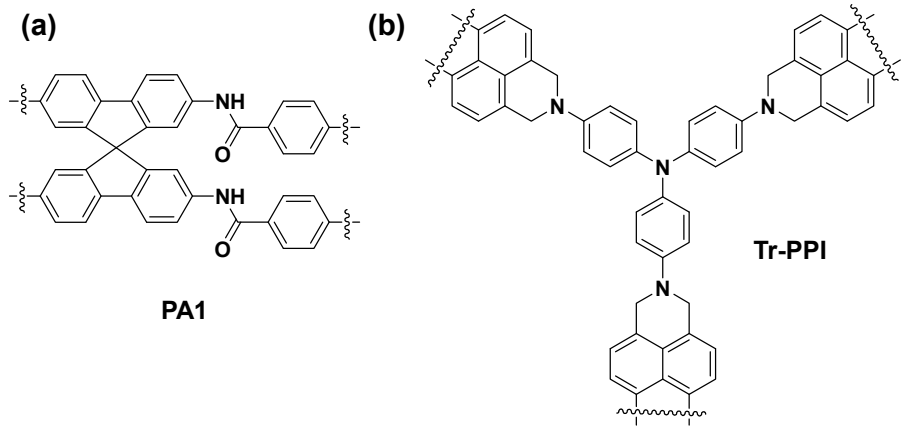

Figure I-21. Structures of microporous organic polymers having (a) amide and (b) imide linkages.

Aldol self-condensation of multiacetyl-containing aromatic compounds was also reported to produce MOPs consisting of α,β-unsaturated ketone and 1,3,5-trisubstituted benzene units formed by dimerization and cyclotrimerization, respectively (Figure I-22a).[69] Among other metal catalyst-free reactions used for the synthesis of MOPs, an electrophilic aromatic substitution reaction of 1,3,5-trihydroxybenzene with a benzaldehyde derivative (Figure I-22b)[70] and a nucleophilic substitution reaction of hexachlorocyclotriphosphazene with a multiamino-functionalized compound are notable (Figure I-22c).[71]

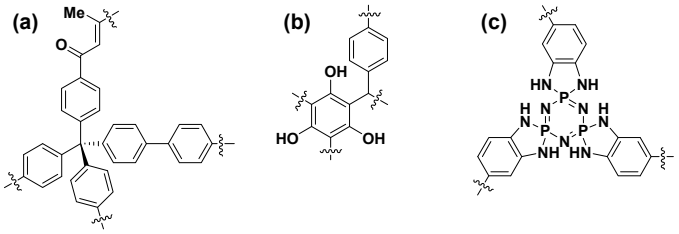

Figure I-22. Structures of microporous organic polymers synthesized by (a) aldol reaction (b) electrophilic aromatic substitution and (c) nucleophilic substitution.

I-3-2. Metal-Doped Porous Polymers

Recently, many efforts to enhance gas adsorption properties of porous materials were reported. As metal-doping strategy was found to be effective for enhancing gas adsorption properties of porous materials theoretically and

experimentally,[72,73] diverse metal ions have been doped in various types of frameworks including MOFs and porous organic polymers. With this strategy, the polymers showed improved features not only in gas adsorption but also in catalysis, electrical properties and photophysical properties.

Lithium ion has been doped for increasing hydrogen uptake. Theoretical calculations showed that lithium ion had the strong interaction with hydrogen by forming the dative bond between electrons in σ-bond of H_2 and empty 2s orbital of Li.[74,75] Also, methane and CO_2 gases were simulated to be captured efficiently through electrostatic interactions with cationic lithium ions doped in COFs as well as MOFs.[76,77] Li *et al.* reported that the Li-doped conjugated microporous polymer and attained the high H_2 storage capability of 6.1 wt% at 77 K.[78] Lately, Zhu group synthesized a microporous organic polymer, PAF-18-OH having hydroxyl groups. After lithiation of OH groups in PAF-18-OH, CO_2 and H_2 uptakes significantly increased by quadrupolar interaction even though the BET surface area decreased from 1121 to 981 m^2 g^{-1} (Figure I-23).[79]

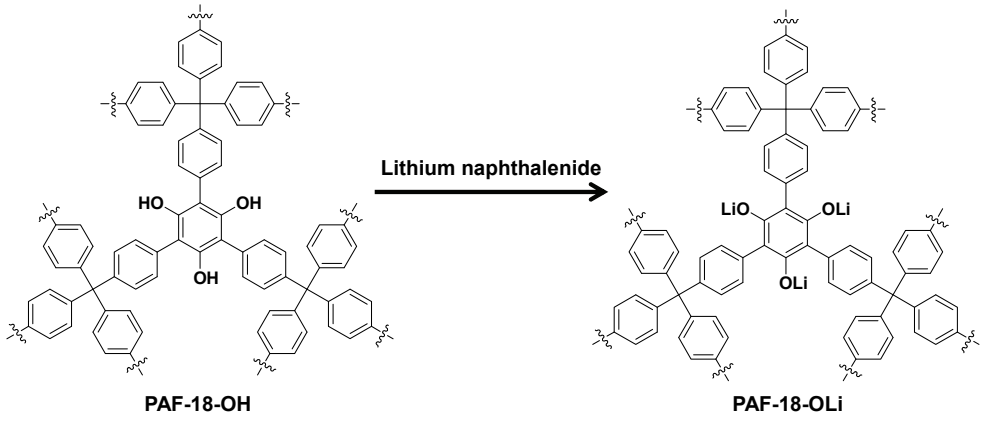

Figure I-23. Schematic description for lithiation of microporous organic polymer (PAF-18-OH).

Transition metals such as rhenium, rhodium and iridium were incorporated in conjugated microporous polymers by Cooper group.[80] The metal ions were introduced by post coordination (Figure I-24a) or by the metal complex polymerization (Figure I-24b). Through two strategies, the porous framework was metalated without the hindrance of π-conjugation. The iridium-containing conjugated polymer, CMP-CpIr-3 was successfully applied in catalysis of reductive amination.

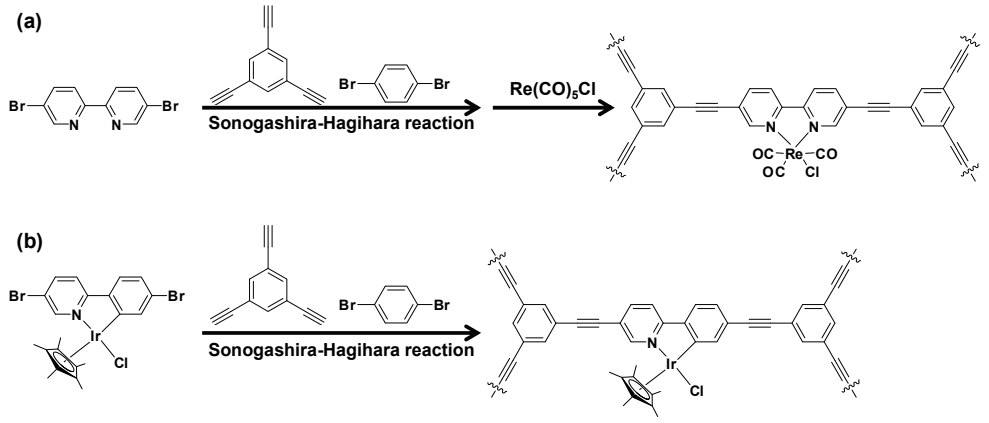

Figure I-24. Schematic descriptions for conjugated microporous polymers metalated by (a) post modification or (b) copolymerization methods.

Porous materials containing lanthanide(III) ions have been also studied. Lanthanide(III) ions were incorporated in MOFs by coordination with carboxylate groups of organic linkers (Figure I-25). Lanthanide(III) ions are d-block metal ions and having flexible high coordination numbers. They can be coordinated with labile ancillary ligands such as water molecules and the open metal site is formed when these ligands are removed. The exposed metal site induces the increase of gas adsorption by dipolar and/or quadrupolar interaction and potential catalytic activity. In addition, lanthanide(III) ions can improve the frameworks with their own luminescent or electrical properties.

To name a few, 1,4-phenyldiacetic acid (Figure I-25a) was reacted with Er(III) ions and the resulting isostructural framework, $Er_2(PDA)_3$ showed high

stability and selective gas adsorption for CO_2 over Ar or N_2 because of size selectivity and host-guest interaction obtained from well-defined porosity.[81] Lee *et al.* prepared lanthanide-organic frameworks by using a phosphine oxide-based tricarboxylate (Figure I-25b) for coordinating Nd(III), Sm(III), Eu(III) and Gd(III) ions, which exhibited enhanced surface areas and gas adsorptions. The resulting optical and magnetic properties of the frameworks were also investigated.[82] The trigonal ligand, 1,3,5-benzenetrisbenzoic acid (Figure I-25c) and various lanthanide(III) ions were used in the preparation of lanthanide-coordinated frameworks by Zou and coworkers. They reported that the effect of the metal ions on gas and vapor adsorptions.[83]

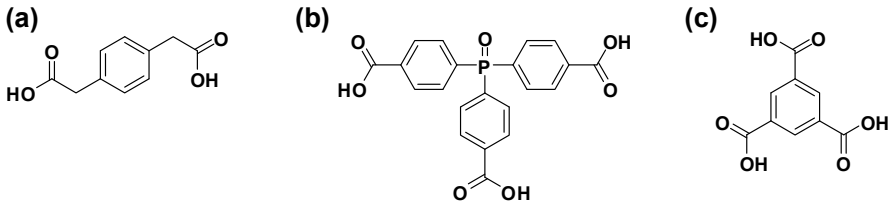

Figure I-25. Structures for ligands in lanthanide-organic frameworks.

I-4. References

1. Weissman, S. I. *J. Chem. Phys.* **1942**, *10*, 214-217.
2. Bünzli, J.-C. G. *Acc. Chem. Res.* **2006**, *39*, 53-61.
3. Binnemans, K. *Chem. Rev.* **2009**, *109*, 4283-4374.
4. Bünzli, J.-C. G.; Piguet, C. *Chem. Soc. Rev.*, **2005**, *34*, 1048-1077.
5. Eliseevaa, S. V.; Bünzli, J.-C. G. *Chem. Soc. Rev.*, **2010**, *39*, 189-227.
6. Flory, P. *J. Discuss Faraday Soc*. **1974**, *57*, 7-18.
7. Kobayashi, M.; Nakaoki, T.; Ishihara, N. *Macromolecules*, **1990**, *23*, 78-83.
8. Girolamo, M.; Keller, A.; Miyasaka. K.; Overbergh, N. *J. Polym. Sci., Polym. Phys. Ed.* **1976**, *14*, 39-61.
9. Saiani, A; Guenet, J.-M. *Macromolecules* **1997**, *30*, 966-972.
10. Korenaga, T.; Oikawa, H.; Nakanishi, H. *J. Macromol. Sci., Part B: Phys.* **1997**, *36*, 487-501.
11. Kim, K. T.; Park, C.; Vandermeulen, G. W. M.; Rider, D. A.; Kim, C.; Winnik, M. A.; Manners, I. *Angew. Chem., Int. Ed.* **2005**, *44*, 7964-7968.
12. Da, J.; Hogen-Esch, T. E. *Macromolecules* **2003**, *36*, 9559-9563.

13. Lis, S.; Wang, Z. M.; Choppin, G. R. *Inorg. Chim. Acta* **1995**, *239*, 139-143.

14. Smirnov, V. A.; Philippova, O. E.; Sukhadolski, G. A.; Khokhlov, A. R. *Macromolecules* **1998**, *31*, 1162-1167.

15. Beck, J. B.; Rowan, S. J. *J. Am. Chem. Soc.* **2003**, *125*, 13922-13923.

16. Weng, W.; Beck, J. B.; Jamieson, A. M.; Rowan, S. J. *J. Am. Chem. Soc.* **2006**, *128*, 11663-11672.

17. Vermonden, T.; van Steenbergen, M. J.; Besseling, N. A. M.; Marcelis, A. T. M.; Hennink, W. E.; Sudhölter, E. J. R.; Cohen Stuart, M. A. *J. Am. Chem. Soc.* **2004**, *126*, 15802-15808.

18. De Paoli, G.; Džolic, Z.; Rizzo, F.; De Cola, L.; Vögtle, F.; Müller, W. M.; Richardt, G.; Žinic, M. *Adv. Funct. Mater.* **2007**, *17*, 821-828.

19. Wang, Q. M.; Ogawa, K.; Toma, K.; Tamiaka, H. *Chem. Lett.* **2008**, *37*, 430-431.

20. Pauling, L. *J. Am. Chem. Soc.* **1940**, *62*, 2643-2657.

21. Wulff, G. *Chem. Rev.* **2002**, *102*, 1-27.

22. Haupt, K.; Mosbach, K. *Chem. Rev.* **2000**, *100*, 2495-2504.

23. Chen, L. X.; Xu, S. F.; Li, J. H. *Chem. Soc. Rev.* **2011**, *40*, 2922-2942.

24. Whitcombe, M. J.; Chianella, I.; Larcombe, L.; Piletsky, S. A.; Noble, J.; Porter, R.; Horgan, A. *Chem. Soc. Rev.* **2011**, *40*, 1547-1571.

25. Ye, L.; Mosbach, K. *Chem. Mater.* **2008**, *20*, 859-868.

26. Wulff, G.; Vesper, R.; Grobe-Einsler, R.; Sarhan, A. *Makromol. Chem.* **1977**, *178*, 2799-2816.

27. Wulff, G.; Heide, B.; Helfmeier, G. *J. Am. Chem. Soc.* **1986**, *108*, 1089-1091.

28. Shea, K. J.; Dougherty, T. K. *J. Am. Chem. Soc.* **1986**, *108*, 1091-1093.

29. Mosbach, K. *Trends Biochem. Sci.* **1994**, *19*, 9-14.

30. Haupt, K.; Mosbach, K. *Trends Biotechnol.* **1998**, *16*, 468-475.

31. Wulff, G.; Schönfeld, R. *Adv. Mater.* **1998**, *10*, 957-959.

32. Urraca, J. L.; Hall, A. J.; Moreno-Bondi, M. C.; Sellergren, B. *Angew. Chem., Int. Ed.* **2006**, *45*, 5158-5161.

33. Hart, B. R.; Shea, K. J. *J. Am. Chem. Soc.* **2001**, *123*, 2072-2073.

34. McNiven, S.; Yokobayashi, Y.; Cheong, S. H.; Karube, I. *Chem. Lett.* **1997**, 1297-1298.

35. Kirsch, N.; Alexander, C.; Lübke, M.; Whitcombe, M. J.; Vulfson, E. N. *Polymer* **2000**, *41*, 5583-5590.

36. Whitcombe, M. J.; Vulfson, E. N. *Adv. Mater.* **2001**, *13*, 467-478.

37. Whitcombe, M. J.; Rodriguez, M. E.; Villar, P.; Vulfson, E. N. *J. Am. Chem. Soc.* **1995**, *117*, 7105-7111.

38. Lübke, M.; Whitcombe, M. J.; Vulfson, E. N. *J. Am. Chem. Soc.* **1998**, *120*, 13342-13348.

39. Ki, C. D.; Oh, C.; Oh, S.-G.; Chang, J. Y. *J. Am. Chem. Soc.* **2002**, *124*, 14838-14839.

40. Ki, C. D.; Chang, J. Y. *Macromolecules* **2006**, *39*, 3415-3419.

41. Jung, B. M.; Kim, M. S.; Kim, W. J.; Chang, J. Y. *Chem. Commun.* **2010**, 46, 3699-3701.

42. Clapp, A. R.; Medintz, I. L.; Uyeda, H. T.; Fisher, B. R.; Goldman, E. R.; Bawendi, M. G.; Mattoussi, H. *J. Am. Chem. Soc.* **2005**, *127*, 18212-18221.

43. Yang, M.; Han, A.; Duan, J.; Li, Z.; Lai, Y.; Zhan, J. *J. Hazard. Mater.* **2012**, *237-238*, 63-70.

44. Pan, D.; Zhang, J.; Li, Z.; Wu, M. *Adv. Mater.* **2010**, *22*, 734-738.

45. Sánchez-Barragán, I.; Costa-Fernández, J. M.; Pereiro, R.; Sanz-Medel, A. *Anal. Chem.* **2005**, *77*, 7005-7011.

46. Stringer, R. C.; Gangopadhyay, S.; Grant, S. A. *Anal. Chem.* **2010**, *82*, 4015-4019.

47. Xu, Z.; Kuang, D.; Zhang, F.; Tang, S.; Deng, P.; Li, J. *J. Mater. Chem. B* **2013**, *1*, 1852-1859.

48. Wan, W.; Biyikal, M.; Wagner, R.; Sellergren, B.; Rurack, K. *Angew. Chem. Int. Ed.* **2013**, *52*, 7023-7027.

49. Liu, C.; Song, Z.; Pan, J.; Wei, X.; Gao, L.; Yan, Y.; Li, L.; Wang, J.; Chen, R.; Dai, J.; Yu, P. *J. Phys. Chem. C* **2013**, *117*, 10445-10453.

50. Holst, J. R.; Cooper, A. I. *Adv. Mater.* **2010**, *22*, 5212-5216.

51. Rowsell, J. L. C.; Yaghi, O. M. *Angew. Chem. Int. Ed.* **2005**, *44*, 4670-4679

52. Dawson, R.; Cooper, A. I.; Adams, D. J. *Prog. Polym. Sci.* **2012**, *37*, 530-563.

53. Furukawa, H.; Ko, N.; Go, Y. B.; Aratani, N.; Choi, S. B.; Choi, E.; Yazaydin, A. O.; Snurr, R. Q.; O'Keeffe, M.; Kim, J.; Yaghi, O. M. *Science* **2010**, *329*, 424-428.

54. Côtè, A. P.; Benin, A. I.; Ockwig, N. W.; O'Keeffe, M.; Matzger, A. J.; Yaghi, O. M. *Science* **2005**, *310*, 1166-1170.

55. McKeown, N. B.; Budd, P. M.; *Macromolecules* **2010**, *43*, 5163-5176.

56. Yuan, Y.; Sun, F.; Ren, H.; Jing, X.; Wang, W.; Ma, H.; Zhao, H.; Zhu, G. *J. Mater. Chem.* **2011**, *21*, 13498-13502.

57. Chen, L.; Honsho, Y.; Seki, S.; Jiang, D. *J. Am. Chem. Soc.* **2010**, *132*, 6742-6748.

58. Lim, H.; Chang, J. Y. *Macromolecules* **2010**, *43*, 6943-6945.

59. Dawson, R.; Adams, D. J.; Cooper, A. I. *Chem. Sci.* **2011**, *2*, 1173-1177.

60. Bieri, M.; Treier, M.; Cai, J.; Aït-Mansour, K.; Ruffieux, P.; Gröning, O.; Gröning, P.; Kastler, M.; Rieger, R.; Feng, X.; Müllen, K.; Fasel, R. *Chem. Commun.* **2009**, 6919-6921.

61. Faury, T.; Clair, S.; Abel, M.; Dumur, F.; Gigmes, D.; Porte, L. *J. Phys. Chem. C* **2012**, *116*, 4819-4823.

62. Ben, T.; Ren, H.; Ma, S.; Cao, D.; Lan, J.; Jing, X.; Wang, W.; Xu, J.; Deng, F.; Simmons, J. M.; Qiu, S.; Zhu, G. *Angew. Chem. Int. Ed. Engl.***2009**, *48*, 9457-9460.

63. Yuan, D.; Lu, W.; Zhao, D.; Zhou, H.-C. *Adv. Mater.* **2011**, *23*, 3723-3725.

64. Liu, J.; Lei, M.; Hu, L. *Green Chem.* **2012**, *14*, 2534-2539.

65. Schwab, M. G.; Fassbender, B.; Spiess, H. W.; Thomas, A.; Feng, X.; Müllen, K. *J. Am. Chem. Soc.* **2009**, *131*, 7216-7217.

66. Rabbani, M. G.; El-Kaderi, H. M. *Chem. Mater.* **2011**, *23*, 1650-1653.

67. Weber, J.; Antonietti, M.; Thomas, A. *Macromolecules* **2008**, *41*, 2880-2885.

68. Rao, K. V.; Haldar, R.; Kulkarni, C.; Maji, T. K.; George, S. J. *Chem. Mater.* **2012**, *24*, 969-971.

69. Zhao, Y.-C.; Zhou, D.; Chen, Q.; Zhang, X.-J.; Bian, N.; Qi, A.-D.; Han, B.-H. *Macromolecules* **2011**, *44*, 6382-6388.

70. Katsoulidis, P.; Kanatzidis, M. G. *Chem. Mater.* **2011**, *23*, 1818-1824.

71. Mohanty, P.; Kull, L. D.; Landskron, K. *Nat. Commun.* **2011**, *2*, 401.

72. Getman, R. B.; Miller, J. H.; Wang, K.; Snurr, R. Q. *J. Phys. Chem. C* **2011**, *115*, 2066-2075.

73. Li, J.-R.; Ma, Y.; McCarthy, M. C.; Sculley, J.; Yu, J.; Jeong, H.-K.; Balbuena, P. B.; Zhou, H.-C. *Coord. Chem. Rev.* **2011**, *255*, 1791-1823.

74. Han, S. S.; Goddard, W. A., III. *J. Am. Chem. Soc.* **2007**, *129*, 8422-8423.

75. Cao, D.; Lan, J.; Wang, W.; Smit, B. *Angew. Chem. Int. Ed.* **2009**, *48*, 4730-4733.

76. Lan, J.; Cao, D.; Wang, W. *Langmuir* **2010**, *26*, 220-226.

77. Lan, J.; Cao, D.; Wang, W.; Smit, B. *ACS Nano* **2010**, *4*, 4225-4237.

78. Li, A.; Lu, R. F.; Wang, Y.; Wang, X.; Han, K. L.; Deng, W. Q. *Angew. Chem., Int. Ed.* **2010**, *49*, 3330-3333.

79. Ma, H.; Ren, H.; Zou, X.; Sun, F.; Yan, Z.; Cai, K.; Wang, D.; Zhu, G. *J. Mater. Chem. A* **2013**, *1*, 752-758.

80. Jiang, J.-X.; Wang, C.; Laybourn, A.; Hasell, T.; Clowes, R.; Khimyak, Y. Z.; Xiao, J.; Higgins, S. J.; Adams, D. J.; Cooper, A. I. *Angew. Chem., Int. Ed.* **2011**, *50*, 1072-1075.

81. Pan, L.; Adams, K. M.; Hernandez, H. E.; Wang, X.; Zheng, C.; Hattori, Y.; Kaneko, K. *J. Am. Chem. Soc.* **2003**, *125*, 3062-3067.

82. W. R. Lee, D. W. Ryu, J. W. Lee, J. H. Yoon, E. K. Koh, C. S. Hong, *Inorg. Chem.* **2010**, *49*, 4723-4725.

83. Lin, Z.; Zou, R.; Xia, W.; Chen, L.; Wang, X.; Liao, F.; Wang, Y.; Lin, J.; Burrell, A. K. *J. Mater. Chem.* **2012**, *22*, 21076-21084.

Chapter II.

Synthesis and Characterization of Organogelators Having Lanthanide(III) Ions and Their Gelation and Luminescent Properties

II-1. Introduction

The lanthanide(III) ions have great potential in display and sensor applications due to their unique narrow luminescence and long lifetime as a result of the intraconfigurational f-f transitions inside the 4f shell. Particularly lanthanide(III)-based organic light-emitting displays (OLEDs) have attracted a lot of attention due to their potential for very high internal quantum efficiency, exceeding the theoretical limit of 25 % for the OLEDs with purely organic molecules.[1] In practical applications, the lanthanide(III) ions are used after complexation with organic compounds because of the difficulty in populating their resonance levels by direct excitation.[2] Lanthanide(III) ion-containing complexes have the organic ligands around the metal ions in proximity as an antenna. Excited species are generated optically or electrically in the organic ligands and, in turn, the excited

ligands light on the lanthanide(III) ions by intramolecular energy transfer. By using this sensitization, the characteristic luminescence from lanthanide(III) ions can be obtained efficiently.

In recent years, a white-light emission has been extensively studied because of its potential applications in lighting and display devices.[3-5] Basically white light is produced by tuning blue, green and red emissions, which are often obtained from Ir(III), Tb(III) and Eu(III) ions doped in an suitable host[6-8] or coordinated with organic ligands.[9-12] A variety of combinations have been proposed for achieving white luminescence. Dinuclear Ir(III)/Eu(III) complexes were reported to produce an almost white-light emission via partial energy transfer from the excited Ir(III) moiety to the Eu(III) complex.[13] In a different approach, white-light with a very broad emission was observed from a mononuclear Ir(III) complex with acetylacetonato and 1-methyl-2-phenylimidazole ligands.[14]

Several research groups used organic chromophoric ligands as blue and green emitting sources. Guo *et al.* obtained white light by tuning blue, green and red emissions from a Eu(III) complex with organic ligands that contained blue- and green-emitting fluorophores.[15] Law *et al.* reported a Eu(III) complex containing a double emission center of bluish-green (ligand) and red f-f emissions [Eu(III)] that produced pure white-light.[16] Xu *et al.* reported that a Al_3Eu_2 heteropentanuclear complex with incomplete energy transfer from the ligand to

the lanthanide center displayed a bright white-light emission.[17] Shelton *et al.* recently utilized the solvent-dependent aggregation behavior of a Eu(III) complex for color tuning to produce white light.[18]

Lanthanide(III) complexes are also processed into a thin film by several methods for device fabrication, of which high-vacuum thermal evaporation is a widely used technique. Alternatively, the complexes are dispersed in inorganic or organic films because many of them have poor film forming ability. The difficulty in this technique is achieving a high concentration of the lanthanide(III) ions in the matrix while preventing cluster formation. Several studies used a dendron as an organic ligand. The dendron having a coordination site as a focal point was complexed with a lanthanide(III) ion to form a lanthanide-cored dendrimer.[19] A polyamidoamine-type dendrimer having multiple amide groups capable of coordination with lanthanide(III) ions was also reported in an attempt to increase the lanthanide(III) concentration.[20] These dendrimer systems showed good processibility, but suffered from the poor efficiency of the antenna groups. To enhance the energy absorption, strong chromophores were introduced into the dendrimer. However they were located only at the periphery of the dendrimer, remaining distant from the lanthanide ion.[20,21]

Furthermore, NIR emissions of lanthanide(III) ions have attracted a great interest in optical amplification as the more information is carried by the light

signal. Even Nd(III), Er(III) and Yb(III) are mainly used in NIR emission application, Er(III) is most widely investigated in telecommunication as doped in silica fibers because emission wavelength of Er(III) at 1.54 μm satisfactorily matches with transparent silica window.[22-25] However, it suffers from several limits such as low molar absorption coefficient of Er(III) ion, heterogeneous dispersion in silica matrix due to low solubility and so on. There have been some efforts to overcome the shortages through coordination of Er(III) with organic ligands such as small molecules[26-31] and polymers[32-34] or incubation of Er(III) in zeolite with organic dyes.[35-38]

In this work, Eu(III) and Tb(III) complexes were prepared with phenanthroline derivatives which gelated *n*-decane. Since Eu(III) and Tb(III) complexes had the same structures except the metal ions, they formed stable mixed gels of different compositions that emitted red and green light from Eu(III) and Tb(III) ions, respectively. Furthermore, The color of emission was able to be tuned by controlling gel compositions and white light was finally obtained by combining emissions of Eu(III) and Tb(III) with those of their ligands. Also, a trimetallic disc-like Eu(III) organogelator mainly comprised of a 1,3,5-benzenetrisacetoacetamide core and phenanthroline derivatives was demonstrated to be processed to be not only organogels in a non-polar solvents but also films by solution or melt casting owing to its disc-like shape and large

molecular weight. Er(III) complex gelated ethylene glycol dimethylacrylate (EGDMA) and fibrous structure was further immobilized by in situ cross-linking in gel state by UV curing. Each state was investigated by absorption spectra and NIR emission was observed from resulting Er(III) film after cross-linking.

II-2. Experimental

Materials. 1,3,5-Triacetoacetamidobenzene,[39] 5-amino-1,10-phenanthroline[40] and 3,4,5-tris(dodecyloxy)benzoic acid[41] were prepared following synthetic procedures reported previously. Ethylene glycol dimethylacrylate (EGDMA) was purified by passing through a column filled with aluminum oxide (Aldrich) to remove the inhibitor. All other chemicals were purchased from Aldrich and used without any further purification. Tetrahydrofuran (THF) was dried over sodium metal and distilled. Other reagent grade solvents were used as received.

Measurements. ^{1}H and ^{13}C NMR spectra were recorded on a Bruker Avance 300 (300 MHz) and Avance 500 (125MHz) spectrometer. Elemental analyses were performed using a Flash EA 1112 elemental analyzer. FT-IR measurements were made on a PERKIN ELMER Spectrum GX I using KBr pellets. X-ray diffraction patterns were obtained using Bruker Xps GADDS (Cu Kα radiation, λ = 1.54 Å). Thermogravimetric analyses (TGA) were performed on a TA modulated TGA2050 with a heating rate of 10 ^{o}C/min under nitrogen. Differential scanning calorimetry (DSC) measurements were made on a TA modulated DSC Q10 with a scanning rate of 1 or 10 ^{o}C/min under

nitrogen.Optical textures of the mesophases were observed with a Leica DM LP equipped with a Mettler Toledo FP 82HT heating stage and a Mettler Toledo FP 90 central process controller. UV-Vis spectra were obtained with the use of a Sinco S-3150 spectrometer. Fluorescence measurements were performed on a Shimadzu RF-5301PC spectrofluorometer. Near-infrared emission spectra were measured with the Peltier-cooled Hamamatsu H9170-75 photomultiplier system. SEM images were obtained by using a JEOL JSM-6330F microscope. TEM images were taken by using a JEM1010 microscope operating at 80 kV. The organogel was heated up to dissociation temperature and dropped on a carbon-coated copper grid which was preheated at the same temperature. The sample was cooled to room temperature and dried.

Synthesis of Compound 1. To a solution of 3,4,5-trioctyloxybenzoic acid (2.0 g, 2.96 mmol) in chloroform (100 mL) was added thionyl chloride (0.43 mL, 5.93 mmol). After stirred for 4 h at rt, the solvent and thionyl chloride were removed by evaporation. The crude product was dissolved in THF (100 mL) followed by addition of a solution of 5-amino-1,10-phenanthroline (0.69 g, 3.56 mmol) and triethylamine (0.41 mL, 2.96 mmol) in THF (10 mL). The reaction mixture was stirred overnight at rt. After evaporation of the solvent, the product was isolated by recrystallization in ethanol. Yield: 78%. ^{1}H NMR (300 MHz,

$CDCl_3$, ppm): δ 9.25 (d, J = 4.8 Hz, Ar-H, 1H), 9.17 (d, J = 2.4 Hz, Ar-H, 1H), 8.35-8.24 (overlap, Ar-H, 3H), 8.11 (s, CONH, 1H), 7.72-7.63 (m, Ar-H, 2H), 7.12 (s, Ar-H, 2H), 4.08 (tt, overlap, OCH_2, 6H), 1.88-1.76 (m, OCH_2CH_2, 6H), 1.54-1.26 (m, alkyl chain proton, 54H), 0.89 (t, J = 3 Hz, CH_3, 9H). ^{13}C NMR (125 MHz, $CDCl_3$, ppm): δ 166.94, 153.48, 150.20, 150.04, 146.54, 144.79, 142.10, 136.07, 131.31, 130.70, 129.04, 128.34, 124.96, 123.58, 122.84, 121.19, 106.45, 73.82, 69.66, 32.12, 32.10, 30.55, 29.95, 29.93, 29.89, 29.84, 29.79, 29.67, 29.62, 29.58, 29.55, 26.29, 22.86, 14.28. IR (KBr, cm^{-1}): 3420, 3249, 2920, 2851, 1643, 1585, 1505, 1468, 1424, 1381, 1338, 1231, 1120, 990, 880, 738, 650. Anal. Calcd for $C_{55}H_{85}N_3O_4$: C, 77.51; H, 10.05; N, 4.93. Found: C, 77.77; H, 9.74; N, 4.87.

Synthesis of Eu2. To a solution of compound **1** (1.0 g, 1.17 mmol) in hot ethanol (100 mL) was added dropwise a solution of europium(III) chloride hexahydrate (0.21 g, 0.59 mmol) in ethanol (3 mL). The reaction mixture was refluxed for 2h. The precipitate was isolated by filtration, washed with ethanol and dried in vacuo. Yield: 85%. IR (KBr , cm^{-1}): 3080, 2924, 2853, 1639, 1572, 1527, 1494, 1468, 1427, 1385, 1337, 1234, 1115, 996, 540, 418. Anal. Calcd for $C_{110}H_{172}Cl_3EuN_6O_9$: C, 66.70; H, 8.75; N, 4.24. Found: C, 66.74; H, 8.72; N, 4.21.

Synthesis of Tb2. To a solution of compound **1** (1.0 g, 1.17 mmol) in hot ethanol was added dropwise a solution of terbium(III) chloride hexahydrate (0.22 g, 0.59 mmol) in ethanol. The reaction mixture was refluxed for 2h. Then, precipitates were isolated by filtration, washed with ethanol and dried in vacuo. Yield: 87%. IR (KBr , cm^{-1}): 3049, 2923, 2852, 1640, 1571, 1529, 1496, 1468, 1426, 1385, 1337, 1234, 1115, 735, 539, 419. Anal. Calcd for $C_{110}H_{172}Cl_3TbN_6O_9$: C, 66.46; H, 8.72; N, 4.23. Found: C, 66.46; H, 8.72; N, 4.12.

Synthesis of Er2. To a solution of compound **1** (1.0 g, 1.17 mmol) in hot ethanol was added dropwise a solution of erbium(III) chloride hexahydrate (0.22 g, 0.59 mmol) in ethanol. The reaction mixture was refluxed for 2h. Then, a precipitate was filtered off, washed with ethanol and dried in vacuo. Yield: 89%. IR (KBr , cm^{-1}): 3083, 2922, 2852, 1641, 1574, 1527, 1496, 1468, 1426, 1384, 1336, 1233, 1114, 735, 541, 419. Anal. Calcd for $C_{110}H_{172}Cl_3ErN_6O_9$: C, 66.18; H, 8.68; N, 4.21. Found: C, 66.18; H, 8.60; N, 4.22.

Synthesis of Eu3. A solution of 1,3,5-triacetoacetamidobenzene (63.17 mg, 0.17 mmol) in N-methyl-2-pyrrolidone (3 mL) was mixed with a solution of NaOH (21.54 mg, 0.54 mmol) in methanol (3 mL). This mixture was slowly

added to a solution of **Eu2** (2.0 g, 1.01 mmol) in hot chloroform (100 mL). The reaction mixture was refluxed overnight. After solvent evaporation, the product was dissolved in chloroform and precipitated in methanol. The precipitate was isolated by filtration, washed with methanol and dried in vacuo. The product was obtained as a brown powder. Yield: 74 %. IR (KBr, cm^{-1}): 3392, 3241, 2922, 2852, 1645, 1584, 1523, 1502, 1470, 1426, 1381, 1337, 1231, 1118, 736, 520, 418. Anal. Calcd for $C_{348}H_{534}Eu_3N_{21}O_{36}$: C, 69.16; H, 8.91; N, 4.87. Found: C, 68.99; H, 9.10; N, 4.63.

Synthesis of Tb3. A solution of 1,3,5-triacetoacetamidobenzene (50.70 mg, 0.14 mmol) dissolved in N-methyl-2-pyrrolidone (10 mL) was mixed with a solution of NaOH (17.29 mg, 0.43 mmol) in small amounts of methanol. This mixture was slowly added to a solution of **Tb2** (805.46 mg, 0.41 mmol) in hot chloroform. The reaction mixture was refluxed overnight. After solvent evaporation, the resulting product was dissolved in chloroform and precipitated in methanol. The precipitate was filtered off, washed with methanol and dried in vacuo. The product was obtained as a orange solid. Yield: 79%. IR (KBr , cm^{-1}): 3247, 2920, 2851, 1643, 1584, 1524, 1505, 1469, 1424, 1384, 1339, 1241, 1120, 739, 538, 458. Anal. Calcd for $C_{348}H_{534}Tb_3N_{21}O_{36}$: C, 68.92; H, 8.87; N, 4.85. Found: C, 68.64; H, 8.92; N, 4.66.

Synthesis of Er3. A solution of 1,3,5-triacetoacetamidobenzene (50.70 mg, 0.14 mmol) dissolved in N-methyl-2-pyrrolidone (10 mL) was mixed with a solution of NaOH (17.29 mg, 0.43 mmol) in small amounts of methanol. This mixture was slowly added to a solution of **Er2** (808.84 mg, 0.41 mmol) in hot chloroform. The reaction mixture was refluxed overnight. After solvent evaporation, the resulting product was dissolved in chloroform and precipitated in methanol. The precipitate was filtered off, washed with methanol and dried in vacuo. The product was obtained as a orange solid. Yield: 83 %. IR (KBr , cm^{-1}): 3248, 2922, 2852, 1646, 1583, 1524, 1500, 1468, 1425, 1380, 1337, 1231, 1118, 738, 524, 415. Anal. Calcd for $C_{348}H_{534}Er_3N_{21}O_{36}$: C, 68.63; H, 8.84; N, 4.83. Found: C, 68.75; H, 8.83; N, 4.76.

Synthesis of Eu4. 2,2,6,6-Tetramethyl-3,5-heptanedione (0.1 mL, 0.47 mmol) was preactivated with NaOH (19.42 mg, 0.49 mmol) in methanol (3 mL). This mixture was added dropwise to a solution of **Eu3** (946.7 mg, 0.16 mmol) in hot chloroform (100 mL). After reflux overnight, solvent was evaporated. The resulting product was isolated by precipitation with chloroform as a good solvent and methanol as a non-solvent. The yellow precipitates were obtained by filtration, washed with methanol and dried in vacuo. Yield: 89%. IR (KBr , cm^{-1}): 3423, 3246, 2922, 2852, 1644, 1583, 1526, 1502, 1468, 1424, 1380,

1338, 1232, 1120, 740, 536, 415. Anal. Calcd for $C_{381}H_{588}Eu_3N_{21}O_{39}$: C, 69.94; H, 9.06; N, 4.50. Found: C, 69.99; H, 9.11; N, 4.53.

Synthesis of Tb4. 2,2,6,6-Tetramethyl-3,5-heptanedione (0.08 mL, 0.38 mmol) and NaOH (15.59 mg, 0.39 mmol) were dissolved in small amounts of methanol. This solution was added dropwise to a solution of **Tb3** (762.60 mg, 0.13 mmol) in chloroform. The reaction mixture was refluxed overnight. After solvent evaporation, the resulting product was dissolved in chloroform and precipitated in methanol. The precipitate was filtered off, washed with methanol and dried in vacuo. The product was obtained as a orange powder. Yield: 90%. IR (KBr , cm^{-1}): 3246, 2921, 2851, 1644, 1584, 1525, 1504, 1468, 1424, 1380, 1339, 1231, 1120, 738, 536, 410. Anal. Calcd for $C_{381}H_{588}Tb_3N_{21}O_{39}$: C, 69.72; H, 9.03; N, 4.48. Found: C, 70.10; H, 8.91; N, 4.30.

Synthesis of Er4. 2,2,6,6-Tetramethyl-3,5-heptanedione (0.08 mL, 0.38 mmol) and NaOH (15.64 mg, 0.39 mmol) were dissolved in small amounts of methanol. This solution was added dropwise to a solution of **Er3** (780.60 mg, 0.13 mmol) in chloroform. The reaction mixture was refluxed overnight. After solvent evaporation, the resulting product was dissolved in chloroform and precipitated in methanol. The precipitate was filtered off, washed with methanol

and dried in vacuo. The product was obtained as a orange powder. Yield: 91%. IR (KBr , cm^{-1}): 3251, 2921, 2851, 1645, 1583, 1526, 1504, 1468, 1425, 1380, 1338, 1231, 1120, 738, 536, 412. Anal. Calcd for $C_{381}H_{588}Er_3N_{21}O_{39}$: C, 69.45; H, 9.00; N, 4.46. Found: C, 69.11; H, 8.93; N, 4.42.

II-3. Results and Discussion

II-3-1. Synthesis and Characterization

Scheme 1 shows the synthetic route for the disc-like lanthanide(III) complexes. Ligand **1** having a rigid phenanthroline moiety tailored with three alkyloxy chains was prepared by amidation reaction of 5-amino-1,10-phenanthroline with 3,4,5-trioctyloxybenzoic acid. 1,10-Phenanthroline is well known for its better coordinating ability than 2,2'-bipyridine[42] and for its good energy absorption property. **Ln2** complexes were prepared by complexation of ligand **1** with lanthanide(III) ions such as europium(III) chloride hexahydrate, terbium(III) chloride hexahydrate and erbium(III) chloride hexahydrate. Complexation was confirmed by elemental analysis. Lanthanide(III) ions in **Ln2** complexes have four exchangeable coordination sites, which are occupied by chloride or water molecules.

Ln3 complexes were prepared by the reaction of **Ln2** complexes with 1,3,5-triacetoacetamidobenzene, which has three 1,3-dicarbonyl moieties. 1,3-Diketones are widely used as ligands in metal coordination, but there have been only a few reports on β-ketoamide complexes. Crans *et al.* reported a coordination behavior for acetoacetamide that was similar to that of a 1,3-diketone in the complexation with oxovanadium(IV), where two carbonyl

oxygens were coordinated to the metal atom.[43] Since acetoacetamides can be easily prepared by the reaction of the corresponding amines with diketene, they could be versatile ligands like 1,3-diketones.

1,3,5-Triacetoacetamidobenzene has a planar structure because three *β*-carbonyl moieties are connected to the benzene ring through an amide bond.[39] **Ln3** complexes have a disc-like structure bearing three equivalents of **Ln2** complexes around a 1,3,5-triacetoacetamidobenzene core. The solubility of 1,3,5-triacetoacetamidobenzene changed dramatically after coordination. 1,3,5-Triacetoacetamidobenzene showed poor solubility in common organic solvents because of the strong intermolecular hydrogen bonding between the NH and carbonyl groups. However, **Ln3** complexes obtained by its coordination with lanthanide(III) ions were very soluble in solvents such as dimethylformamide, tetrahydrofuran and dichloromethane, suggesting that all carbonyl oxygen atoms of 1,3,5-triacetoacetamidobenzene were involved in coordination.

Ln3 complexes were further reacted with 2,2,6,6-tetramethylheptane-3,5-dione to replace the OH ligands because the luminescence properties of lanthanide ions are strongly influenced by the OH groups, which serve as efficient quenchers of the emission. The resulting heteroleptic **Ln4** complexes contain six 1,10-phenanthroline units derived from **Ln2** complexes and six *β*-diketonate groups derived from 1,3,5-triacetoacetamidobenzene and 2,2,6,6-

tetramethylheptane-3,5-dione. **Ln4** complexes were soluble in a wide variety of solvents including octanol, ethyl acetate, dichloromethane and toluene.

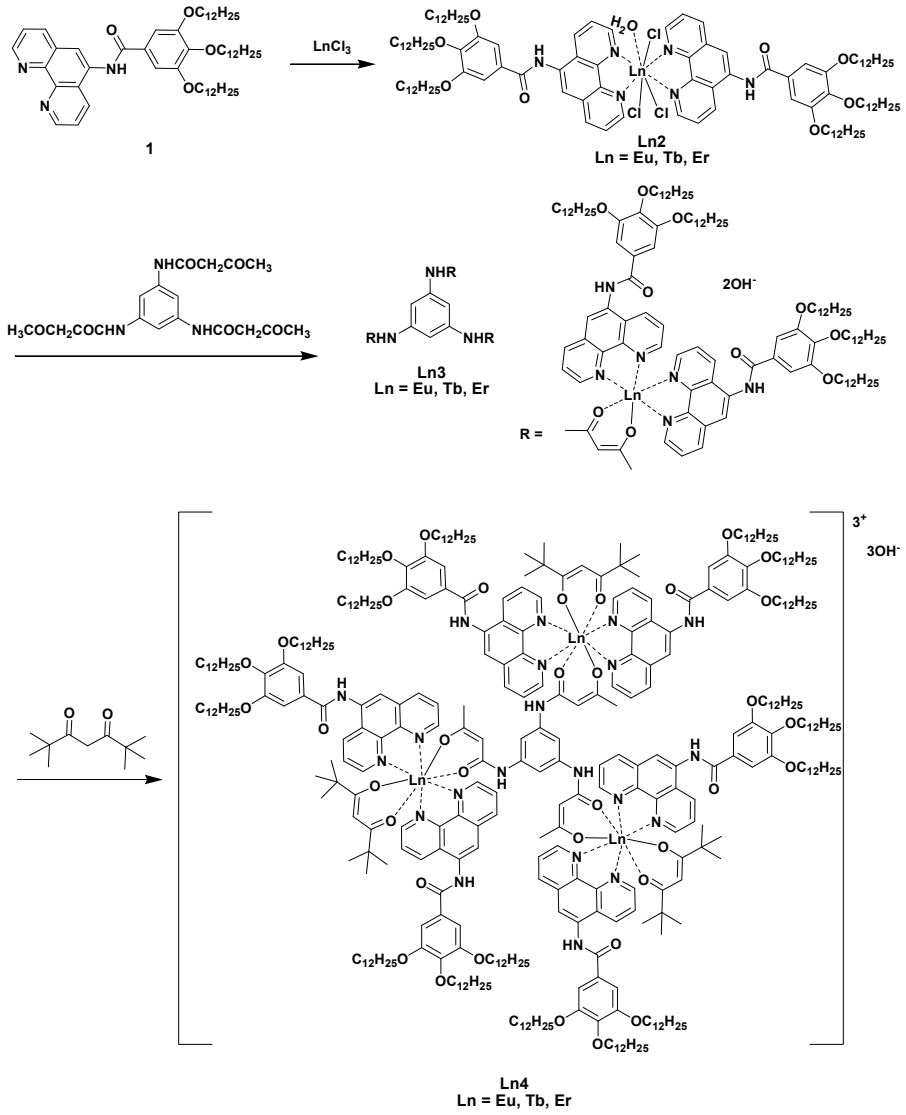

Scheme II-1. Synthesis of lanthanide(III) complexes.

Ln2 complexes showed not only mesophases but also organogelation depending on metal ions. However any self-assembled structure did not appear in **Ln3** complexes probably due to the strong intermolecular interaction. Interestingly, **Ln4** complexes exhibited liquid crystal phases and sol-gel transitions again after coordination with 2,2,6,6-tetramethylheptane-3,5-dione.

Europium(III) and terbium(III) complexes in **Ln2** or **Ln4** structures showed thermotropic mesomorphism. However, in the case of erbium complexes, mesophase was not exhibited. It was presumed that erbium(III) ion affected self-assembly of compounds by its size or electronic structure. Liquid crystal structures were confirmed by XRD (Figure II-1). **Eu2** and **Tb2** showed smectic orderings having d_{100}-spacings of 33.72 and 33.98 Å and d_{200}-spacings of 16.55 and 16.67 Å respectively. **Eu4** and **Tb4** showed hexagonal packing structures having d_{200}-spacings of 38.75, 36.81 and 37.12 Å and d_{210}-spacings of 28.32, 27.78 and 27.96 Å respectively. These *d*-spacings are in the ratio of $1/2:1/\sqrt{7}$, which is in good agreement with a hexagonal lattice with the lattice parameter of a = 87.20 and 85.01 Å. All phase transition temperatures and corresponding enthalpies were determined by DSC (Table II-1). Birefringences of all complexes were investigated by POM as shown in Figure II-2.

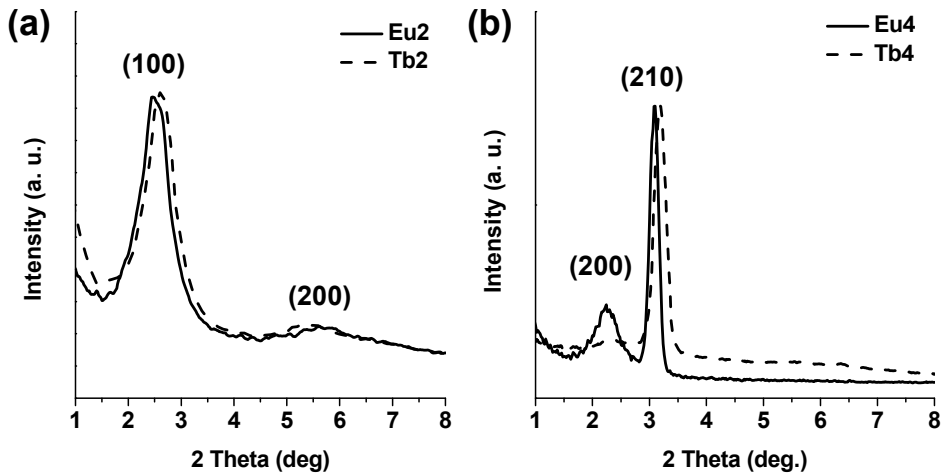

Figure II-1. Small angle X-ray diffractograms of (a) **Eu2** and **Tb2** and (b) **Eu4** and **Tb4**.

Table II-1. DSC analyses of **Eu2**, **Tb2**, **Eu4** and **Tb4**. The scanning rate of compounds was 10 ^{o}C min^{-1} and 1 ^{o}C min^{-1}, respectively.

	T, ^{o}C [ΔH, kJ/mol]	
	Second heating	Second cooling
Eu2	Cr 240.13 (63.15) I	I 223[a] Sm 214.72 (41.28) Cr
Tb2	Cr 216.75 (44.25) I	I 216.1[a] Sm 177.88 (20.55) Cr
Eu4	Cr 131.85 (1.74) I	I 124.5[a] Col_h 119.02 (2.52) Cr
Tb4	Cr 92.86 (5.77) I	I 90.4[a] Col_h 65.36 (5.39) Cr

Abbreviations: Cr) crystalline; Sm) smetic mesophase; Col_h) columnar hexagonal mesophase; I) isotropic. [a] Determined by POM.

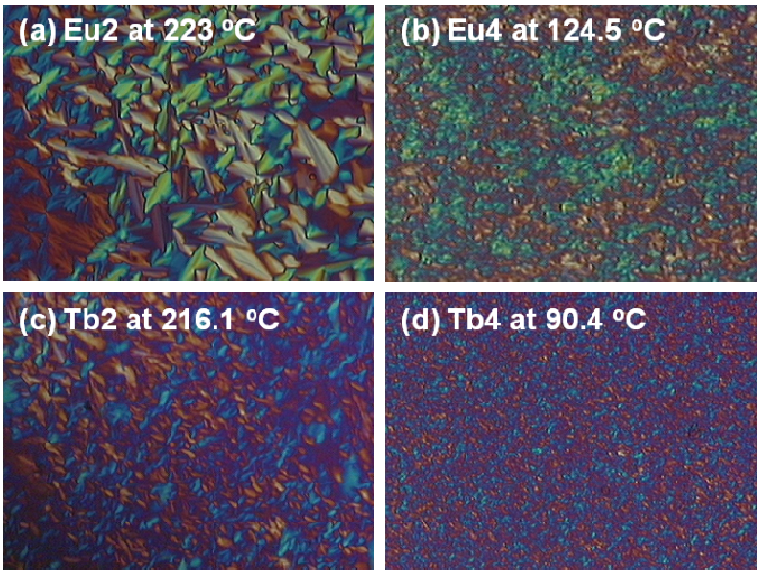

Figure II-2. POM images of (a) **Eu2**, (b) **Eu4**, (c) **Tb2** and (d) **Tb4** on second cooling.

Organogelation was investigated by a vial inversion method. In the case of **Ln2**, gelation occurred in *n*-decane by only **Eu2** and **Tb2**. **Er2** did not show a sol-gel transition until 2 wt% in *n*-decane. However, all **Ln4** complexes could gelate *n*-hexane as well as *n*-decane because of lower melting point confirmed by DSC and better solubility in non-polar solvent than **Ln2**. Their critical gelation concentrations were less sensitive to kind of metal ions and considerably lower than **Ln2,** indicating that **Ln4** could form the fibrous structure easily (Table II-2). In the bulky structure of **Ln4**, atomic effect might be reduced compared to **Ln2** during gelation.

Table II-2. Critical gelation concentrations of lanthanide(III) complexes.

		CGC (*n*-decane)	CGC (*n*-hexane)
Ln2	**Eu2**	0.7 wt%	-
	Tb2	1.9 wt%	-
	Er2	-	-
Ln4	**Eu4**	0.4 wt%	0.5 wt%
	Tb4	0.4 wt%	0.6 wt%
	Er4	0.5 wt%	0.7 wt%

In Figure II-3, photographs of various gels in vial are shown. Entangled fiber network structures were measured by TEM after drying on the carbon-coated copper grids. Dry gels from **Eu2** (1 wt% in *n*-decane) and **Tb2** (2 wt% in *n*-decane) showed fiber diameters ranged from 20 nm to 80 nm and those from **Eu4**, **Tb4** and **Er4** (1 wt% in *n*-hexane) from 0.02 to 1 μm as shown in Figure II-4.

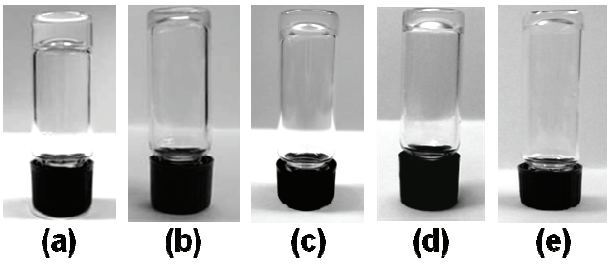

Figure II-3. Photograph of gels obtained from (a) 1 wt% of **Eu2** in *n*-decane, (b) 2 wt% of **Tb2** in *n*-decane, (c) 1 wt% of **Eu4** in *n*-decane, (d) 1 wt% of **Tb4** in *n*-decane and (e) 1 wt% of **Er4** in *n*-decane.

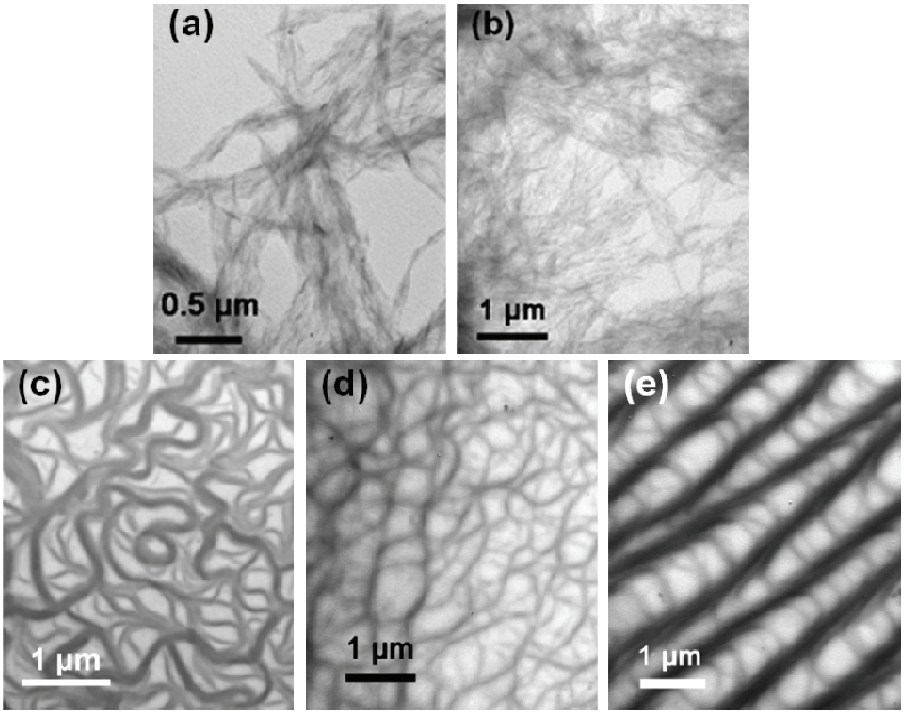

Figure II-4. TEM images of dry gels obtained from (a) 1 wt% of **Eu2** in *n*-decane, (b) 2 wt% of **Tb2** in *n*-decane, (c) 1 wt% of **Eu4** in *n*-decane, (d) 1 wt% of **Tb4** in *n*-decane and (e) 1 wt% of **Er4** in *n*-decane.

II-3-2. White-Light Emission from Mixed Organogels

The most fascinating property of lanthanide(III) ions is their characteristic luminescence. As Eu(III) and Tb(III) ions were coordinated with the same ligands, Eu(III) and Tb(III) complexes exhibited almost the same absorption spectra, but their emission spectra were quite different. Figure II-5a shows the UV-Vis absorption and emission spectra of **Eu2** and **Tb2** in chloroform. When

excited at 330 nm, **Eu2** gave emissions corresponding to two transitions at 595 nm ($^5D_0 \rightarrow {}^7F_1$) and 618 nm ($^5D_0 \rightarrow {}^7F_2$), although the red $^5D_0 \rightarrow {}^7F_2$ transition was much more intense. **Tb2** gave a greenish emission with four transitions at 496 nm ($^5D_4 \rightarrow {}^7F_6$), 551 nm ($^5D_4 \rightarrow {}^7F_5$), 588 nm ($^5D_4 \rightarrow {}^7F_4$) and 625 nm ($^5D_4 \rightarrow {}^7F_3$) and gave an intense and broad emission at around 440 nm from its ligands, which was not significant for **Eu2**. The intense emission at around 440 nm was attributed to partial energy transfer from the ligand to Tb(III).

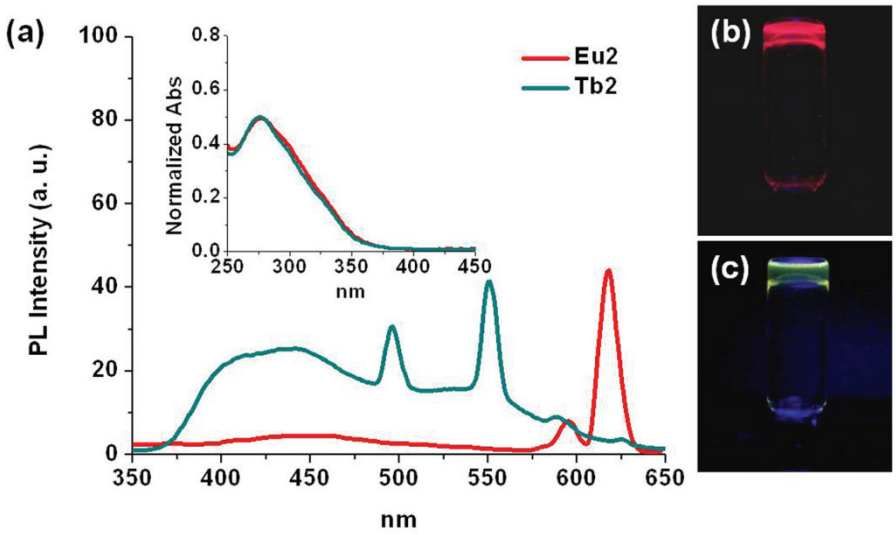

Figure II-5. (a) Emission spectra from **Eu2** and **Tb2** in chloroform excited at 330 nm. The absorption spectra of the two complexes are included as an inset. (b and c) Photographs of organogels of **Eu2** (b) and **Tb2** (c) (2 wt% in *n*-decane) taken under 365 nm irradiation.

Due to their structural similarities, **Eu2** and **Tb2** also formed homogeneous mixed gels.[44] The emission spectra of a mixture of **Eu2** and **Tb2** in *n*-decane (2 wt%) measured in the sol and gel states showed peaks corresponding to emissions from the ligands and sensitized Eu(III) and Tb(III). The emission peaks from Eu(III) appeared at 595 and 618 nm and from Tb(III) at 496 and 551 nm when excited at 330 nm. Furthermore, a broad emission was observed around 470 nm that was attributed primarily to the ligands of **Tb2**. After examining the emission spectra of the mixed gels with various compositions, a ratio of **Eu2** / **Tb2** of 1 : 19 by weight was deemed to provide an optimum white-light emission.

The critical gelation concentration of the mixture of **Eu2** and **Tb2** (1 : 19 by weight) (**Eu2-Tb2**) was 1.3 wt% in *n*-decane which was higher than that of **Eu2** (0.7 wt%) but lower than that of **Tb2** (1.9 wt%), suggesting the absence of orthogonal self-assembly of **Eu2** or **Tb2**.[42] The same ligand structures of two complexes were supposed to enhance intermolecular interactions between **Eu2** and **Tb2** to form a homogenous mixed gel. The TEM image of the dry gel revealed entangled fibers with diameters ranged from 20 nm to 80 nm without evidence of self-sorting (Figure II-6a).[45,46]

The absorption and emission spectra of **Eu2-Tb2** in *n*-decane (2 wt %) obtained in the sol and gel states are described in Figure II-6b. In the sol state at

100 ^{o}C, the absorption bands of the ligands appeared below 400 nm with a λ_{max} of 275 nm and their emission bands were between 360 and 600 nm when excited at 330 nm. However, the emissions from the Eu(III) and Tb(III) ions were barely noticeable. After gelation at 25 ^{o}C, the absorption maximum was red-shifted by 8 nm probably because of intermolecular ground state interactions[50] and interestingly, Eu(III) and Tb(III) emissions intensified significantly with a slight diminution of emission from the ligands, suggesting efficient intramolecular energy transfer from the ligands to the core metal ions. The most intensive transitions in **Eu2** ($^5D_0 \rightarrow {}^7F_2$) and **Tb2** ($^5D_4 \rightarrow {}^7F_5$) were enhanced 22 and 2 times, respectively after gelation.

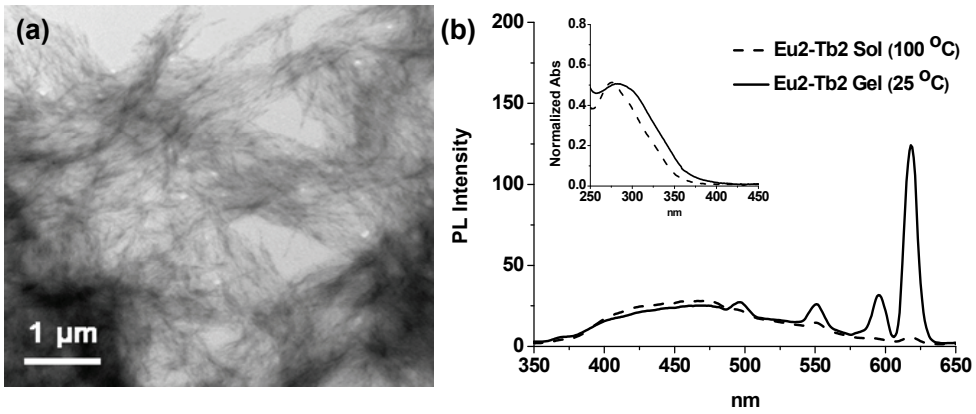

Figure II-6. (a) TEM image of the dry gel obtained from **Eu2-Tb2** in *n*-decane (2 wt%). (b) Emission spectra of the sol and gel of **Eu2-Tb2** in *n*-decane (2 wt%) when excited at 330 nm. The absorption spectra of two states are shown in the inset.

Emission quenching of Eu(III) and Tb(III) in the sol state could be a result of non-radiative transitions, which are dependent on temperature. Accordingly, the effect of temperature on luminescence intensity was investigated by using a solution of **Eu2** in *n*-decane, which was prepared to have the same **Eu2** concentration (0.1 wt%) as in **Eu2-Tb2**. At 0.1 wt% and 25 ^{o}C, **Eu2** couldn't gelate *n*-decane. The luminescence intensity of the solution for the $^{5}D_{0}\rightarrow{}^{7}F_{2}$ transition of Eu(III) increased on cooling from 100 to 25 ^{o}C, but this increase was only 5-fold (Figure II-7a). The same experiment was carried out using a solution of **Eu2-Tb2** in toluene (2 wt%) in which gelation did not occur. The luminescence intensity only increased 2-fold on cooling (Figure II-7b). These results suggested that emission quenching was reduced significantly by gelation.

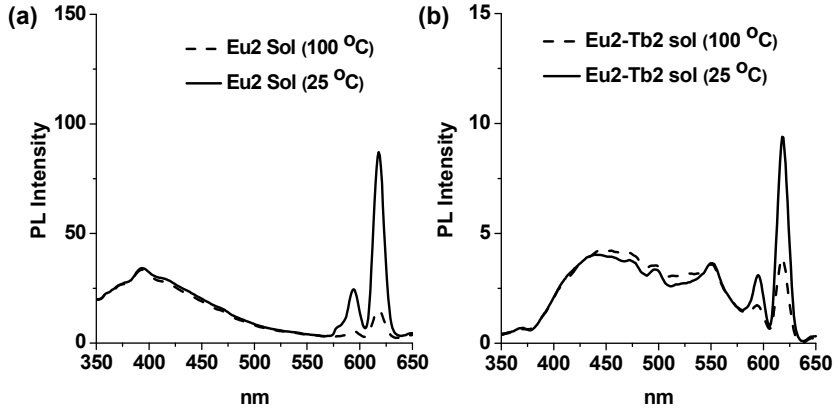

Figure II-7. Emission spectra obtained from (a) a solution of **Eu2** (0.1 wt%) in *n*-decane and (b) a solution of **Eu2-Tb2** (2 wt%) in toluene when excited at 330 nm.

Similar emission intensity increases by gelation were observed for **Eu2** and **Tb2** gels formed in *n*-decane (2 wt %), indicating that the luminescences of the two components were unperturbed in the mixed gels. The absorption maxima of **Eu2** and **Tb2** were also found to be red-shifted by 8 nm by gelation (Figure II-8 and II-9).

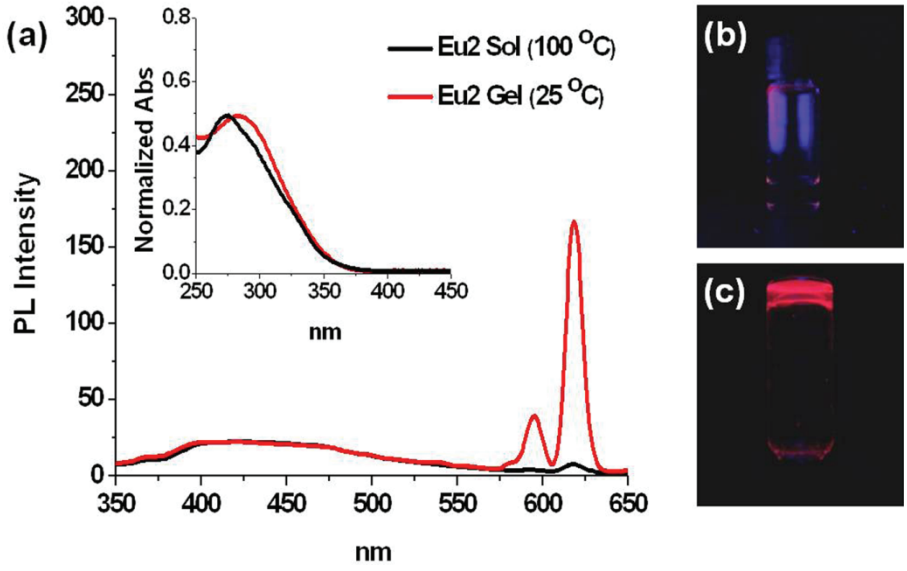

Figure II-8. (a) Emission spectra of the sol (100 °C) and gel (25 °C) of **Eu2** in *n*-decane (2 wt%) excited at 330 nm. The absorption spectra of two states are shown in the inset. (b and c) Photographs of the sol (b) and the gel (c) of **Eu2** in *n*-decane (2 wt%) under 365 nm irradiation.

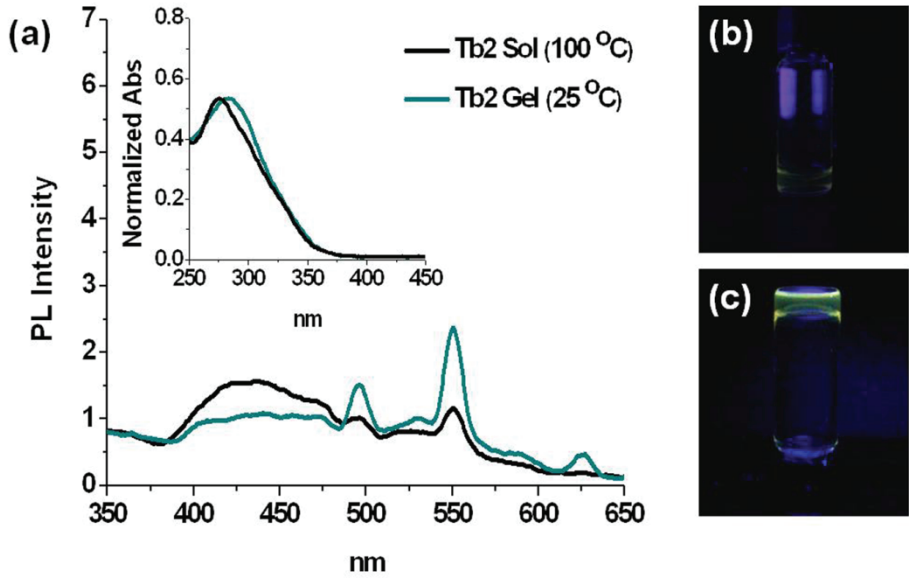

Figure II-9. (a) Emission spectra of the sol (100 °C) and gel (25 °C) of **Tb2** in *n*-decane (2 wt%) excited at 330 nm. The absorption spectra of two states are shown in the inset. (b and c) Photographs of the sol (b) and the gel (c) of **Tb2** in *n*-decane (2 wt%) under 365 nm irradiation.

Figure II-10a and II-10b show photographs of the sol (100 °C) and gel (25 °C) of **Eu2-Tb2** (2 wt%, *n*-decane) taken under 365 nm irradiation, respectively. The two-component gel exhibited white luminescence. In the sol state, the CIE color coordinates of **Eu2-Tb2** were x = 0.20 and y = 0.23 in the blue region and these changed to x = 0.36 and y = 0.30 in the white region by gelation (Figure II-10c).

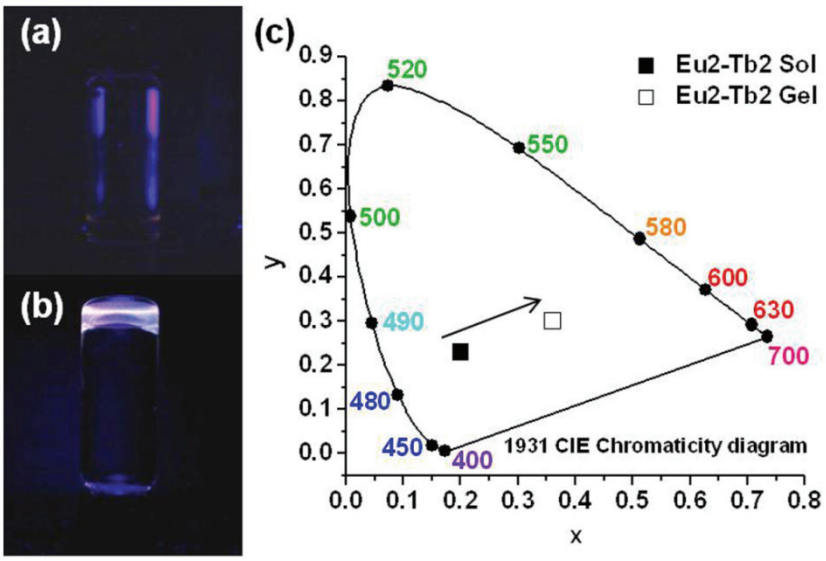

Figure II-10. Photographs of the sol at 100 °C (a) and gel at 25 °C (b) of **Eu2-Tb2** (2 wt%, *n*-decane) taken under 365 nm irradiation. (c) CIE color coordinates of **Eu2-Tb2** at the sol and gel states in *n*-decane (2 wt%).

Emission spectra of **Eu4** and **Tb4** in chloroform are shown in Figure II-11. **Eu4** showed three transitions in red region at 581 nm ($^5D_0 \rightarrow {}^7F_0$), 595 nm ($^5D_0 \rightarrow {}^7F_1$) and 618 nm ($^5D_0 \rightarrow {}^7F_2$) as reported data.[44] A ligand-centered emission appeared between 360 and 600 nm. On the other hand, **Tb4** did not show the luminescence from Tb(III) ion. A broad emission in greenish blue region was only observed from the ligands, suggesting the poor energy transfer from the triplet states of the ligands to the emitting level of Tb(III) ion.[47-49]

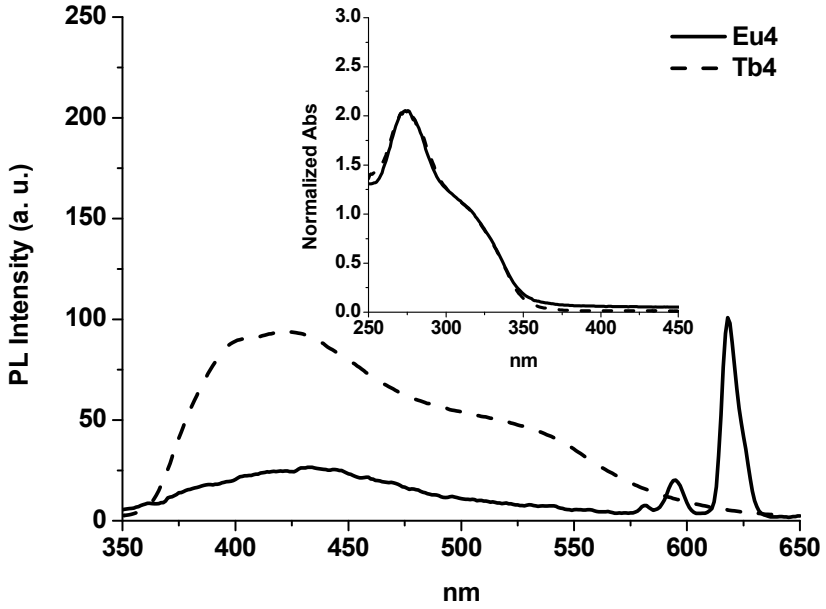

Figure II-11. Emission spectra from **Eu4** and **Tb4** in chloroform excited at 330 nm. The absorption spectra of the two complexes are shown in the inset.

Emission spectra of sol and gel states of **Eu4** and **Tb4** in *n*-decane (1 wt%) are described in Figure II-12. The organogel of **Eu4** showed the significantly enhanced emission intensities from europium(III) ion at 581 nm, 595 nm and 618 nm with the decrease of the emission intensity from the ligands compared with the solution.[44] The metal-centered emission was not observed in the organogel of **Tb4** as in the solution but the emission from the ligands was enhanced after gelation.

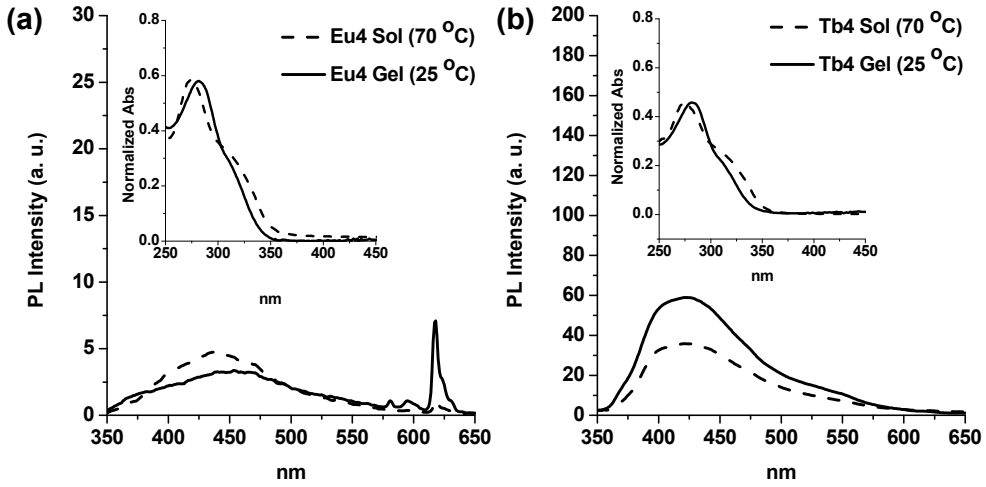

Figure II-12. Emission spectra of the sol (70 °C) and gel (25 °C) of **Eu4** (a) and **Tb4** (b) in *n*-decane (1 wt%) excited at 330 nm. The absorption spectra of two states are shown in the inset.

Eu4 and **Tb4** formed a homogeneous mixed gel in *n*-decane (**Eu4-Tb4**), showing a whitish luminescence at the ratio of 3 : 1 by weight. The critical gelation concentration of **Eu4-Tb4** (3 : 1 by weight) was 0.5 wt%. The TEM image of the dry gel revealed entangled fibers with diameters ranged from 60 nm to 180 nm (Figure II-13a). Emission spectra of **Eu4-Tb4** in *n*-decane (1 wt%) at sol and gel states are shown in Figure II-13b. The CIE color coordinates of a **Eu4-Tb4** solution were x = 0.18 and y = 0.13 in the blue region, which were shifted to x = 0.24 and y = 0.18 in the boundary of the white region after gelation.

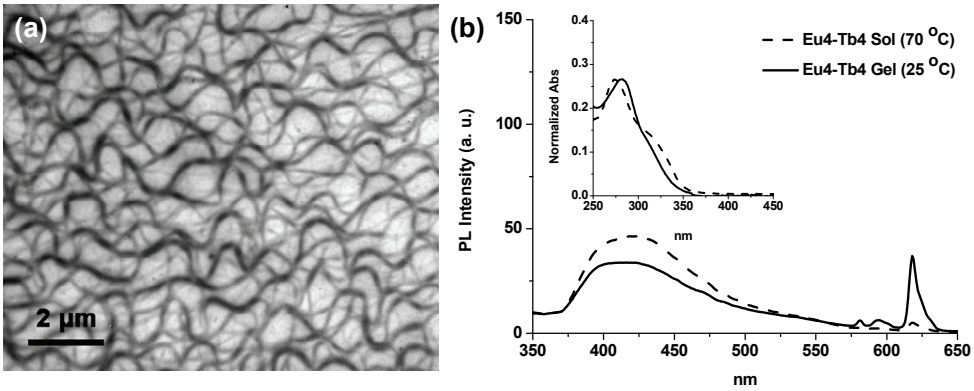

Figure II-13. (a) TEM image of the dry gel obtained from **Eu4-Tb4** (3 : 1 by weight) in *n*-decane (1 wt%). (b) Emission spectra of the sol (70 ^{o}C) and gel (25 ^{o}C) of **Eu4-Tb4** in *n*-decane (1 wt%) excited at 330 nm. Absorption spectra of two states are shown in the inset.

II-3-3. Film-Forming Properties of the Europium(III) Complex

One of the distinguishing features of **Eu4** was a film-forming property. A thin film was prepared by spin-casting at 1500 rpm on a quartz plate from a 5 wt% dichloromethane solution to investigate the optical absorption and photoluminescence (PL) property. **Eu4** showed an absorption maximum at 274 nm in the chloroform solution (10^{-6} M). In the film and gel states, the maximum absorption peaks were red-shifted by 4 and 8 nm, respectively, which was ascribed to the intermolecular ground state interactions.[50] Regardless of the different absorption patterns, all the samples showed the same PL emission peaks

corresponding to the transitions from the excited state $^5D_0$ to the ground states ^7F_J of europium (III). Three transitions were observed at 595 nm ($^5D_0 \rightarrow {}^7F_1$), 618 nm ($^5D_0 \rightarrow {}^7F_2$) and 656 nm ($^5D_0 \rightarrow {}^7F_3$). The $^5D_0 \rightarrow {}^7F_2$ transition was the strongest, showing the typical red color emission of europium (III).[51]

The PL intensity of the $^5D_0 \rightarrow {}^7F_2$ transition increased with the increase in the concentration of **Eu4** up to 10^{-4} M in toluene, but decreased markedly at higher concentrations because the concentration quenching occurred. Also, the PL intensity at 25 and 75 ^oC were insignificantly changed in 10^{-3} and 10^{-4} M of toluene soltions having similar concentration with 1 wt% of gel (Figure II-14).

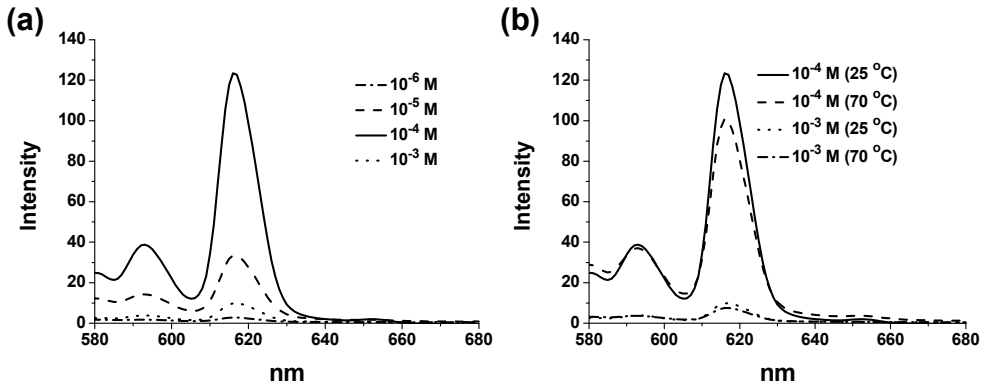

Figure II-14. (a) Emission spectra of **Eu4** in toluene with various concentrations obtained at 25 ^oC (λ_{ex} = 310 nm). (b) Emission spectra of **Eu4** in toluene obtained at 25 and 70 ^oC (λ_{ex} = 310 nm).

Concentration quenching effect was diminished in the gel state. Figure II-15 shows the UV-Vis and PL spectra of **Eu4** in the solution and gel states. A 1 wt% solution of **Eu4** in *n*-decane (1.13 x 10^{-3} M) prepared at 70 °C showed a weak PL emission due to the quenching. As the solution turned into a gel at 25 °C, the PL intensity of the $^5D_0 \rightarrow {}^7F_2$ transition was increased by about 6 times. Since the PL intensity is also dependent on temperature, the emission spectra of **Eu4** in toluene (10^{-3} M) were measured at 25 and 70 °C. The PL intensity of the solution for the $^5D_0 \rightarrow {}^7F_2$ transition was increased, but only by 31 % on cooling from 70 to 25 °C (Figure II-16).

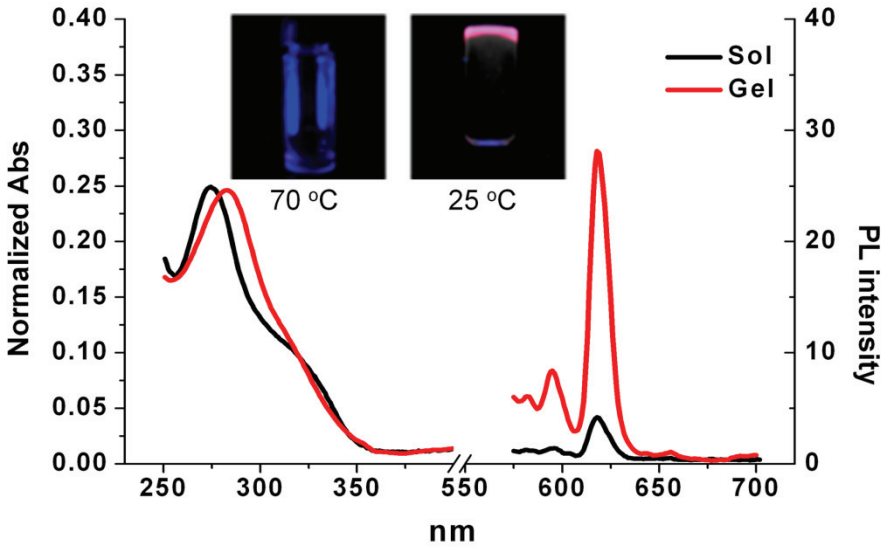

Figure II-15. UV-Vis spectra (left) and emission spectra excited at 275 nm (right) of **Eu4** in the solution and gel states. Photographs of the sol (left) and the gel (right) were taken after 365 nm irradiation.

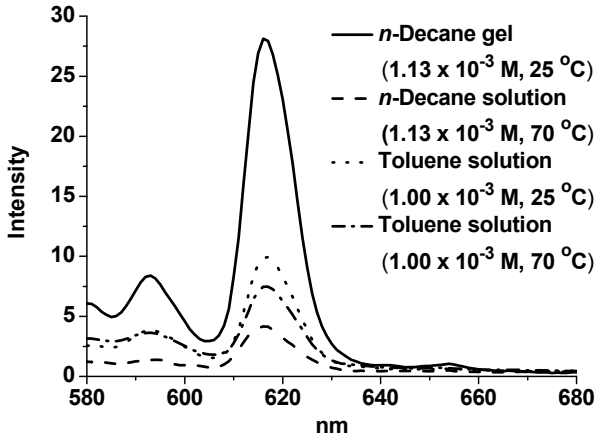

Figure II-16. Emission spectra of **Eu4** in *n*-decane at 25 and 70 °C and in toluene at 25 and 70 °C (λ_{ex} = 310 nm).

This result suggests that the probability of emission quenching was reduced significantly by gelation. Additionally, a freestanding film with a thickness of about 54 μm obtained by melt casting on a silicon-coated substrate at 140 °C also showed bright red color upon UV irradiation at 365 nm (Figure II-17).

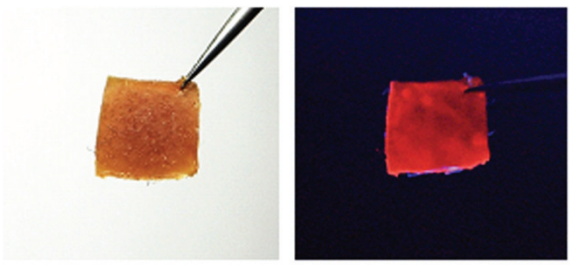

Figure II-17. Photographs of a freestanding film of **Eu4** (left) and after 365 nm irradiation (right).

II-3-4. NIR-Emitting Er(III) Film Through the Gel-State Polymerization

Although organogels have been used in various fields, they still suffer from intrinsically weak durabilities in many cases. To immobilize gel fibers effectively, polymerization was required to occur in the gel state without disruption of the fibers. **Er4** showed a gelation behavior not only in aliphatic solvents but also in EGDMA, one of the well-known cross-linking agents in radical polymerizations. The CGC of **Er4** in EGDMA was found to be 4 wt% and the fiber network in the gel was investigated by TEM and SEM measurements (Figure II-18).

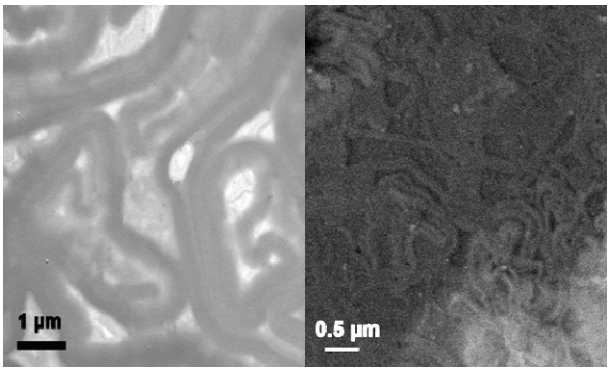

Figure II-18. TEM (left) and SEM (right) images of the dry gel obtained from **Er4** in EGDMA (5 wt%).

Because **Er4** gel in EGDMA was sensitive to heat, UV polymerization was carried out with 2,2-dimethoxy-2-phenylacetophenone (DMPA) as a

photoinitiator. DMPA (2 wt%) was dissolved to 5 wt% of **Er4** in EGDMA by gentle heating. Once the gel was formed, the gel was irradiated by a high pressure mercury arc lamp (3 mW cm^{-2}). Under UV light, the gel maintained its shape without collapsing. Photograph of each step was taken as shown in Figure II-19. **Er4** gel with DMPA was placed on quartz plate by means of drop casting and the transparent **Er4** film was obtained after UV irradiation (Figure II-20). In SEM images (Figure II-21), the surface of the film was measured to be rugged compared to a normal EGDMA film, supporting that the fibrous structure was supposed to be maintained during gelation and embedded in the cross-linked film. The film showed a thickness of 84 μm averagely and became no more soluble in common organic solvents and fusible by heat.

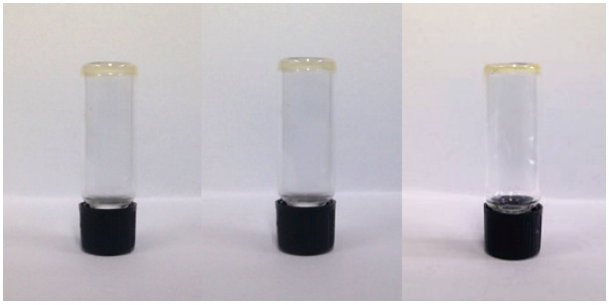

Figure II-19. Photographs of **Er4** gel in EGDMA at 5 wt% (left), with DMPA (middle) and after UV irradiation (right).

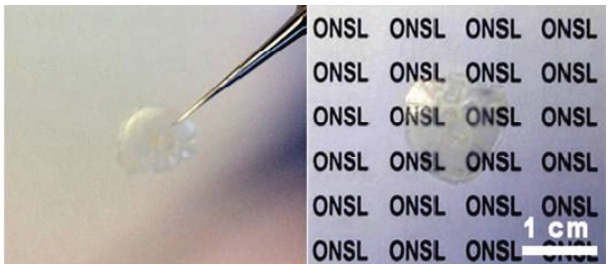

Figure II-20. Photographs of **Er4** film after cross-linking by UV irradiation.

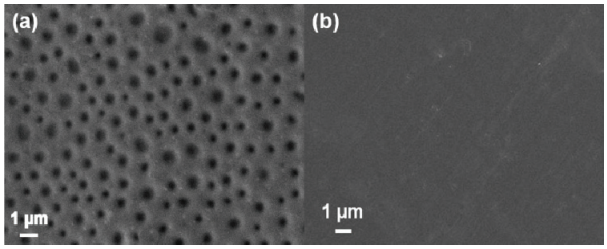

Figure II-21. SEM images of films obtained from (a) 5 wt% of **Er4** in EGDMA and (b) only EGDMA after UV cross-linking.

Absorption spectra of **Er4** in sol, gel and film state were investigated (Figure II-22). **Er4** in sol state (1 wt% in EGDMA) showed an absorption maximum at 291 nm, but in gel state (5 wt% in EGDMA), it was blue-shifted by 20 nm. The film state showed comparable absorption spectrum to gel state, indicating that **Er4** gel fiber network was probably maintained in the film during cross-linking. Excitation (λ_{em} = 1533 nm) and emission (λ_{ex} = 325 nm) spectra are shown in Figure II-23. Excitation spectrum of NIR emission is similar to absorption

spectrum of **Er4** film, suggesting the energy transfer occurred from peripheral ligand to Er(III). Also the resulting emission spectrum was considered to be obtained from the frozen fiber network inside the film. Emission spectrum is generated by intraconfigurational 4f-4f transition from $^4I_{13/2}$ level to $^4I_{15/2}$ level in Er(III). Broad NIR emission ranged from 1450 nm to 1650 nm and full width at half maximum (fwhm) was found to be around 100 nm useful for wavelength division multiplexing (WDM) around 1.54 μm.[52,53]

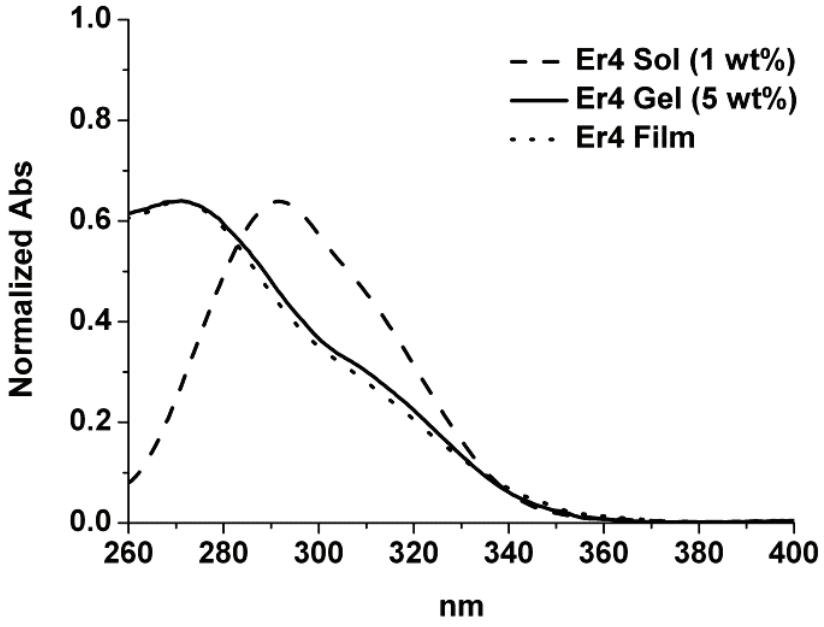

Figure II-22. Absorption spectra of **Er4** in sol, gel and film states.

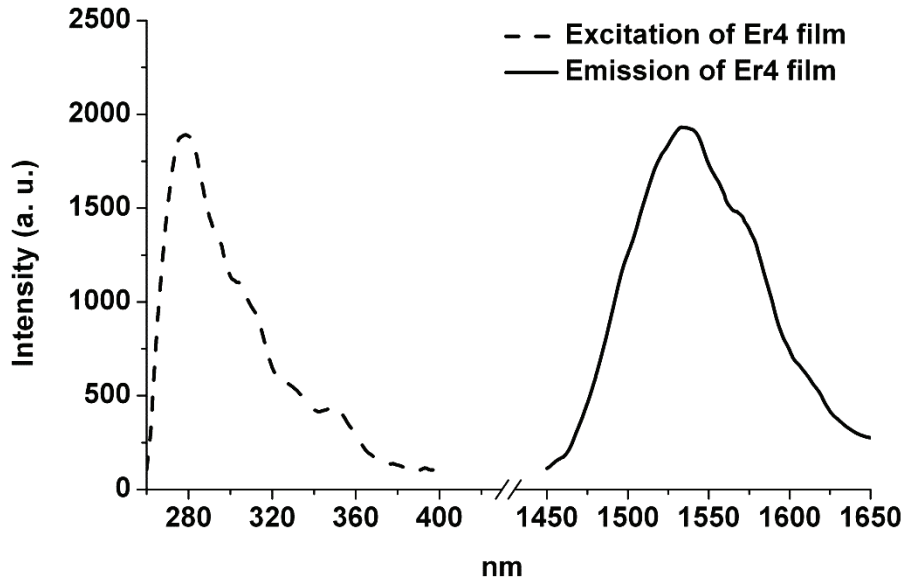

Figure II-23. Excitation (λ_{em} = 1533 nm) and emission (λ_{ex} = 325 nm) spectra of **Er4** film.

II-4. Conclusions

Organogelators containing Eu(III), Tb(III) and Er(III) ions were synthesized and their self-assembled properties were characterized. **Eu2** and **Tb2** formed stable organogels in *n*-decane. A metal-centered emission was significantly enhanced in the gel state as compared with the sol state. Two-component mixed gels were obtained from a mixture of two gelators without evidence of self-sorting. A white luminescence was achieved by controlling the composition of the mixed gel to give a bluish ligand-centered emission that was well-balanced by the red and green emissions from Eu(III) and Tb(III) core ions. Trimetallic organogelators, **Eu4** and **Tb4**, also formed a homogeneous mixed gel in *n*-decane. The mixed gel of **Eu4** and **Tb4** had a bluish emissions from the ligands and the red emissions from Eu(III) ions and showed a whitish luminescence. Especially, **Eu4** could be processed into a thin film or free-standing film without losing its photoluminescence. Furthermore, a film could be fabricated from a gel fiber network through the gel-state polymerization. **Er4** gelated EGDMA and the resulting gel was cross-linked after in situ UV irradiation in gel state. The fiber network was embedded in the film during polymerization and photphysical properties were investigated.

II-5. References

1. Binnemans, K. *Chem. Rev.* **2009**, *109*, 4283-4374.
2. Binnemans, K. *J. Mater. Chem.* **2009**, *19*, 448-453.
3. Farinola, G. M.; Ragni, R. *Chem. Soc. Rev.* **2011**, *40*, 3467-3482.
4. Kido, J.; Okamoto, Y. *Chem. Rev.* **2002**, *102*, 2357-2368.
5. Ulbricht, C.; Beyer, B.; Friebe, C.; Winter, A.; Schubert, U. S. *Adv. Mater.* **2009**, *21*, 4418-4441.
6. Balamurugan, A.; Reddy, M. L. P.; Jayakannan, M. *J. Phys. Chem. B* **2009**, *113*, 14128-14138.
7. Li, S.; Zhong, G.; Zhu, W.; Li, F.; Pan, J.; Huang, W.; Tian, H. *J. Mater. Chem.* **2005**, *15*, 3221-3228.
8. Sasabe, H.; Takamatsu, J.; Motoyama, T.; Watanabe, S.; Wagenblast, G.; Langer, N.; Molt, O.; Fuchs, E.; Lennartz, C.; Kido, J. *Adv. Mater.* **2010**, *22*, 5003-5007.
9. Zucchi, G.; Jeon, T.; Tondelier, D.; Aldakov, D.; Thuéry, P.; Ephritikhine, M.; Geffroy, B. *J. Mater. Chem.* **2010**, *20*, 2114-2120.
10. Pyo, S. W.; Lee, S. P.; Lee, H. S.; Kwon, O. K.; Hoe, H. S.; Lee, S. H.; Ha, Y.-k.; Kim, Y. K.; Kim, J. S. *Thin Solid Films* **2000**, *363*, 232-235.

11. He, L.; Qiao, J.; Duan, L.; Dong, G.; Zhang, D.; Wang, L.; Qiu, Y. *Adv. Funct. Mater.* **2009**, *19*, 2950-2960.
12. He, L.; Duan, L.; Qiao, J.; Dong, G.; Wang, L.; Qiu, Y. *Chem. Mater.* **2010**, *22*, 3535-3542.
13. Coppo, P.; Duati, M.; Kozhevnikov, V. N.; Hofstraat, J. W.; De Cola, L. *Angew. Chem. Int. Ed.* **2005**, *44*, 1806-1810.
14. Bolink, H.; De Angelis, F.; Baranoff, E.; Klien, C.; Fantacci, S.; Coronado, E.; Sessolo, M.; Kalyanasundaram, K.; Grätzel, M.; Nazeeruddin, M. K. *Chem. Commun.* **2009**, 4672-4674.
15. He, G.; Guo, D.; He, C.; Zhang, X.; Zhao, X.; Duan, C. *Angew. Chem., Int. Ed.* **2009**, *48*, 6132-6135.
16. Law, G.-L.; Wong, K.-L.; Tam, H.-L.; Cheah, K.-W.; Wong, W.-T. *Inorg. Chem.* **2009**, *48*, 10492-10494.
17. Xu, H.-B.; Chen, X.-M.; Zhang, Q.-S.; Zhang, L.-Y.; Chen, Z.-N. *Chem. Commun.* **2009**, 7318-7320.
18. Shelton, A. H.; Sazanovich, I. V.; Weinstein, J. A.; Ward, M. D. *Chem. Commun.* **2012**, *48*, 2749-2751.
19. Kawa, M.; Fréchet, J. M. J. *Chem. Mater.* **1998**, 10, 286-296.
20. Cross, J. P.; Lauz, M.; Badger, P. D.; Petoud, S. *J. Am. Chem. Soc.* **2004**, *126*, 16278-16279.

21. Vicinelli, V.; Ceroni, P.; Maestri, M.; Balzani, V.; Gorka, M.; Vögtle, F. *J. Am. Chem. Soc.* **2002**, *124*, 6461-6468.

22. Zhu, X.; Wong, W.-K.; Wong, W.-Y.; Yang, X.-P. *Eur. J. Inorg. Chem.* **2011**, *2011*, 4651-4674.

23. Kuriki, K.; Koike, Y.; Okamoto, Y. *Chem. Rev.* **2002**, *102*, 2347-2356.

24. Artizzu, F.; Mercuri, M. L.; Serpe, A.; Deplano, P. *Coord. Chem. Rev.* **2011**, *255*, 2514-2529.

25. Bünzli, J.-C. G.; Comby, S.; Chauvin, A.-S.; Vandevyver, C. D. B. *J. Rare Earths* **2007**, *25*, 257-274.

26. Oh, J. B.; Nah, M.-K.; Kim, Y. H.; Kang, M. S.; Ka, J.-W.; Kim, H. K. *Adv. Funct. Mater.* **2007**, *17*, 413-424.

27. Baek, N. S.; Kim, Y. H.; Roh, S.-G.; Kwak, B. K.; Kim, H. K. *Adv. Funct. Mater.* **2006**, *16*, 1873-1882.

28. Beverina, L.; Crippa, M.; Sassi, M.; Monguzzi, A.; Meinardi, F.; Tubino , R.; Pagani, G. A. *Chem. Commun.* **2009**, 5103-5105.

29. Song, L.; Hu, J.; Wang, J.; Liua, X.; Zhen, Z. *Photochem. Photobiol. Sci.* **2008**, *7*, 689-693.

30. Li, Y.; Yang, H.; He, Z.; Liu, L.; Wang, W.; Li, F.; Xu, L. *J. Mater. Res.* **2005**, *20*, 2940-2946.

31. Wang, H.; Qian, G.; Wang, M.; Zhang, J.; Luo, Y. *J. Phys. Chem. B* **2004**, *108*, 8084-8088.

32. Song, L.-M.; Zhen. Z.; Liu, X.-H. *Mater. Lett.* **2010**, *64*, 1745-1747.

33. Fan, W. ; Feng, J.; Song, S.; Lei, Y.; Zhou, L.; Zheng, G.; Dang, S.; Wang, S.; Zhang, H. *Nanoscale* **2010**, *2*, 2096-2103.

34. Kamimura, M.; Kanayama, N.; Tokuzen, K.; Soga, K.; Nagasaki, Y. *Nanoscale* **2011**, *3*, 3705-3713.

35. Tiseanu, C.; Lórenz-Fonfría, V. A.; Parvulescu, V. I.; Gessner, A.; Kumke, M. U. *J. Appl. Phys.* **2008**, *104*, 033530.

36. Hashimoto, S.; Kirikae, S.; Tobita, S. *Phys. Chem. Chem. Phys.* **2002**, *4*, 5856-5862.

37. Monguzzi, A.; Macchi, G.; Meinardi, F.; Tubino, R.; Calzaferri, G. *Appl. Phys. Lett.* **2008**, *92*, 123301.

38. Mech, A.; Monguzzi, A.; Meinardi, F.; Mezyk, J.; Macchi, G.; Tubino, R. *J. Am. Chem. Soc.* **2010**, *132*, 4574-4576.

39. Jeong, M. J.; Park, J. H.; Lee, C.; Chang, J. Y. *Org. Lett.* **2006**, *8*, 2221-2224.

40. Binnemans, K.; Lenaerts, P.; Driesen, K.; Görller-Walrand, C. *J. Mater. Chem.* **2004**, *14*, 191-195.

41. Lim, G. S.; Jung, B. M.; Lee, S. J.; Song, H. H.; Kim, C.; Chang, J. Y. *Chem. Mater.* **2007**, *19*, 460-467.

42. Accorsi, G.; Listorti, A.; Yoosaf, K.; Armaroli, N. *Chem. Soc. Rev.* **2009**, *38*, 1690-1700.

43. Crans, D. C.; Khan, A. R.; Mahroof-Tahir, M.; Mondal, S.; Miller, S. M.; la Cour, A.; Anderson, O. P.; Jakusch, T.; Kiss, T. *J. Chem. Soc., Dalton Trans.* **2001**, 3337-3345.

44. Kim, H.; Chang, J. Y. *Soft Matter* **2011**, *7*, 7952-7955.

45. Willemen, H. M.; Vermonden, T.; Marcelis, A. T. M.; Sudhölter, E. J. R. *Langmuir* **2002**, *18*, 7102-7106.

46. Escuder, B.; Martí, S.; Miravet, J. F. *Langmuir* **2005**, *21*, 6776-6787.

47. Latva, M.; Takalo, H.; Mukkala, V. M.; Matachescu, C.; Rodríguez-Ubis, J. C.; Kankare, J. *J. Lumin.* **1997**, *75*, 149-169.

48. Silva, W. E. ; Belian, M. F.; Freire, R. O.; de Sá, G. F.; Alves Jr, S. *J. Phys. Chem. A* **2010**, *114*, 10066-10075.

49. Cardinaels, T.; Ramaekers, J.; Nockemann, P.; Driesen, K.; Van Hecke, K.; Van Meervelt, L.; Lei, S.; De Feyter, S.; Guillon, D.; Donnio, B.; Binnemans, K. *Chem. Mater.* **2008**, *20*, 1278-1291.

50. Hayer, A.; de Halleux, V.; Köhler, A.; El-Garoughy, A.; Meijer, E. W.; Barberá, J.; Tant, J.; Levin, J.; Lehmann, M.; Gierschner, J.; Cornil, J.;

Geerts, Y. H. *J. Phys. Chem. B* **2006**, *110*, 7653-7659.

51. Lenaerts, P. ; Driesen, K.; Van Deun, R.; Binnemans, K. *Chem. Mater.* **2005**, *17*, 2148-2154.

52. Van Deun, R.; Nockemann, P.; Görller-Walrand, C.; Binnemans, K. *Chem. Phys. Lett.* **2004**, *397*, 447-450.

53. Polman, A. *J. Appl. Phys.* **1997**, *82*, 1-39.

Chapter III.

Preparation of a Molecularly Imprinted Polymer Containing Europium(III) Ions for Luminescent Sensing

III-1. Introduction

The lanthanide(III) ions have attracted great interests in sensor applications due to their unique photophysical properties. Their luminescence resulting from intraconfigurational f-f transition is narrow, long-lasting and sensitive to the coordination environments, which makes them a promising candidate for signal transducers. Since the lanthanide(III) ions have very low molar absorptivities, it is difficult to populate their resonance levels by direct excitation. As an alternative, indirect excitation of the lanthanide(III) ions via an organic-based antenna is widely used to obtain strong luminescence. The organic ligands located around the lanthanide(III) ions absorb light and sensitize the lanthanide(III) ions by intramolecular energy transfer.[1]

Molecular imprinting is a practical method for preparing artificial receptors. In the molecular imprinting process, a complex of a functional vinyl monomer and a template is copolymerized with a cross-linking agent and subsequent removal of the template from the polymerized matrix generates binding cavities.[2-8] In sensor applications of molecularly imprinted polymers, the bound molecules are usually analyzed by an indirect method such as choromatography.[2,3] However, this method has a drawback such that an additional separation process is required. Several direct sensing methods have been developed, involving the detection of changes in optical properties upon molecular binding[9] by using quantum dots,[10,11] dyes[12,13] and fluorescent polymers[14] as probes. The use of the lanthanide(III) ions to signal the detection has also been reported.[15-19] In these studies, the sensors were designed to detect organophosphonates and organophosphates, which have strong binding affinity for europium(III) ions. The imprinted polymer matrices contained both the europium(III) ions and the sensitizing chromophore moieties. Once the target molecules were bound to the ions by coordination, there was observed an increase of luminescence intensity, regardless of their structures. This result was attributed to the fact that the luminescence of the europium(III) ions is sensitive to the coordination number and geometry as well as the ligand structure.

In this work, a facile synthesis of a luminescence sensor based on the

europium(III) ion-containing molecularly imprinted polymer was described. Different from previous works, this study uses non-chromophoric monomers for coordination with the europium(III) ions and for polymerization. As a result, the europium(III) ion-containing imprinted polymer showed significant luminescence only after binding of chemicals bearing sensitizing chromophore moieties. This type of sensor may be suitable for detecting chromophoric toxic chemicals, such as aromatic acid herbicides and insecticides. Picloram was selected as a model template because it is a widely used chlorinated herbicide persistent in water or soil, which is a suspicious endocrine disruptor and also a detriment to the environment.[20]

III-2. Experimental

Materials. 3-Allylpentane-2,4-dione was synthesized according to the reported procedure.[21] Azobisisobutyronitrile (AIBN) was recrystallized in methanol before use. Ethylene glycol dimethacrylate (EGDMA) was purified by passing through a column filled with aluminum oxide (Aldrich) to remove the inhibitor. All other chemicals and reagent grade solvents were purchased from Aldrich and used without any further purification.

Measurements. ^{1}H NMR spectra were recorded on a Bruker Avance 300 spectrometer (300 MHz). UV-Vis spectra were obtained with the use of a Sinco S-3150 spectrometer. Fluorescence measurements were performed on a Shimadzu RF-5301PC spectrofluorometer. The pH values of solutions were measured using a Schott Lab-860 pH meter.

Polymerization of the Europium(III) Complex. To a solution of 3-allylpentane-2,4-dione (578 mg, 4.12 mmol) in ethanol (100 mL) was added a solution of NaOH (164.89 mg, 4.12 mmol) in water (5 mL). Then, solutions of europium(III) chloride hexahydrate (503.60 mg, 1.37 mmol) in ethanol (2 mL) and picloram (331.87 mg, 1.37 mmol) in ethanol (2 mL) were added dropwise

in sequence. After stirring 2 h at room temperature, EGDMA (3.89 mL, 20.62 mmol) and AIBN (225.69 mg, 1.37 mmol) were added and the reaction mixture was refluxed for 4 h. The white precipitates were isolated by filtration, washed with tetrahydrofuran, water and methanol and dried in vacuo.

Extraction of the Europium(III) Ions and the Template Molecules. The cross-linked polymers were stirred overnight in a HCl and ethanol solution (1 : 9, v/v) and isolated by filtration. The polymers were soxhlet extracted with ethanol for 2 days, collected and dried in vacuo.

Incorporation of the Europium(III) Ion into the Polymer Matrix (MIP-Eu). To a mixture of the extracted polymer (1.20 g) in ethanol (100 mL) and a solution of NaOH (81.86 mg, 2.05 mmol) in water (2 mL) was added a solution of europium(III) chloride hexahydrate (250.00 mg, 0.68 mmol) in ethanol (2 mL). The reaction mixture was refluxed overnight. The white precipitates were isolated by filtration, washed with water and methanol and dried in vacuo.

Preparation of the Europium(III) Coordinated Non-Imprinted Polymer (NIP-Eu). This polymer was prepared in the same manner as **MIP-Eu** except that picloram was omitted.

Rebinding and Selectivity Test. In rebinding test, picloram was dissolved in methanol (10 mL) at various concentrations (0, 0.05, 0.1, 0.2, 0.3, 0.4 mM). Then, the pH of each solution was adjusted to 6 with a 0.1 M aqueous NaOH solution. **MIP-Eu** or **NIP-Eu** (100 mg) was added to the solutions. After incubation for 1 h, luminescence at 616 nm was monitored. In selectivity test, picloram and its analogs were dissolved in methanol (10 mL) at a concentration of 0.4 mM and the pH of each solution was adjusted to 6 with a 0.1 M aqueous NaOH solution. **MIP-Eu** or **NIP-Eu** (100 mg) was added to solutions. After incubation for 1 h, luminescence at 616 nm was monitored. All measurements were repeated three times.

III-3. Results and Discussion

III-3-1. Synthesis and Characterization

Scheme III-1 shows the fabrication of the europium(III) ion-containing molecularly imprinted polymer. 3-allylpentane-2,4-dione and picloram (4-amino-3,5,6-trichloro-2-pyridinecarboxylic acid, template) were used as ligands for the complexation with the europium(III) ion. 3-Allylpentane-2,4-dione has a *β*-diketone structure and an allyl group. *β*-Diketone is well known for its good coordinating ability and widely used as a ligand in metal coordination.[22] Three *β*-diketone ligands were first coordinated with the europium(III) ion by the reaction of 3-allylpentane-2,4-dione and europium(III) chloride hexahydrate in basic aqueous ethanol. Generally, the coordination number of a trivalent europium ion complex is eight or nine. The chloride or water molecules were replaced by occupying the remaining two exchangeable coordination sites with picrolam. Picloram has an aromatic ring which can function as a sensitizing chromophore and two coordination sites, pyridinic nitrogen and carboxylic oxygen.

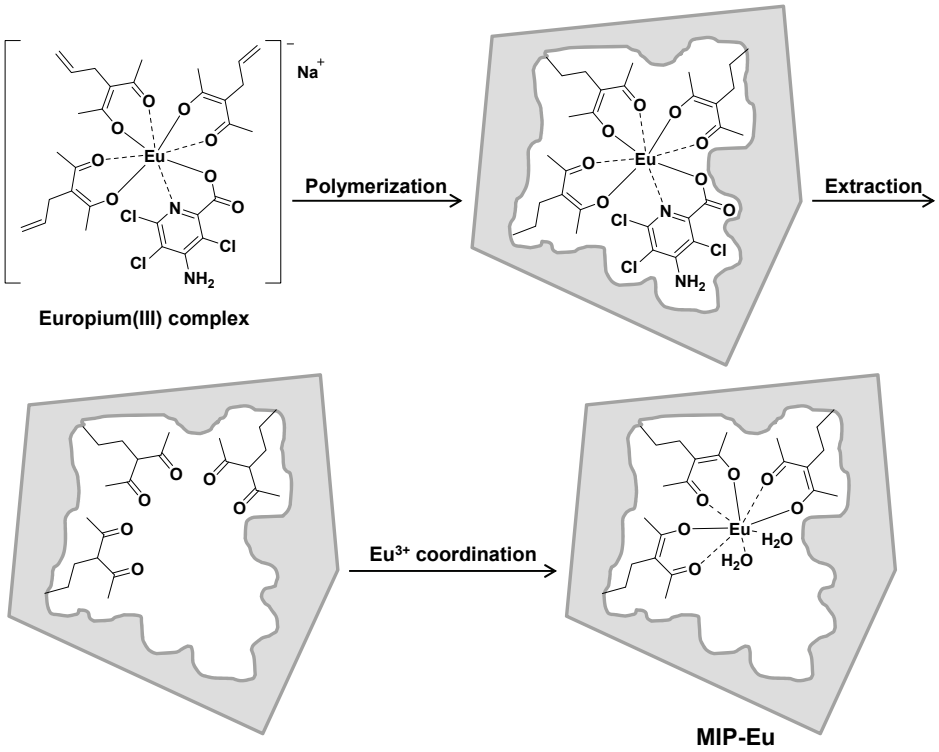

Scheme III-1. Schematic description of the preparation of the europium(III) ion-containing molecularly imprinted polymer.

Figure III-1 shows the changes in emission of the *β*-diketone coordinated europium(III) ion by the addition of picloram at pH 6 under excitation at 320 nm. The emission intensity increased continuously until one equivalent of picrolam was added to the europium(III) ion, suggesting the formation of a europium(III) ion complex coordinated with three *β*-diketones and one picrolam.

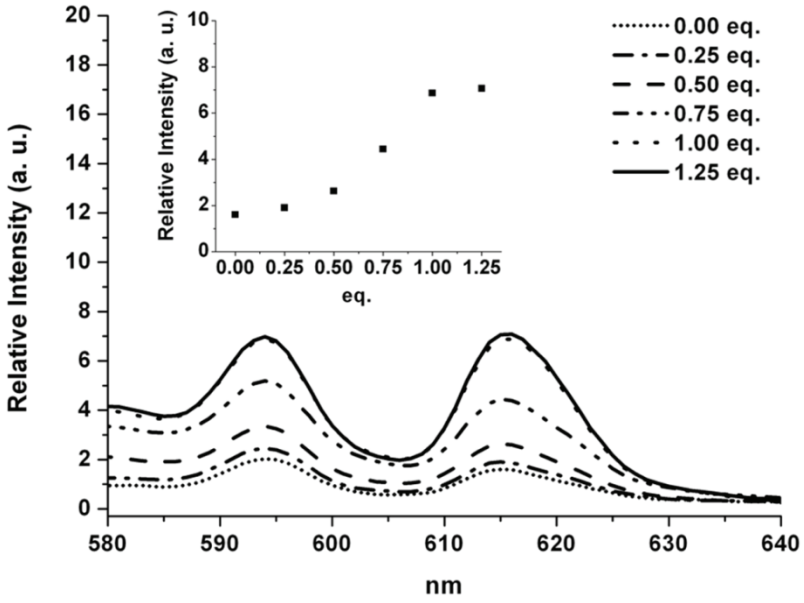

Figure III-1. The changes in the emission of the *β*-diketone coordinated europium(III) ion by addition of picloram at pH 6 under excitation at 320 nm. The *β*-diketone coordinated europium(III) ion was prepared from 1 eq. of europium(III) ion and 3 eq. of 3-allylpentane-2,4-dione in MeOH. The inset shows the changes in the 616 nm emission.

Without isolation of the complex, the copolymerization of its allylic groups with ethylene glycol dimethacrylate (EGDMA) was carried out using azobisisobutyronitrile (AIBN) as an initiator. The radical polymerization of allyl monomers generally produces oligomers because of the chain transfer to the monomers,[23-26] but they are copolymerized with acrylates.[27,28] A

considerably large amount of initiator was required to obtain a cross-linked, insoluble polymer as white fine powders.

The template molecules together with the europium(III) ions were removed from the polymer matrix by solvent extraction with HCl/ethanol, and then only the europium(III) ions were reintroduced into the polymer matrix by reacting the polymer with europium(III) chloride hexahydrate. By this process, the europium(III) ions were placed in the binding cavities of the imprinted polymer (**MIP-Eu**) through coordination with three *β*-diketo groups. A non-imprinted polymer (**NIP-Eu**) was also prepared in the same manner as **MIP-Eu** except that picloram was omitted.

III-3-2. Rebinding Test

The ability of **MIP-Eu** to recognize the template (picrolam) was investigated by photoluminescence spectroscopy. For the rebinding test, picloram solutions of various concentrations in methanol were prepared and their pHs were adjusted to 6 with a 0.1 M aqueous NaOH solution. **MIP-Eu** was added to each solution and incubated for 1 h. The emissions of the mixtures were measured at an excitation wavelength of 250 nm. Figure III-2a shows the spectra obtained by subtracting the spectrum of the **MIP-Eu** in methanol from the original spectra of the mixtures. The characteristic and narrow emission peaks of the

europium(III) ions appeared at 594 and 616 nm, corresponding to $^5D_0 \rightarrow {}^7F_1$ and $^5D_0 \rightarrow {}^7F_2$ transitions, respectively. The intensities of these peaks increased with the increase in the picrolam concentration.

Figure III-2b shows the plots of the changes in the emission intensity of **MIP-Eu** and **NIP-Eu** vs the concentration of picrolam. A $\Delta I/I_0$ parameter was used to analyze the luminescence changes, where I_0 was the emission intensity in the absence of picloram and ΔI was equal to $I - I_0$. The emission of **MIP-Eu** was much more sensitive to the picrolam concentration than that of **NIP-Eu** was. The $\Delta I/I_0$ of **MIP-Eu** increased sharply with the increase in the picrolam concentration up to 0.1 mM and then slowly increased thereafter. At the concentration of 0.1 mM, the enhancement of the emission intensity of **MIP-Eu** was more than four times that of **NIP-Eu**, demonstrating the high recognition ability of **MIP-Eu**. Because the europium(III) ions were placed in the binding cavities, the template molecules were likely trapped in the cavities via coordination with the europium(III) ions.

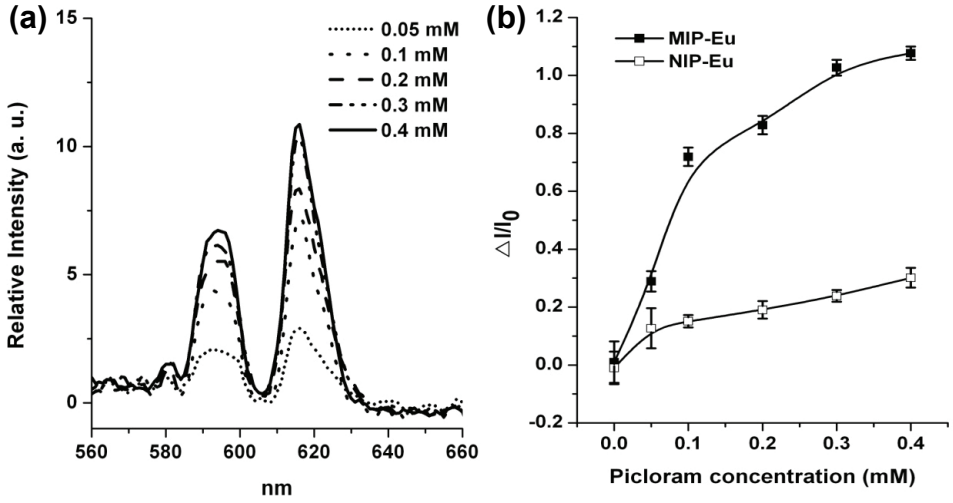

Figure III-2. (a) Emission spectra of **MIP-Eu** in aqueous methanol in the presence of various concentrations of picloram. Emission spectra were obtained at 250 nm excitation. (b) The concentration effect of picloram on emissions of **MIP-Eu** and **NIP-Eu**. ΔI: emission intensity change upon addition of picloram ($I - I_0$), I_0: emission intensity in the absence of picloram.

The binding affinity of **MIP-Eu** for picrolam was also confirmed by visual observation. Figure III-3 shows the photographs of the as-synthesized polymer, **MIP-Eu** and the picloram-bound **MIP-Eu**. The polymers did not have a distinct color in daylight. Under irradiation at 365 nm, however, the as-synthesized polymer containing the europium(III) ions and picloram appeared bright red. The imprinted polymer (**MIP-Eu**) did not show visible emission

owing to the absence of a chromophoric ligand, but exhibited a red color after incubation for 1 h in a 0.4 mM picloram solution in methanol.

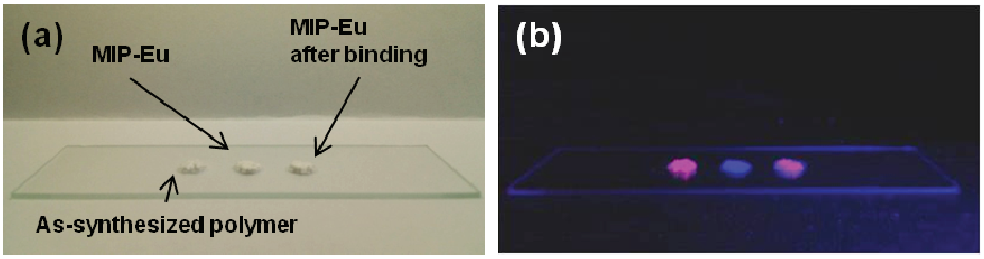

Figure III-3. Photographs of the as-synthesized polymer, **MIP-Eu** and **MIP-Eu** incubated in a 0.4 mM picloram solution in methanol for 1 h taken in (a) daylight and (b) under 365 nm irradiation.

Picloram molecules trapped in cavities were coordinated with europium(III) ions. But, the coordination was dependent on the pH. Ligands are protonated in acidic condition or europium(III) oxides are possibly formed after competition between hydroxide ions and ligands in basic condition. Both cases result in the disruption of the coordination.[29] The pH of picloram solution (0.4 mM) was adjusted with 0.1 M of aqueous HCl and NaOH solutions and found that the emission was most intensified after binding picloram at the pH 6 as shown in Figure III-4.

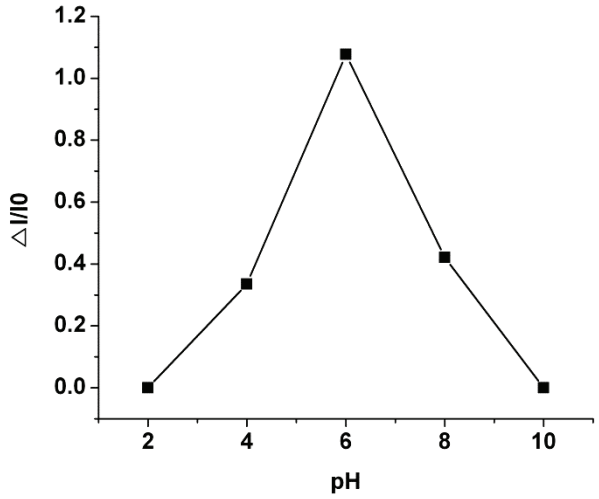

Figure III-4. The effect of pH on emission of **MIP-Eu** in 0.4 mM of picloram solution. ΔI : emission intensity change upon addition of picloram ($I-I_0$), I_0 : emission intensity without picloram.

III-3-3. Selectivity Test

The specific recognition ability of **MIP-Eu** was investigated for the template and its structural analogs, dicamba and 2-amino-4,6-dichloropyrimidine-5-carboxaldehyde (ADC) by photoluminescence spectroscopy. The rebinding test was carried out in the same manner as described above. Solutions of picloram and its analogs in methanol were prepared to have a concentration of 0.4 mM and a pH of 6. After incubation of **MIP-Eu** for 1 h, the emissions of the mixtures were measured at an excitation wavelength of 250 nm. Figure III-5a shows the spectra obtained by subtracting the spectrum of the **MIP-Eu** in

methanol from the original spectra of the mixtures. Figure III-5b shows the changes in the emission intensity ($\Delta I/I_0$) of **MIP-Eu** by addition of analytes. **MIP-Eu** showed the highest recognition ability for picrolam and lowest recognition ability for ADC. Although dicamba has the carboxylic oxygen which can function as a possible coordination site, its binding affinity to **MIP-Eu** was much lower than that of picrolam, proving that the template was most accessible to the europium(III) ion for coordination.

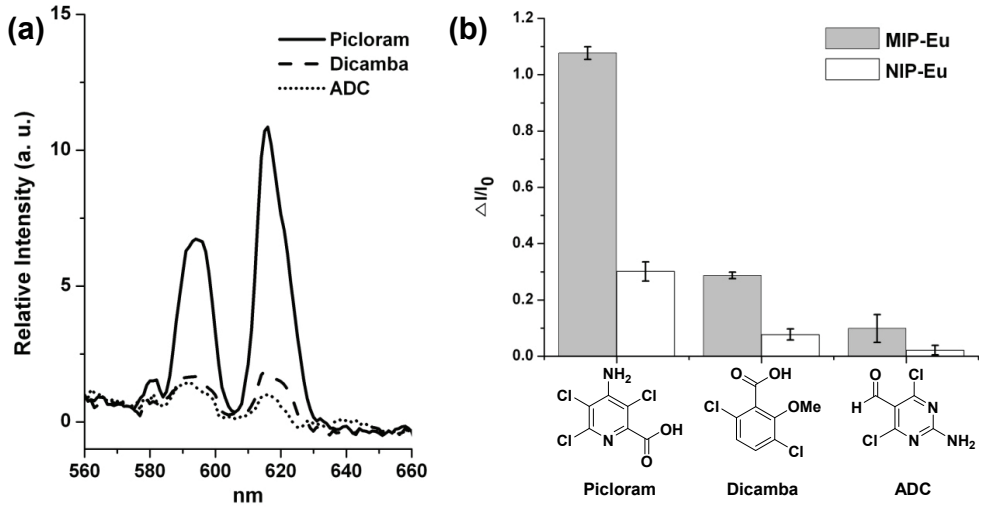

Figure III-5. (a) Emission spectra of **MIP-Eu** in aqueous methanol in the presence of picloram and its analogs (0.4 mM). Emission spectra were obtained at 250 nm excitation. (b) Structures of analytes and their effect on emissions of **MIP-Eu** and **NIP-Eu**. ΔI: emission intensity change upon addition of picloram ($I - I_0$), I_0: emission intensity in the absence of picloram.

III-4. Conclusions

It was demonstrated that the molecularly imprinted polymer bearing the europium(III) ions could be used for the direct detection of the chromophoric template molecule. The europium(III) ion was located in the binding cavities, which were produced in the non-chromophoric cross-linked polymer matrix. In the binding process, the template was trapped in the cavity to coordinate with the europium(III) ion. The imprinted polymer had high recognition ability for the template and showed enhanced luminescence emission in its presence. Since the luminescence emission of the europium(III) ion is very sensitive to the chromophoric ligand, this system has great potential to detect chromophoric chemicals.

III-5. References

1. Binnemans, K. *Chem. Rev.* **2009**, *109*, 4283-4374.
2. Wulff, G. *Chem. Rev.* **2002**, *102*, 1-28.
3. Haupt, K.; Mosbach, K. *Chem. Rev.* **2000**, *100*, 2495-2504.
4. Ye, L.; Mosbach, K. *Chem. Mater.* **2008**, *20*, 859-868.
5. Ki, C. D.; Oh, C.; Oh, S. G.; Chang, J. Y. *J. Am. Chem. Soc.* **2002**, *124*, 14838-14839.
6. Lee, K.; Ki, C. D.; Kim, H.; Chang, J. Y. *Macromolecules* **2004**, *37*, 5544-5549.
7. Jung, B. M.; Kim, M. S.; Kim, W. J.; Chang, J. Y. *Chem. Commun.* **2010**, *46*, 3699-3701.
8. Kim, W. J.; Jung, B. M.; Kang, S. H.; Chang, J. Y. *Soft Matter* **2011**, *7*, 4160-4162.
9. Liao, Y.; Wang, W.; Wang, B. *Bioorg. Chem.* **1999**, *27*, 463-476.
10. Liu, J.; Chen, H.; Lin, Z.; Lin, J. M. *Anal. Chem.* **2010**, *82*, 7380-7386.
11. Zhang, W.; He, X. W.; Chen, Y.; Li, W. Y.; Zhang, Y. K. *Biosens. Bioelectron.* **2011**, *26*, 2553-2558.
12. Tong, A.; Dong, H.; Li, L. *Anal. Chim. Acta* **2002**, *466*, 31-37.
13. Malosse, L.; Buvat, P.; Adès, D.; Siove, A. *Analyst* **2008**, *133*, 588-595.

14. Li, J.; Kendig, C. E.; Nesterov, E. E. *J. Am. Chem. Soc.* **2007**, *129*, 15911-15918.

15. Jenkins, A. L.; Uy, O. M.; Murray, G. M. *Anal. Chem.* **1999**, *71*, 373-378.

16. Jenkins, A. L.; Yina, R.; Jensen, J. L. *Analyst* **2001**, *126*, 798-802.

17. Jenkins, A. L.; Bae, S. Y. *Anal. Chim. Acta* **2005**, *542*, 32-37.

18. Southard, G. E.; Van Houten, K. A.; Ott, E. W.; Murray, G. M. *Anal. Chim. Acta* **2007**, *581*, 202-207.

19. Southard, G. E.; Van Houten, K. A.; Murray, G. M. *Macromolecules* **2007**, *40*, 1395-1400.

20. Zhang, Y.; Zeng, G. M.; Tang, L.; Niu, C. G.; Pang, Y.; Chen, L. J.; Feng, C. L.; Huang, G. H. *Talanta* **2010**, *83*, 210-215.

21. Kalaitzakis, D.; Rozzell, J. D.; Smonou, I; Kambourakis, S. *Adv. Synth. Catal.* **2006**, *348*, 1958-1969.

22. Gao, L. H.; Guan, M.; Wang, K. Z.; Jin, L. P.; Huang, C. H. *Eur. J. Inorg. Chem.* **2006**, *2006*, 3731-3737.

23. Gaylord, N. G. *J. Polym. Sci.* **1956**, *22*, 71-78.

24. Inoue, S.; Kumagai, T.; Tamezawa, H.; Aota, H.; Matsumoto, A.; Yokoyama, K.; Matoba, Y.; Shibano, M. *J. Polym. Sci., Part A: Polym. Chem.* **2011**, *49*, 156-163.

25. Negrell-Guirao, C.; David, G.; Boutevin, B.; Chougrani, K. *J. Polym. Sci., Part A: Polym. Chem.* **2011**, *49*, 3905-3910.

26. Tamezawa, H.; Kumagai, T.; Aota, H.; Matsumoto, A.; Totsuka, T.; Fujie, H. *J. Polym. Sci., Part A: Polym. Chem.* **2012**, *50*, 2732-2737.

27. Venkatesh, R.; Vergouwen, F.; Klumperman, B. *J. Polym. Sci., Part A: Polym. Chem.* **2004**, *42*, 3271-3284.

28. Matsumoto, A.; Miwa, Y.; Inoue, S.; Enomoto, T; Aota, H. *Macromolecules* **2010**, *43*, 6834-6842.

29. Harbuzaru, B. V.; Corma, A.; Rey, F.; Jordá, J. L.; Ananias, D.; Carlos, L. D.; Rocha, J. *Angew. Chem. Int. Ed.* **2009**, *48*, 6476-6479.

Chapter IV.

Preparation of a Yb(III)-Incorporated Porous Polymer by Post-Coordination: Enhancement of Gas Adsorption and Catalytic Activity

IV-1. Introduction

Microporous organic polymers (MOPs) with high surface area and physicochemical stability have attracted considerable attention as gas adsorbents.[1-4] Compared to traditionally used porous materials such as zeolites and activated carbons, MOPs have an advantage in their synthesis and modification. A variety of building blocks and synthetic methodologies are available for MOPs. In addition, MOPs can be further functionalized using diverse chemical methods which, combined with an appropriately selected building block, will provide the MOPs with the desired property for a specific application.

Several factors govern the gas adsorption behaviors of MOPs, including surface area, pore shape and size, and functionality of the framework. Many

efforts to enhance gas adsorption properties of MOPs, particularly for carbon dioxide (CO_2) and hydrogen (H_2), have been reported.[5-21] For example, several studies demonstrated that an introduction of a polar functional group into an MOP enhanced its CO_2 uptake significantly.[13-18] The effects of metal ions on the gas adsorption of MOPs have been also studied. Lithium ion-doped porous polymers showed an increase in CO_2 and H_2 adsorptions.[19-21] High expectations have been also given for metal-containing MOPs for their use in the catalysis of an organic reaction.[22-28]

In this work, a Yb(III)-incorporated microporous polymer (**Yb-ADA**) was synthesized from adamantane derivative and 2,5-dibromoterephthalic acid. Yb is an element in the lanthanide series that has the most common oxidation state of +3. An Yb(III) ion normally has a coordination number of six to nine. Depending on coordination conditions, it has labile small molecules such as water as ligands that are easily eliminated to form open metal sites. The cationic open metal sites are known to induce chemical binding with H_2 as well as CO_2.[29,30] Furthermore, Yb(III) complexes are widely used as a Lewis catalyst in organic reactions such as aldol condensation, cyanation, and Michael reaction.[31-33] Yb(III) catalysts supported on ion exchange resins were also reported to show a similar catalytic activity.[34,35] Herein the synthesis of **Yb-ADA** and its enhanced gas adsorption and catalytic activity were demonstrated.

IV-2. Experimental

Materials. 1,3,5,7-Tetrakis(4-ethynylphenyl)adamantane was synthesized by according to the literature.[36] All chemicals purchased from Aldrich and TCI were used without any further purification. Other reagent grade solvents were used as received.

Measurements. ^{1}H NMR spectra were recorded on a Bruker Avance 300 spectrometer (300 MHz). Solid state ^{13}C CP/MAS NMR spectra were recorded on a Bruker Avance 400 WB spectrometer (100 MHz) equipped with CP-MAS. Fourier transform infrared (FT-IR) measurements were made on a PERKIN ELMER Spectrum GX I using KBr pellets. Thermogravimetric analyses (TGA) were performed on a TA modulated TGA2050 with a heating rate of 10 ^{o}C/min under nitrogen. N_2 and CO_2 uptakes were measured by using a Belsorp-Max (BEL Japan, Inc.) apparatus. Ultra-high purity grade N_2, H_2, and CO_2 gases were used for all adsorption measurements. X-ray photoelectron spectroscopy (XPS) measurements were performed on a KRATOS AXIS-Hsi spectrometer equipped with a Mg K_{α} X-ray source.

Preparation of the Adamantane-Based Porous Polymer (ADA). To a solution of 1,3,5,7-tetrakis(4-ethynylphenyl)adamantane (100 mg, 0.19 mmol) and 2,5-dibromoterephthalic acid (80 mg, 0.25 mmol) in DMF (3 mL) were added $PdCl_2(PPh_3)_2$ (30 mg, 0.04 mmol) and CuI (10 mg, 0.05 mmol). After degassing for 10 min, diisopropylamine (3 mL) was added dropwise to the reaction mixture. After stirring for 24 h at 90 ^oC, the precipitated polymer was isolated by filtration and acidified in an aqueous HCl solution (1 N, 10 mL). The resulting polymer was filtered, washed with water, DMF, and acetone, and Soxhlet extracted with MeOH. The polymer was dried in vacuum at 150 ^oC. Yield: 84%. IR (KBr, cm^{-1}): 3394, 3035, 2933, 2901, 2855, 2198, 1684, 1606, 1507, 1447, 1406, 1359, 1207, 1190, 1117, 1017, 834, 784, 730, 564.

Preparation of the Yb(III)-Coordinated ADA Polymer (Yb-ADA). ADA (60 mg) was dispersed in EtOH (50 mL) and then the pH was adjusted to 8 with an aqueous NaOH solution (2 M). A solution of ytterbium(III) chloride hexahydrate (103.33 mg, 0.27 mmol) in water (2 mL) was added dropwise to the polymer suspension. After stirring for 10 h at rt, the product was isolated by filtration and washed with water, ethanol, and acetone. The polymer was dried in vacuum at 150 ^oC. Yield: 92 %. IR (KBr, cm^{-1}): 3747, 3620, 3394, 2931,

2855, 2195, 1698, 1636, 1522, 1405, 1363, 1272, 1118, 1017, 835, 779, 675, 569.

General Procedure for Acetalization. To a solution of an aldehyde (0.1 mmol) and trimethyl orthoformate (0.03 mL, 0.3 mmol) in MeOH (10 mL) was added a catalyst (30 mg). The reaction mixture was stirred for 12 h at rt. The catalyst was removed by filtration. After evaporation of the solvent, the residue was analyzed by ^{1}H NMR spectroscopy.

IV-3. Results and Discussion

IV-3-1. Synthesis and Characterization

The adamantane-based porous polymer (**ADA**) was synthesized from an ethynyl-functionalized adamantane derivative and 2,5-dibromoterephthalic acid through Sonogashira–Hagihara cross-coupling. A slight excess amount of the ethynyl-functionalized adamantane monomer with respect to 2,5-dibromoterephthalic acid was used because of side reactions such as homocoupling between ethynyl groups.[37,38] **ADA** had two carboxyl groups which could be utilized for Yb(III) coordination. Under basic conditions, the carboxyl group was deprotonated and the resulting carboxylate was reacted with Yb(III) chloride hexahydrate to form a Yb(III) complex. A synthetic pathway of **ADA** and Yb(III)-coordinated **ADA** (**Yb-ADA**) is shown in Scheme IV-1.

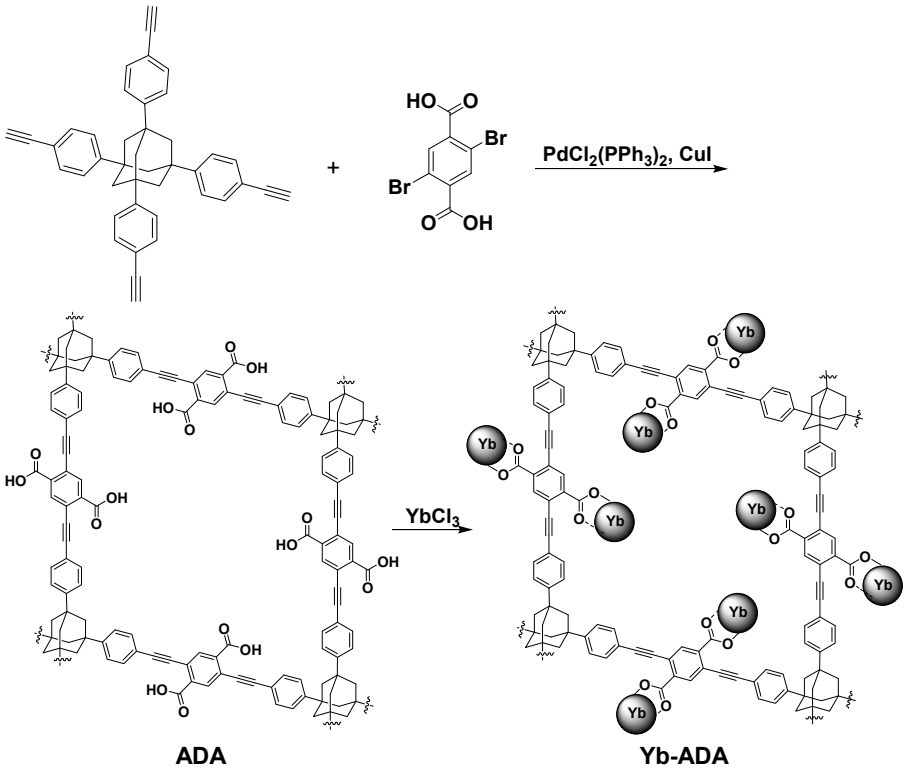

Scheme IV-1. Synthesis of **ADA** and **Yb-ADA**.

The incorporation of Yb(III) ions in **ADA** was confirmed by XPS measurements. The O 1s and C 1s peaks appeared at the binding energy of 530 and 283 eV, respectively in **ADA** (Figure IV-1). After coordination with Yb(III), the polymer (**Yb-ADA**) emitted Yb 4d photoelectrons with the corresponding binding energy at 185 eV in addition to O 1s and C 1s photoelectrons. The Cl 2p photoelectrons were also detected at 198 eV because an Cl anion could remain as a counter ion for Yb(III). On the assumption that

Yb(III) ions were distributed homogeneously in **Yb-ADA**, atomic ratios of C, O, and Yb were estimated by using XPS elemental analysis. The ratio of C : O : Yb was found to be 86.36 : 13.64 : 0 in **ADA** and 69.88 : 27.79 : 2.33 in **Yb-ADA**. The concentration of Yb was smaller than the value calculated from the ideal structure probably because various coordination structures could be formed. The XPS elemental analysis results and theoretical compositions are summarized in Table IV-1. Theoretical values were calculated on the hypothesis that all ethynyl groups were participated in the coupling reaction and Yb(III) was coordinated with one carboxylate group.

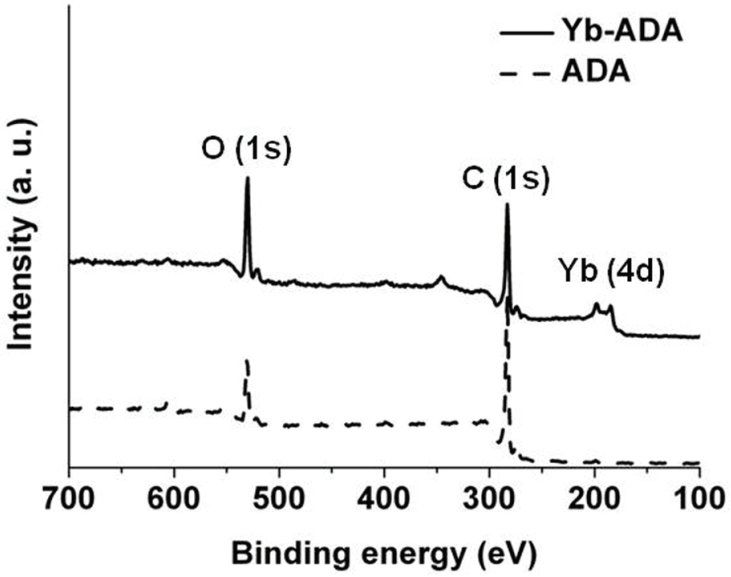

Figure IV-1. XPS spectra of **ADA** and **Yb-ADA**.

Table IV-1. Atomic composition of **ADA** and **Yb-ADA** determined by XPS

Polymer		Atomic composition (%)		
		C	O	Yb
ADA	Theoretical	88.57	11.43	-
	XPS analysis	86.36	13.64	-
Yb-ADA	Theoretical	68.89	26.67	4.44
	XPS analysis	69.88	27.79	2.33

Figure IV-2 shows the ^{13}C NMR spectra of **ADA** and **Yb-ADA**. In **ADA**, the carbon peaks from the carboxyl and ethynyl groups appeared at 165 and 80 ppm, respectively. The peak for aromatic carbons adjacent to the adamantane ring appeared at 149 ppm and the peaks for other aromatic carbons appeared at 130 and 123 ppm. The admantane carbon peaks were shown at 38 and 44 ppm. All these peaks were also observed in **Yb-ADA**, indicating that the **ADA** structure was preserved while coordinated.

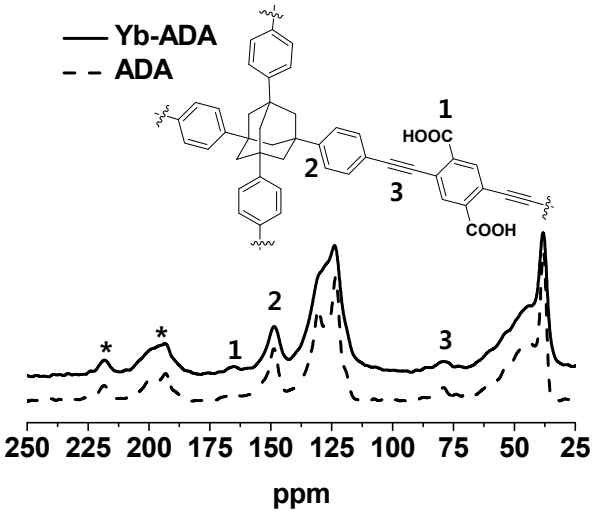

Figure IV-2. Solid-state ^{13}C NMR spectra of **ADA** and **Yb-ADA**.

Thermal properties of **ADA** and **Yb-ADA** were investigated by TGA (Figure IV-3). Both **ADA** and **Yb-ADA** were thermally stable up to 200 ^{o}C and degraded gradually as the temperature increased further. **ADA** and **Yb-ADA** had char yields of 65 and 73 wt%, respectively at 800 ^{o}C. The higher char yield of **Yb-ADA** could be caused by the coordinated Yb(III) ions.

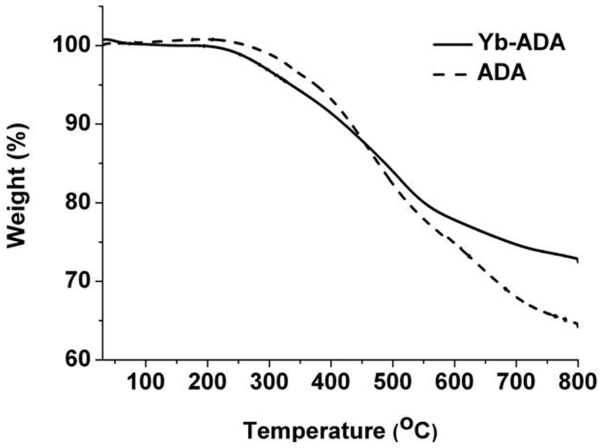

Figure IV-3. TGA thermograms of **ADA** and **Yb-ADA**.

IV-3-2. Gas Adsorption Properties

The N_2 adsorption/desorption isotherms and pore distributions of **ADA** and **Yb-ADA** are shown in Figure IV-4. The Brunauer-Emmett-Teller (BET) surface area of **ADA** calculated from the N_2 adsorption isotherm at 77 K was 970 $m^2 g^{-1}$. As the Yb(III) ions were incorporated into **ADA**, the surface area of the polymer (**Yb-ADA**) was reduced to 885 $m^2 g^{-1}$. The incorporation of Yb(III) ions into **ADA** also appeared to change the pore size distribution when calculated by nonlocal density function theory (NLDFT) with a cylindrical model. Given the calculation, the proportion of ultrafine micropores (< 1 nm) was reduced after coordination and larger micropores were observed more in **Yb-ADA**. One possible explanation for this result was that the pore structure was changed by coordination and deviated from the cylindrical model. The

micropore volume decreased from 0.36 to 0.34 cm^3 g^{-1} after coordination, leading to the surface area decrease.

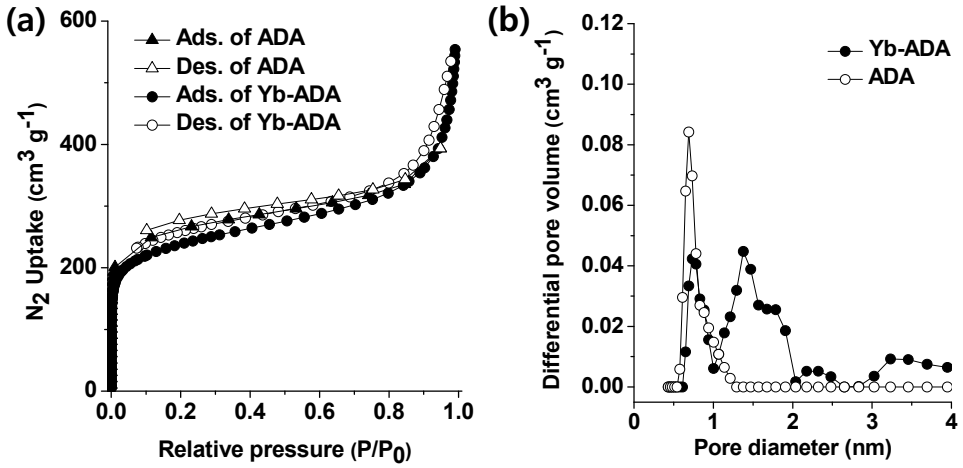

Figure IV-4. (a) N_2 adsorption/desorption isotherms at 77 K for **ADA** and **Yb-ADA** and (b) their pore size distributions calculated using NLDFT.

The CO_2 adsorptions were measured up to 1 bar at 273 and 298 K (Figure IV-5a). **ADA** showed the CO_2 adsorption of 2.57 and 1.56 mmol g^{-1} at 273 and 298 K, respectively. **Yb-ADA** exhibited significantly enhanced CO_2 adsorption capacity of 3.49 and 2.36 mmol g^{-1} at 273 and 298 K, respectively even though it had a smaller surface area compared to **ADA**. This result was attributable to the fact that the cationic open metal sites of Yb(III) interacted with CO_2 electrostatically.[39-41] The interaction between Yb(III) and CO_2 was further

proved by the heat of adsorption measurement (Figure IV-5b). The heat of adsorption was obtained from the CO_2 adsorption isotherms at 273 and 298 K. **Yb-ADA** showed a larger initial heat of adsorption (31.7 KJ mol^{-1}) than **ADA** (28.5 KJ mol^{-1}).

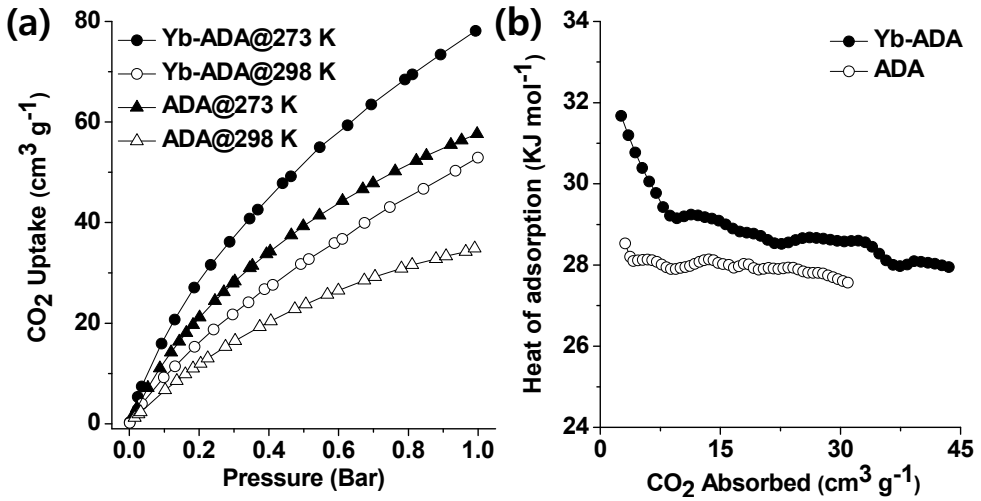

Figure IV-5. (a) CO_2 adsorptions at 273 and 298 K for **ADA** and **Yb-ADA** and (b) their isosteric heats of adsorption for CO_2.

The capture of CO_2 from flue gas is of great interest because CO_2 is considered one of the main causes of global warming. Flue gas usually comprises mostly nitrogen and approximately 15% CO_2.[42,43] Accordingly, the high selectivity of CO_2 over N_2 at low pressures is essential for the efficient separation of CO_2 in flue gas. The initial CO_2 and N_2 adsorption isotherms at

298 K are compared in Figure IV-6. The comparison of initial adsorptions has been reasonably used to investigate the interaction between a gas and a porous polymer while excluding other factors such as gas-gas interactions and pore shapes.[44-46] The CO_2 and N_2 adsorption isotherms showed linear slopes within the pressure range of 0.0 to 0.1 bar. The initial CO_2 adsorption slope of **Yb-ADA** was steeper than that of **ADA**, while two polymers showed a similar initial slope in the N_2 adsorption. The selectivity of CO_2 over N_2 was calculated based on the initial uptake slopes. The CO_2/N_2 selectivity of **Yb-ADA** was 38, which was 2.7 times higher than that of **ADA** (14).

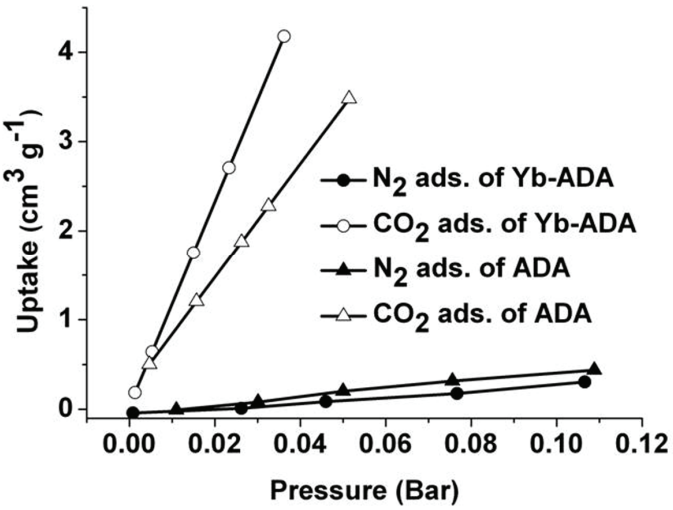

Figure IV-6. CO_2 and N_2 adsorption isotherms of **ADA** and **Yb-ADA** at 298 K within the pressure range of 0.0 to 0.1 bar.

Figure IV-7 shows the H_2 adsorption isotherms at 77 and 87 K. The H_2 uptake of **ADA** also increased after coordination with Yb(III) from 1.15 wt% to 1.40 wt% at 77 K and from 0.81 wt% to 0.95 wt% at 87 K. The initial heats of adsorption of **Yb-ADA** and **ADA**, calculated from adsorption isotherms at 77 and 87 K, were 11.5 and 7.7 KJ mol^{-1}, respectively. The gas adsorption properties of the polymers are summarized in Table IV-2. Micropore volume and total pore volume were determined at P/P_0 = 0.1 and P/P_0 = 0.995, respectively. Also, CO_2 uptakes were measured at 273 K and at 298 K in parenthesis and H_2 uptakes at 77 K and 87 K in parenthesis.

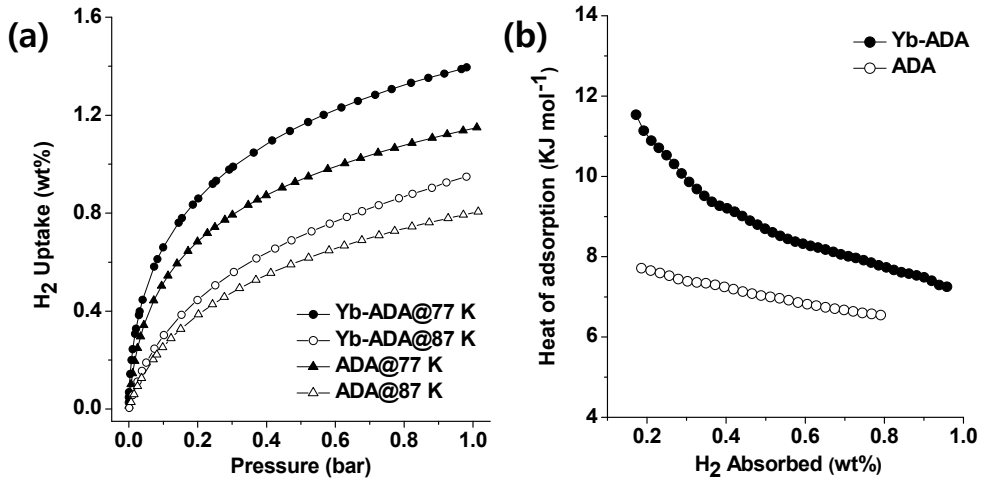

Figure IV-7. (a) H_2 adsorption isotherms at 77 and 87 K for **ADA** and **Yb-ADA** and (b) their isosteric heats of adsorption for H_2.

Table IV-2. Surface areas (S_{BET}), micropore volumes (V_{micro}), total pore volumes (V_{total}), fraction of micropore volume ($V_{0.1/total}$), and CO_2 and H_2 uptakes of **ADA** and **Yb-ADA.**

Polymer	S_{BET} ($m^2 g^{-1}$)	V_{micro} ($cm^3 g^{-1}$)	V_{total} ($cm^3 g^{-1}$)	$V_{0.1/total}$	CO_2 uptake @ 1 bar (mmol g^{-1})	H_2 uptake @ 1 bar (wt%)
ADA	970	0.36	0.82	0.44	2.57 (1.56)	1.15 (0.81)
Yb-ADA	885	0.34	0.85	0.40	3.49 (2.36)	1.40 (0.95)

IV-3-3. Catalytic Activity

The catalytic activity of **ADA** and **Yb-ADA** in a condensation reaction was investigated. An acetal formation reaction of 4-bromobenzaldehyde and furfural with trimethyl orthoformate was arranged as a model reaction and determined conversion yields by ^1H NMR spectroscopy. **ADA** with catalytic carboxyl groups produced acetals in very low yields of 5% and 28 % for 4-bromobenzaldehyde and furfural, respectively. In contrast, in the presence of **Yb-ADA**, 4-bromobenzaldehyde and furfural were completely converted to the corresponding acetals under the same reaction conditions. Without the polymers, the reaction did not occur (Table IV-3). **Yb-ADA** was reused 5 times consecutively in the acetalization of 4-bromobenzaldehyde and furfural.

Conversion yields were almost retained, implying that **Yb-ADA** as a heterogeneous catalyst could be reused after recovery without severe loss of activity (Figure IV-8).

Table IV-3. Conversion yields in acetalization of 4-bromobenzaldehyde and furfural.

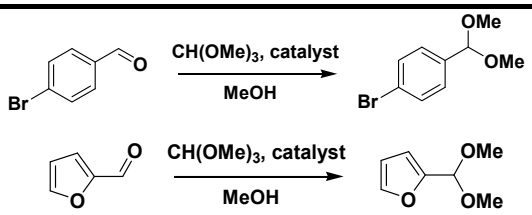

Catalyst	Yield (%) 4-bromobenzaldehyde	Furfural
Without the catalyst	0	0
ADA	5	28
Yb-ADA	100	100

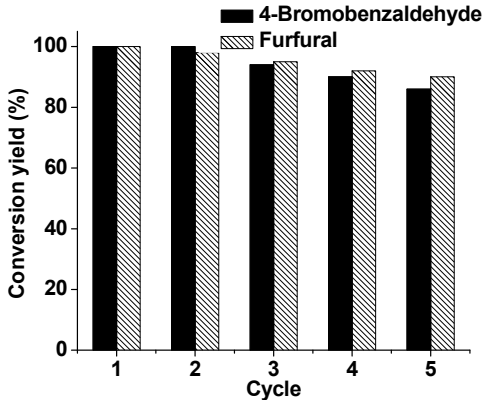

Figure IV-8. Conversion yields of **Yb-ADA** in 5 cycles of acetalization.

IV-4. Conclusions

The synthesis of the adamantane-based porous polymer containing Yb(III) ions by post-coordination was reported. The polymer showed the enhancement of gas adsorption and catalytic activity in acetalization. Following the inclusion of Yb(III) ions, CO_2 uptake of the polymer was enhanced by about 50% at 298 K and H_2 uptake by 21% at 77 K. The Yb(III)-coordinated polymer also functioned as a heterogeneous catalyst in acetalization. These results suggested that cationic open metal sites of Yb(III) in the polymer strongly interacted with electron rich parts of H_2 and CO_2 for adsorption, and with an unshared electron pair on the oxygen atom for catalysis. This work demonstrates that the introduction of metal ions of interest into MOPs is an efficient way to further optimize their properties.

IV-5. References

1. McKeown, N. B.; Budd, P. M. *Macromolecules* **2010**, *43*, 5163-5176.
2. Holst, J. R.; Cooper, A. I. *Adv. Mater.* **2010**, *22*, 5212-5216.
3. Dawson, R.; Cooper, A. I.; Adams, D. J. *Prog. Polym. Sci.* **2012**, *37*, 530-563.
4. Wu, D.; Xu, F.; Sun, B.; Fu, R.; He, H.; Matyjaszewski, K. *Chem. Rev.* **2012**, *112*, 3959-4015.
5. Lim, H.; Cha, M. C.; Chang, J. Y. *Polym. Chem.* **2012**, *3*, 868-870.
6. Lim, H.; Cha, M. C.; Chang, J. Y. *Macromol. Chem. Phys.* **2012**, *213*, 1385-1390.
7. Lim, H.; Chang, J. Y. *Macromolecules* **2010**, *43*, 6943-6945.
8. Li, B.; Gong, R.; Wang, W.; Huang, X.; Zhang, W.; Li, H.; Hu, C.; Tan, B. *Macromolecules* **2011**, *44*, 2410-2414.
9. Y. Yampolskii, *Macromolecules* **2012**, *45*, 3298-3311.
10. Moon, S.-Y.; Mo, H.-R.; Ahn, M.-K.; Bae, J.-S.; Jeon, E.; Park, J.-W. *J. Polym. Sci. Part A: Polym. Chem.* **2013**, *51*, 1758-1766.
11. Germain, J.; Fréchet, J. M. J.; Svec, F. *Small* **2009**, *5*, 1098-1111.
12. Dawson, R.; Cooper, A. I.; Adams, D. J. *Polym. Int.* **2013**, *62*, 345-352.

13. Lu, W.; Yuan, D.; Sculley, J.; Zhao, D.; Krishna, R.; Zhou, H.-C. *J. Am. Chem. Soc.* **2011**, *133*, 18126-18129.

14. Dawson, R.; Adams, D. J.; Cooper, A. I. *Chem. Sci.* **2011**, *2*, 1173-1177.

15. Ren, S.; Dawson, R.; Laybourn, A.; Jiang, J.-X.; Khimyak, Y.; Adams, D. J.; Cooper, A. I. *Polym. Chem.* **2012**, *3*, 928-934.

16. Dawson, R.; Ratvijitvech, T.; Corker, M.; Laybourn, A.; Khimyak, Y. Z.; Cooper, A. I.; Adams, D. J. *Polym. Chem.* **2012**, *3*, 2034-2038.

17. Shanmugam, N.; Lee, K.-T.; Cheng, W.-Y.; Lu, S.-Y. *J. Polym. Sci. Part A: Polym. Chem.* **2012**, *50*, 2521-2526.

18. Yu, H.; Shen, C.; Tian, M.; Qu, J.; Wang, Z. *Macromolecules* **2012**, *45*, 5140-5150.

19. Cao, D.; Lan, J.; Wang, W.; Smit, B. *Angew. Chem. Int. Ed.* **2009**, *48*, 4730-4733.

20. Ma, H.; Ren, H.; Zou, X.; Sun, F.; Yan, Z.; Cai, K.; Wang, D.; Zhu, G. *J. Mater. Chem. A* **2013**, *1*, 752-758.

21. Li, A.; Lu, R.-F.; Wang, Y.; Wang, X.; Han, K.-L.; Deng, W.-Q. *Angew. Chem. Int. Ed.* **2010**, *49*, 3330-3333.

22. Chen, L.; Yang, Y.; Jiang, D. *J. Am. Chem. Soc.* **2010**, *132*, 9138-9143.

23. Chen, L.; Yang, Y.; Guo, Z.; Jiang, D. *Adv. Mater.* **2011**, *23*, 3149-3154.

24. Xie, Z.; Wang, C.; deKrafft, K. E.; Lin, W. *J. Am. Chem. Soc.* **2011**, *133*, 2056-2059.

25. Jiang, J.-X.; Wang, C.; Laybourn, A.; Hasell, T.; Clowes, R.; Khimyak, Y. Z.; Xiao, J.; Higgins, S. J.; Adams, D. J.; Cooper, A. I. *Angew. Chem. Int. Ed.* **2011**, *50*, 1072-1075.

26. Thiel, K.; Zehbe, R.; Roeser, J.; Strauch, P.; Enthalerd, S.; Thomas, A. *Polym. Chem.* **2013**, *4*, 1848-1856.

27. Lei, J.; Li, D.; Wang, H.; Wang, Z.; Zhou, G. *J. Polym. Sci. Part A: Polym. Chem.* **2011**, *49*, 1503-1507.

28. Morisaki, Y.; Gon, M.; Chujo, Y. *J. Polym. Sci. Part A: Polym. Chem.* **2013**, *51*, 2311-2316.

29. Getman, R. B.; Miller, J. H.; Wang, K.; Snurr, R. Q. *J. Phys. Chem. C* **2011**, *115*, 2066-2075.

30. Mu, B.; Schoenecker, P. M.; Walton, K. S. *J. Phys. Chem. C* **2010**, *114*, 6464-6471.

31. Kobayashi, S.; Sugiura, M.; Kitagawa, H.; Lam, W. W.-L. *Chem. Rev.* **2002**, *102*, 2227-2302.

32. Inanaga, J.; Furuno, H.; Hayano, T. *Chem. Rev.* **2002**, *102*, 2211-2225.

33. Aspinall, H. C.; Bickley, J. F.; Greeves, N.; Kelly, R. V.; Smith, P. M. *Organometallics* **2005**, *24*, 3458-3467.

34. Yu, L.; Chen, D.; Li, J.; Wang, P. G. *J. Org. Chem.* **1997**, *62*, 3575-3581.

35. Dondoni, A.; Massi, A. *Tetrahedron Lett.* **2001**, *42*, 7975-7978.

36. Lu, W.; Yuan, D.; Zhao, D.; Schilling, C. I.; Plietzsch, O.; Muller, T.; Bräse, S.; Guenther, J.; Blümel, J.; Krishna, R.; Li, Z.; Zhou, H.-C. *Chem. Mater.* **2010**, *22*, 5964-5972.

37. Elangovan, A.; Wang, Y.-H.; Ho, T.-I. *Org. Lett.* **2003**, *5*, 1841-1844.

38. Jiang, J.-X.; Su, F.; Trewin, A.; Wood, C. D.; Niu, H.; Jones, J. T. A.; Khimyak, Y. Z.; Cooper, A. I. *J. Am. Chem. Soc.* **2008**, *130*, 7710-7720.

39. Lee, W. R.; Ryu, D. W.; Lee, J. W.; Yoon, J. H.; Koh, E. K.; Hong, C. S. *Inorg. Chem.* **2010**, *49*, 4723-4725.

40. Pan, L.; Adams, K. M.; Hernandez, H. E.; Wang, X.; Zheng, C.; Hattori, Y.; Kaneko, K. *J. Am. Chem. Soc.* **2003**, *125*, 3062-3067.

41. Lin, Z.; Zou, R.; Xia, W.; Chen, L.; Wang, X.; Liao, F.; Wang, Y.; Lin, J.; Burrell, A. K. *J. Mater. Chem.* **2012**, *22*, 21076-21084.

42. D´Alessandro, D. M.; Smit, B.; Long, J. R. *Angew. Chem. Int. Ed.* **2010**, *49*, 6058-6082.

43. Drage, T. C.; Snape, C. E.; Stevens, L. A.; Wood, J.; Wang, J.; Cooper, A. I.; Dawson, R.; Guo, X.; Satterley, C.; Irons, R. *J. Mater. Chem.* **2012**, *22*, 2815-2823.

44. Rabbani, M. G.; El-Kaderi, H. M. *Chem. Mater.* **2012**, *24*, 1511-1517.

45. An, J.; Geib, S. J.; Rosi, N. L. *J. Am. Chem. Soc.* **2010**, *132*, 38-39.

46. Banerjee, R.; Furukawa, H.; Britt, D.; Knobler, C.; O'Keeffe, M.; Yaghi, O. M. *J. Am. Chem. Soc.* **2009**, *131*, 3875-3877.

국문요약

란탄족 원소는 f-f 전이로 인하여 좁은 발광 스펙트럼과 긴 발광 수명을 나타내는 독특한 광학적 성질을 가지고 있다. 본 연구에서는 발광성을 띠는 란탄족 원소를 방향족의 유기물 안에 도입하여 유기 젤화제를 만들었으며, 유기 용매의 젤화 거동을 관찰하였고 젤화에 의한 란탄족 원소의 발광 세기 증가와 발광색의 변화 등을 관찰하였다. 란탄족 원소의 종류에 따라서 젤화제는 가시광선 영역의 발광뿐만 아니라 근적외선 영역의 발광까지 나타낼 수 있었으며, 다양한 형태의 필름으로도 제조되었다. 또한 란탄족 원소는 그 광학적 성질로 인하여 분자 날인 고분자에서 신호 변환 장치로 활용되었으며, 다공성 고분자에 도핑되어 고분자의 기체 흡착 거동과 촉매 특성의 향상에 쓰였다.

먼저 유기젤의 경우, 유로피움과 터븀 이온을 phenanthroline 유도체에 배위결합 시켜서 유기 젤화제 **Eu2** 와 **Tb2** 를 합성하였고, *n*-decane 의 젤화 거동을 관찰하였다. **Eu2** 와 **Tb2** 의 유기젤은 각각 빨간색과 초록색의 발광을 나타내었으며, 해당 건조젤을 TEM 으로 확인하였을 때, 20 에서 80 nm 두께의 섬유조직이 형성되었음을

확인하였다. 구조적 유사성으로 인하여 두 젤화제의 혼합물도 *n*-decane의 젤화 거동을 보였다. 각 이온의 고유 발광 특성을 유지하여, 유로피움의 발광이 595 와 618 nm 에서, 터븀의 발광은 496 과 551 nm 에서 관찰되었다. 또한 주로 **Tb2** 의 리간드에서 나오는 형광이 470 nm 에서 관찰되었다. **Eu2** 와 **Tb2** 의 비율이 1 : 19 일 때, 색좌표 (1931 CIE color coordinates) 에서 (0.36, 0.30) 값을 나타내는 백색광을 얻었다. 혼합된 건조젤을 TEM 으로 조사하였을 때, 20 에서 80 nm 의 두께를 갖는 섬유구조가 상분리 없이 관찰되었다. **Eu2** 와 **Tb2** 를 이용하여 세 개의 금속 이온을 갖는 **Eu4** 와 **Tb4** 를 합성하였다. **Eu4** 는 리간드의 발광뿐만 아니라, 빨간색 영역의 유로피움 발광도 나타나는 반면, **Tb4** 는 리간드의 녹청색 발광만 보였다. **Eu4** 와 **Tb4** 역시 혼합젤을 형성하였고 3 : 1 의 비율에서 백색 영역의 발광이 관찰되었다. **Eu4** 는 필름형성 특성을 보였다. 어븀 이온이 도입된 **Er4** 를 합성하여 EGDMA 에서의 젤화 거동을 조사하였다. 젤 상태에서의 중합 반응을 통하여 제조한 어븀 이온을 갖는 경화성 필름은 광통신에 이용할 수 있는 NIR 발광을 보였다.

두 번째로, 유로피움 이온을 분자 날인 고분자에 도입하여 방향족 분자를 광학적으로 감지하는 센서를 제조하였다. 유로피움 이온과 3-

allylpentane-2,4-dione 의 컴플렉스와 EGDMA 의 공중합을 통하여 인식자리에 유로피움 이온을 갖는 분자 인식 고분자를 합성하였다. 주형분자로는 제초제로 쓰이고 환경 호르몬으로써 위험성을 지니며 토양이나 물에 잔존하기 쉬운 picloram 을 선택하였다. 분자 날인 고분자의 인식자리에 있는 유로피움은 picloram 존재 시 594 과 616 nm 에서 강한 발광을 보였다. 또한 다른 구조적 유사체들과 비교하였을 때 picloram 을 선택적으로 검출함을 확인하였다.

마지막으로, 이터븀 이온을 함유한 다공성 고분자 (**Yb-ADA**) 를 제조하고 그에 따른 기체 흡착 거동과 촉매 성능의 향상에 대해 연구하였다. 아다만탄 기제의 모노머와 2,5-dibromoterephthalic acid 로부터 다공성 고분자를 제조한 후, 이터븀 이온을 도입하였다. 금속 이온이 도입되면서 전체적인 BET 비표면적은 970 에서 885 $m^2 g^{-1}$ 로 감소하였지만, 이산화탄소 흡착량은 1.56 에서 2.36 mmol g^{-1} 로 증가하였고 수소 흡착량은 1.15 에서 1.40 wt% 로 증가하였다. 또한 **Yb-ADA** 는 이터븀의 영향으로 bromobenzaldehyde 와 furfural 의 아세탈 반응에서 촉매 활성을 보였으며, 재사용이 가능한 것을 확인하였다.

주요어 : 란탄족, 발광, 유기젤, 분자날인, 다공성 고분자, 촉매.

학번 : 2008-20639

List of Publications

(1) Hyungwoo Kim and Ji Young Chang, "Synthesis of a film-forming europium(III) complex and its organogelation and photoluminescent properties", *Soft Matter* **2011**, *7*, 7952-7955.

(2) Hyungwoo Kim, Young do Kim and Ji Young Chang, "Preparation of a molecularly imprinted polymer containing europium(III) ions for luminescent sensing", *J. Polym. Sci. Part A: Polym. Chem.* **2012**, *50*, 4990-4994.

(3) Hyungwoo Kim and Ji Young Chang, "White light emission from a mixed organogel of lanthanide(III)-containing organogelators", *RSC Adv.* **2013**, *3*, 1774-1780.

(4) Hyungwoo Kim, Taejin Choi, Min Chul Cha and Ji Young Chang, "Preparation of a porous polymer by a catalyst-free diels-alder reaction and its structural modification by post-reaction", *J. Polym. Sci. Part A: Polym. Chem.* **2013**, *51*, 3646-3653.

(5) Hyungwoo Kim, Min Chul Cha, Hyun Woo Park and Ji Young Chang, "Preparation of a Yb(III)-incorporated porous polymer by post-coordination: enhancement of gas adsorption and catalytic activity", *J. Polym. Sci. Part A: Polym. Chem.* **2013**, *51*, 5291-5297.

List of Presentations

(1) 2009년 4월, 춘계 한국고분자학회, “Preparation of PEG-folate-immobilized mesoporous silica particles”

(2) 2009년 8월, IRTG meeting, “Synthesis and Characterization of Europium(III) Complexes Bearing 1,3,5-Tris(acetoacetamido)benzene and Phenanthrolines”

(3) 2009년 10월, 추계 한국고분자학회, “Synthesis and characterization of europium(lll) complexes bearing 1,3,5-Tris(acetoacetamido)benzene and phenanthrolines”

(4) 2010년 4월, 춘계 한국고분자학회, “Synthesis and Self-Assembly of Europium (III) Complexes Bearing 1,3,5-Tris(acetoacetamido)benzene and Phenanthrolines”

(5) 2010년 6월, IRTG meeting, “Synthesis and Self-Assembly of Europium(III) Complexes Bearing 1,3,5-Tris(acetoacetamido)benzene and Phenanthroline Moieties”

(6) 2011년 1월, IRTG meeting, “Synthesis of a small molecule having a coordination site and its photovoltaic application”

(7) 2011년 4월, 춘계 한국고분자학회, “Synthesis of a small molecule having a coordination site and its photovoltaic application”

(8) 2012년 4월, 춘계 한국고분자학회, “Preparation of molecularly imprinted polymers containing europium(III) and their luminescent sensing”

(9) 2012년 8월, ACS fall meeting in Philadelphia, “Synthesis and self-assembly of an organogelator containing europium(lll) ions and its photoluminescent properties”

(10) 2012년 10월, 추계 한국고분자학회, “White-light emission from a mixed organogel of lanthanide(lll)-containing organogelators”

(11) 2013년 2월, IRTG meeting, “White-light emission from a mixed organogel of lanthanide(III)-containing organogelators”

(12) 2013년 4월, 춘계 한국고분자학회, “Synthesis of lanthanide(III) complexes and their self-assembly and optical properties”

(13) 2013년 8월, German-Korean Polymer Symposium with IRTG meeting, “Preparation of a Porous Polymer by a Catalyst-Free Diels-Alder Reaction and Its Structural Modification by Post-Reaction”

(14) 2013년 10월, 추계 한국고분자학회, “Preparation of a Yb(III)-Incorporated Porous Polymer by Post-Coordination: Enhancement of Gas Adsorption and Catalytic Activity”